Lsz
9 000004 122426

OF 1915

ANALELE UNIVERSITATII BUCURESTI

fizica

Nuclear Physics • Plasma Physics • Optics and Spectroscopy • Laser Physics • Solid State Physics • Polymers Physics • Electron Physics • Biophysics • Earth Physics

ANUL XXIX – 1980

F I Z I C Ă

COMITETUL DE REDACȚIE

Redactor responsabil :	Prof. dr. doc. *Gheorghe Brătescu*
Redactor responsabil adj. :	Prof. dr. *Ion Petrea*
Membri :	Prof. dr. *Vasile Mihu*
	Conf. dr. *Constantin Vrejoiu*
	Conf. dr. *Dumitru Ciobotaru*
	Conf. dr. *Grecu Voicu*
Secretar de redacție :	Lector dr. *Ion Licea*

REDACȚIA
TIPOGRAFIA UNIVERSITĂȚII BUCUREȘTI
Șoseaua Panduri nr. 90
Telefon 13 40 00/122

OF 1915

ANALELE UNIVERSITĂȚII BUCUREȘTI

1989

FIZICĂ

BUDAPESTI MŰSZAKI ÉS GAZDASÁGTUDOMÁNYI EGYETEM
Országos Műszaki Információs Központ és Könyvtár
2001

SUMAR • CONTENTS

NUCLEAR PHYSICS

S. MUSCALU : Calculus of the Antisymmetric Spin Functions in the Three-Body Case 3

PLASMA PHYSICS

G. G. BRĂTESCU, MAGDA CAZAN-CORBASCA : Coefficients d'ionisation et potentiels explosifs dans les vapeurs de l'alcool méthylique (CH_3OH) 9

OPTICS AND SPECTROSCOPY

G. G. BRĂTESCU, T. TUDOR, G. NEMEȘ, M. RISTICI : The Coherence of Sidebands of Electrically Intensity Modulated Light 15

G. G. BRĂTESCU, F. GRUZSNICZKI : The Influence of the Hyperfine Structure on the Profile Fineness of Radiations emitted by Mercury and the Intensity Anomaly of the Hyperfine Components of the Green Radiation 21

T. TUDOR, A. DUMITRICĂ, D. APOSTOL : Optical Frequency Translator Using Two K.D.P. Crystals in Tandem 31

LASER PHYSICS

M. RISTICI, A. I. CIURA, T. TUDOR : Longitudinal Mode-Locking in a HE.–NE. Laser by Nonlinear Absorption in Neon . . 37

SOLID STATE PHYSICS

B. LOGOFĂTU, A. DAFINEI, I. DAFINEI : Deposition and Study of some Properties of Tin Oxide Films 43

MICHAELA LOGOFĂTU, B. LOGOFĂTU, M. F. LĂZĂRESCU, M. T. DUMITRIU : Some Indium Arsenide Photoconductive Properties 47

H. V. ALEXANDRU, Z. CSIKI, G. BACIU : The Study of Defects in the ADP Single Crystals by the X-ray Topography Method 51

POLYMERS PHYSICS

I. C. PETREA, C. A. STĂNESCU, M. COJOCARU, E. BARNA : Dielectric Properties of Plasticizated Elastomer Mixtures . 57

E. BARNA, L. M. IONESCU, I. C. PETREA : Mesure de résistence spécifique et évaluation d'une transition isotrope-smectique C 63

L. GEORGESCU, C. A. STĂNESCU : Deduction of Flory and Huggins Formula for Macromolecular Solutions of the Basis of Ising's Model 69

C. A. STĂNESCU : Applications of Decorated Lattices to Solutions. I. Equilibrium Polymerisation in a Decorated Lattice Model. 75

LIVIA IONESCU, I. C. PETREA, E. BARNA : Etude des interfaces des microdomaines de segregation d'un copolymere séquencé organisé 81

ELECTRON PHYSICS

V. GHEORGHE, S. I. SPÂNULESCU : Noise Rejection by Discrete Restoration of Signal Spectrum 89

BIOPHYSICS

SILVIA INDREI, V. GHEORGHE, GABRIELA ANGEL : Transmembrane Potential Measurement Through a Collagen Membrane 99

EARTH PHYSICS

ST. LASCU : Notices on the Variation of Seismic Waves Velocity Beneath the Vrance zone. 107

⁂

Le proffeseur NICOLAE BĂRBULESCU *a son 80-ème anniversaire* 113

BME KÖZPONTI F KÖNYVTÁR
F 8482
FOLYÓIRAT OSZTÁLY

Budapesti Műszaki Egyetem
Központi Könyvtára
Folyóiratok
P280/1980

BUDAPESTI MŰSZAKI EGYETEM KÖZPONTI KÖNYVTÁR 1848

ANALELE UNIVERSITĂŢII BUCUREŞTI, FIZICĂ XXIX, 1980, PAG. 3–8

CALCULUS OF THE ANTISYMMETRIC SPIN FUNCTIONS IN THE THREE-BODY CASE

S. MUSCALU

Faculty of Physics, University of Bucharest *

ABSTRACT

The three body problem, in the short range interaction forces case was always an object for study, and the problem of splitting the deuteron by nucleons was approached with in different ways [1–7]. For comparison with the experimental results, the amplitude of nucleon scattering on deuterium with splitting of the deuterons has to be written for real particles taking into account the spin and isospin variables. The purpose of the present paper in the getting of the antisymmetric spin functions in the three-body case.

We start off by examining the system of two particles, the state of which is determined by the respective moments $\vec{J}(1)$ and $\vec{J}(2)$. We admit that their projection operators do commute with each other

$$[\hat{J}_l(1), \hat{J}_k(2)] = 0, \qquad l, k = 1, 2, 3 \tag{1}$$

In this case the total system can find itself in states with simultaneously definite values of the squared moments.

$$|\vec{J}(1)|^2 = j_1(j_1 + 1)\,\hbar^2, \; |\vec{J}(2)|^2 = j_2(j_2 + 1)\,\hbar^2 \tag{2}$$

Their projections on one, let it be the z, axis the values

$$J_z(1) = m_1\hbar, \; J_z(2) = m_2\hbar \tag{3}$$

Such states are described by the wave functions [8]

$$|j_1 m_1 j_2 m_2 > = |j_1 m_1 > |j_2 m_2 > \tag{4}$$

---

* National Center of Physics, P. O. BOX 5211, Măgurele, Bucharest.

Fixing down the j_1 and j_2 values there are $(2j_1 + 1)\,(2j_2 + 1)$ functions differing from one another by the m_1 and m_2 values.

Let us now determine the operator

$$\hat{\vec{J}} = \hat{\vec{J}}(1) + \hat{\vec{J}}(2) \tag{5}$$

that we shall call total momentum operator of the system. The wave functions (4) are eigen functions of the total momentum operator projection

$$\hat{J}_z = \hat{J}_z(1) + \hat{J}_z(2) \tag{6}$$

to which correspond the eigen values

$$J_z = m\hbar = (m_1 + m_2)\,\hbar \tag{7}$$

The total momentum square operator

$$\hat{\vec{J}}^2 = |\hat{\vec{J}}(1)|^2 + |\hat{\vec{J}}(2)|^2 + 2\hat{\vec{J}}(1)\,\hat{\vec{J}}(2) \tag{8}$$

commutes with the operators $|\vec{\hat{J}}(1)|^2$ and $|\vec{\hat{J}}(2)|^2$ and may thus have its value simultaneously defined with those of the squared moments of each sistem component. However, functions (4) are not eigen-functions of the operator (8) because the third term in (8) mixes the states differing in the values of m_1 and m_2 by one unit. From the function (4) one can build up such linear combinations which were eigen functions of $|\hat{\vec{J}}|^2$ too. Due to the linearity of operator $\hat{J}_z$ these linear combinations should be at the same time its eigen-functions. Thus, the state corresponding to definite values of squared total moment, total moment projection and squared $|\vec{J}(1)|^2$ and $|\vec{J}(2)|^2$ moments can be written as follows

$$|j_1 j_2 m_1 m_2> = \sum_{m_1, m_2} (j_1 j_2 m_1 m_2\,|\,jm)\,|\,j_1 m_1>|\,j_2 m_2> \tag{9}$$

where $(j_1 j_2 m_1 m_2\,|\,jm)$ are coefficients [8 – 9] accounting for the different contributions of the functions in (9). These coefficients constitute the transformation matrix from the component momentr projections representation of the system to the total momentum and its projection representation. The coefficients differ from zero only if the condition

$$m = m_1 + m_2 \tag{10}$$

is fulfilled.

The actual problem is to establish antisymmetric spin functions in the case of neutrons scattering on deuterium. We shall use the notation ${}_m\chi^j_a$ where j is the total momentum in the three body final state and m

is the total momentum projection on the chosen direction. In the case of antisymmetric spin functions the spins of the final state pairedly interacting particles are antiparallel, that is these functions describe the singlet state of the system.

We suppose that in the final state are interacting the pairedly particles n_1 and p, and the third particle n_2 with spin $\frac{1}{2}$ has its spin peojection on the chosen direction, $\frac{1}{2}$. We first obtain the spin function for the pairedly interacting particles n_1 and p. We note with j_1 and j_2 the spins of the two particles and with m_1 and m_2 their projections on the z axis. As the spins of the paired particles are antiparallel, it comes out that

$$m_{12} = m_1 + m_2 = j_1 + j_2 - 1 \tag{11}$$

where $m_1 = j_1 - 1$ and $m_2 = j_2$, or $m_1 = j_1$ and $m_2 = j_2 - 1$. Using relation (9) we get

$$\begin{aligned}|j_{12}m_{12}> = {} & (j_1j_2j_1-1j_2 \,|\, j_{12}j_1-1+j_2)\,|j_1j_1-1>|j_2j_2> + \\ & + (j_1j_2j_1j_2-1 \,|\, j_{12}j_1+j_2-1)\,|j_1j_1>|j_2j_2-1> + \\ & + (j_1j_2j_1j_2 \,|\, j_{12}j_1+j_2)\,|j_1j_1>|j_2j_2> + \\ & + (j_1j_1j_1-1j_2-1 \,|\, j_{12}j_1-1+j_2-1)\,|j_1j_1-1>|j_2j_2-1>\end{aligned} \tag{12}$$

The couplings given by the third and fourth terms in (12) are not materialized since $m_{12} = m_1 + m_2 = \pm 1$, which does not correspond to the proposed problem, that is $m_{12} = m_1 + m_2 = 0$.
Thus,

$$\begin{aligned}|j_{12}m_{12}> = {} & (j_1j_2j_1-1j_2 \,|\, j_{12}j_1-1+j_2)\,|j_1j_1-1>|j_1j_2> + \\ & + (j_1j_2j_1j_3-1 \,|\, j_{12}j_1+j_2-1)\,|j_1j_1>|j_2j_2-1>\end{aligned} \tag{13}$$

where the coefficients have the values [9]:

$$(j_1j_2j_1-1j_2 \,|\, j_{12}j_1-1+j_2) = -\sqrt{\frac{j_1-m_{12}+j_2}{2j_1+1}} = -\frac{1}{\sqrt{2}}$$

$$(j_1j_2j_1j_2-1 \,|\, j_{12}j_1+j_2-1) = \sqrt{\frac{j_1+m_{12}+j_2}{2j_1+1}} = \frac{1}{\sqrt{2}}$$

With these coefficients, relation (13) becomes:

$$|j_{12}m_{12}> = \frac{1}{\sqrt{2}}\,[\,|j_1j_1>|j_2j_2-1> - |j_1j_1-1>|j_2j_2>\,] \tag{14}$$

This is the antisymmetric spin function for paired particles n_1p interacting in the final state.

In the final state we are dealing with a system component the operators of which $\hat{\vec{J}}(1)$, $\hat{\vec{J}}(2)$, $\hat{\vec{J}}(3)$ commute with one another and have for their eigenfunctions $|j_1m_1>$, $|j_2m_2>$ and $|j_3m_3>$ respectively.

The operator $\hat{\vec{J}} = \hat{\vec{J}}(1) + \hat{\vec{J}}(2) + \hat{\vec{J}}(3)$ will be the total momentum operator of the system. Therefore from system component functions corresponding to given, j_1, j_2 and j_3 values we have to build up wave functions that were eigen functions of $|\hat{\vec{J}}|^2$ and $\vec{J}_z$ with eigen values $|\vec{J}|^2 = j(j+1)\hbar$ and $J_z = m\hbar$ respectively, where $m = m_1 + m_2 + m_3$. To obtain the function $|jm>$ we have to couple the function (14) with that of the third unpaired particle n_2, $|j_3m_3>$, where $j_3 = \frac{1}{2}$ and $m_3 = \frac{1}{2}$ or $-\frac{1}{2}$. At the start we admit that the actual state is $m_3 = \frac{1}{2}$.

Therefore, $j = j_{12} + j_3 = \frac{1}{2}$ and $m = m_{12} + m_3 = j_{12} + j_3$, where $m_{12} = j_{12}$ and $m_3 = j_3$, or $m_{12} = j_3$ and $m_3 = j_{12}$, which do not correspond to the state proposed for realisation.

It results that:

$$|jm> = \sum_{m_{12},m_3} (j_{12}j_3m_{12}m_3\,|jm)\,|j_{12}m_{12}>|j_3m> \tag{15}$$

which, after performing the summation with the above values, becomes

$$|jm> = (j_{12}j_3j_{12}j_3\;jm)\,|j_{12}m_{12}>|j_3m_3> \tag{16}$$

Function $|j_{12}m_{12}>$ is given by (14) and the coefficient, [9], is given by

$$(j_{12}j_3j_{12}j_3|\;j_{12} + j_3j_{12} + j_3) = \sqrt{\frac{j_{12} + m + \frac{1}{2}}{2j_{12} + 1}} = 1$$

With this value ofor the coefficient and taking (14) into account, the relation (16) becomes:

$$|jm> = \frac{1}{\sqrt{2}}\,[\,|j_1j_1>|j_2j_2 - 1>|j_3j_3> - |j_1j_1 - 1>|j_2j_2>|j_3j_3>] \tag{17}$$

Introducing the notations $|j_1j_1> = a_{n1}$, $|j_2j_2> = a_p$, $|j_3j_3> = a_{n2}$, $|j_1j_1 - 1> = b_{n1}$, $|j_3j_3 - 1> = b_{n2}$ and $|j_2j_2 - 1> = b_p$, the relation (17) becomes:

$$|jm> = \frac{1}{\sqrt{2}}\,(a_{n1}b_pa_{n2} - b_{n1}a_pa_{n2}) \tag{18}$$

The expression (18) is the antisymmetric spin function for the case when in the final state interact paired particles n_1p with total spin $j_{12} = 0$ and the third particle has the spin $j_3 = \frac{1}{2}$ and its projection alongside the privileged direction $m_3 = \frac{1}{2}$. With the above introduced notation, this expression takes the form:

$$ {}_{-1/2}\chi_a^{1/2}(n_1p\,;\,n_2) = \frac{1}{\sqrt{2}}\,(a_{n1}b_pa_{n2} - b_{n1}a_pa_{n2}) \tag{19} $$

In the case $m_3 = -\frac{1}{2}$ we have to couple function (14) with the function of the unpaired particle $|j_3m_3> = |j_3j_3-1> = b_{n2}$. Performing the same as before we obtain:

$$ \begin{aligned} {}_{-1/2}\chi_a^{1/2}(n_1p\,;\,n_2) = (j_{12}j_3j_{12}j_3-1\,|j_{12}+j_3j_{12}+j_3-1)\cdot\frac{1}{\sqrt{2}}\,[\,|j_1j_1>|j_2j_2> - \\ - |j_1j_1-1>|j_2j_2>]\cdot|j_3j_3-1> \end{aligned} \tag{20} $$

where [9],

$$ (j_{12}j_3j_{12}j_3-1\,|j_{12}+j_3j_{12}+j_3-1) = \sqrt{\frac{j_{12}-m+\frac{1}{2}}{2j_{12}+1}} = 1 $$

Carrying in (20) the value of the coefficient and taking into account the before introduced notations we obtain:

$$ {}_{-1/2}\chi_a^{1/2}\,(n_1p\,;\,n_2) = \frac{1}{\sqrt{2}}\,(a_{n1}b_pb_{n2} - b_{n1}a_pb_{n2}) \tag{21} $$

If in the final state interact the paired particles n_2p and the unpaired particle is n_1, using the symmetry conditions (8) we get from relations (19) and (21)

$$ {}_{1/2}\chi_a^{1/2}\,(n_2p\,;\,n_1) = \frac{1}{\sqrt{2}}\,(a_{n2}b_pa_{n1} - b_{n2}a_pa_{n1}) \tag{22} $$

and

$$ {}_{-1/2}\chi_a^{1/2}(n_2p\,;\,n_1) = \frac{1}{\sqrt{2}}\,(a_{n2}b_pb_{n1} - b_{n2}a_pb_{n1}) \tag{23} $$

Also, if in the final state interact the paired particles n_1n_2 and the unpaired particle is p, using the same symmetry conditions we obtain from relations (19) and (21)

$$ {}_{1/2}\chi_a^{1/2}\,(n_1n_2\,;\,p) = \frac{1}{\sqrt{2}}\,(a_{n1}b_{n2}a_p - b_{n1}a_{n2}a_p) \tag{24} $$

and

$$_{-1/2}\chi_a^{2/2}\,(n_1n_2\,;\,p) = \frac{1}{\sqrt{2}}\,(a_{n1}b_{n2}b_p - b_{n1}a_{n2}b_p) \tag{25}$$

Relations (19), (21), (22), (23), (24) and (25) represent the spin antisymmetrie spin functions in the three body case for all possible final state combinations. The paired particles have zero total spin and the unpaired $\frac{1}{2}$ spin particle has its projection alongside the z direction $\frac{1}{2}$ or $-\frac{1}{2}$. Using these functions one may write, fro each separated case, the scattering amplitude of nucleons on deuterons.

REFERENCES

1. L. D. BLOHINȚEV, E., I. DOLINSCHI, V. S. POPOV, JETF, *42*, 1636 (1962).
2. I. S. SAPIRO, Nucl. Phys., *38*, 128 (1962).
3. V. V. KOMAROV, A. M. POPOVA, Nucl. Phys., *54*, 278 (1964).
4. A. M. POPOVA, S. MUSCALU, Nucl. Phys. (in Russian), *1*, 776 (1965).
5. A. M. POPOVA, S. MUSCALU, Nucl. Phys. (in Russian), *3*, 813 (1966).
6. S. MUSCALU, Analele Univ. Buc., ser. St. naturii, *17*, 96 (1968).
7. S. MUSCALU, Analele Univ. Buc., ser. Șt. naturii, *21*, 5 (1972).
8. A. S. RAVIDOV, *Quantum Mechanics*, Moscow, 1963.
9. A. M. BALDIN, V. I. GOLDANSCHI, I. L. ROZENTALI, *Kinematics of nuclear reactions*, Moscou, 1959.

Received, November 23, 1979

ANALELE UNIVERSITĂŢII BUCUREŞTI, FIZICĂ XXIX, 1980, PAG. 9–14

COÉFFICIENTS D'IONISATION ET POTENTIELS EXPLOSIFS DANS LES VAPEURS DE L'ALCOOL MÉTHYLIQUE (CH_3-OH)

G. G. BRĂTESCU, MAGDA CAZAN-CORBASCA
Faculté de Physique, Université de Bucarest *

RÉSUMÉ

On a mesuré les potentiels explosifs dans les vapeurs de l'alcool méthylique et tracé les courbes de Paschen $V_e = f(pd)$ pour des éléctrodes de Al et Ni. On a tracé aussi les courbes $\frac{\alpha}{p_0} = f\left(\frac{E}{p_0}\right)$, $\eta = f\left(\frac{E}{p_0}\right)$ et $\gamma = f\left(\frac{E}{p_0}\right)$, en comparant les valeurs trouvées avec celles qui correspondent à d'autres alcools.

Introduction

Cet ouvrage s'inscrit parmis les recherches effectuées sur les propriétés électriques des vapeurs des differents alcools et autres substances organiques [1–11].

On a déterminé expérimentalement les potentiels explosifs – Paschen – dans les vapeurs de l'alcool méthylique, pour des électrodes d'Al et de Ni, et on a tracé les courbes de Paschen correspondantes $V_e = f(p \,.\, d)$, où V_e est le potentiel explosif, p la pression des vapeurs et d la distance entre les électrodes. De même que dans les traveaux antérieurs, concernant les vapeurs d'autres alcools, on a testé le mode dans lequel la nature des électrodes influence la valeur du potentiel explosif minim et du produit $(p \,.\, d)$ correspondant, de même que l'allure de la courbe de Paschen.

On a calculé les coéfficients d'ionization α et γ de Townsend, en employant les relations (1) et (2) :

$$\frac{\alpha}{p_0} = A e^{-\frac{B}{\frac{E}{p_0}}} \tag{1}$$

$$V_e = \frac{1}{\eta} \ln\left(1 + \frac{1}{\gamma}\right) \tag{2}$$

---

* Centre National de Physique, Măgurele–Bucarest B.P. 5211.

où p_0 est la pression réduite à la température de 0°C ; E l'intensité du champ électrique, A et B deux constantes dépendantes de la nature du gas et $\eta = \frac{\alpha}{E}$, [13].

La constante $A = 6{,}77$ cm^{-1} Torr^{-1} provient de l'ouvrage [9] et les valeurs $B = 1248{,}13$ V cm^{-1} Torr^{-1}, pour l'électrode de Al et $B = 1647{,}00$ V cm^{-1} Torr^{-1}, pour l'électrode de Ni ont été calculées à l'aide de l'équation :

$$B = \frac{V_{e\,\min}}{(p_0 d)_{\min}} \tag{3}$$

Le dispositif expérimental employé et le mode dans lequel les déterminations ont été effectuées ont été décrits dans un ouvrage antérieur [2].

Résultats expérimentaux

On a travaillé à des pressions situées dans le domaine de 0,7 –10 Torr et à des distances entre les électrodes comprises entre 1,0 et 2, 5 mm Dans la figure 1 sont tracées les courbes de Paschen.

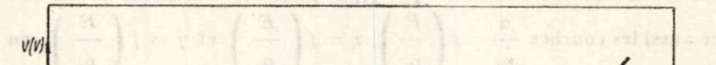

Fig. 1. Les courbes de Paschen pour les vapeurs de l'alcool méthylique avec des électrodes de Al et de Ni.

On a obtenu les valeurs suivantes :

$V_{e\,\min} = 477 \pm 1$ V pour l'électrode de Al

$V_{e\,\min} = 476 \pm 1$ V pour l'électrode de Ni

$(pd)_{\min} = 4{,}1 \pm 0{,}1$ mm Torr pour l'électrode de Al

$(pd)_{\min} = 3{,}1 \pm 0{,}1$ mm Torr pour l'électrode de Ni

Les valeurs différentes pour les produits $(pd)_{\min}$ sont attribuées en partie aux valeurs différentes du travail d'extraction électronique de Al et de Ni (pour Al $\varphi = 4{,}20$ eV et pour Ni $\varphi = 4{,}96$ eV).

Comparativement aux vapeurs d'autres alcools où la courbe de Paschen pour l'électrode de Al est plus arrondie et pour l'électrode de Ni affilée dans la région du minimum [3], dans le cas des vapeurs de l'alcool méthilique, les deux courbes ont une allure ressemblante. De même les valeurs du potentiel explosif minim pour des électrodes de Al et de Ni ne diffèrent pas dans la limite des erreurs expérimentales, à l'encontre des autres vapeurs d'alcool étudiés, où dans le cas de l'électrode de Al ses valeurs sont plus basses que dans le cas de l'électrode de Ni.

Le produit $(pd)_{\min}$ dans le cas de l'électrode de Al est plus élevé que dans le cas de l'électrode de Ni, ce qu'on retrouve aussi aux autres vapeurs d'alcool étudiés (voir le tableau I).

Tableau I

Substance	Electrode : Al		Electrode : Ni	
	$V_{e\,\min}$ (V)	$(pd)_{\min}$(mm Torr)	$V_{e\,\min}$ (V)	$(pd)_{\min}$(mm Torr)
Alcool méthylique CH_3-OH	477,00	4,10	476,00	3,10
Alcool éthylique CH_3CH_2-OH	447,00	4,40	450,00	2,55
Alcool propilique $CH_3(CH_2)_2-OH$	456,50	3,05	471,50	3,15
Alcool butilique $CH_3-(CH_2)_3-OH$	435,00	3,60	496,00	2,75

On peut attribuer ce comportement différent des vapeurs de l'alcool méthylique à sa structure moléculaire différente par rapport aux autres alcools étudiés.

Les figures (2), (3), (4) et (5) représentent les courbes : $\frac{\alpha}{p_0} = f\left(\frac{E}{p_0}\right)$, $\frac{1}{\eta} = f\left(\frac{E}{p_0}\right)$ et $\gamma = f\left(\frac{E}{p_0}\right)$.

On constate que les minimum des courbes $\frac{1}{\eta}$ sont très rapprochés du point de Stoletov des courbes $\frac{\alpha}{p_0}$ correspondantes [12], [13].

Les valeurs des cœfficients γ sont plus élevées que dans le cas des vapeurs d'autres alcools étudiés.

Conclusions

On constate, de même que dans le cas d'autres substances organiques, des valeurs élevées des potentiels explosifs dues à la complexité structurale des molécules, une part de l'énergie des électrons en interaction avec les molécules du gaz, se dissipe dans une série de processus non suivis d'ionisation ; comme, par exemple les excitations, les disociations [3] [4]

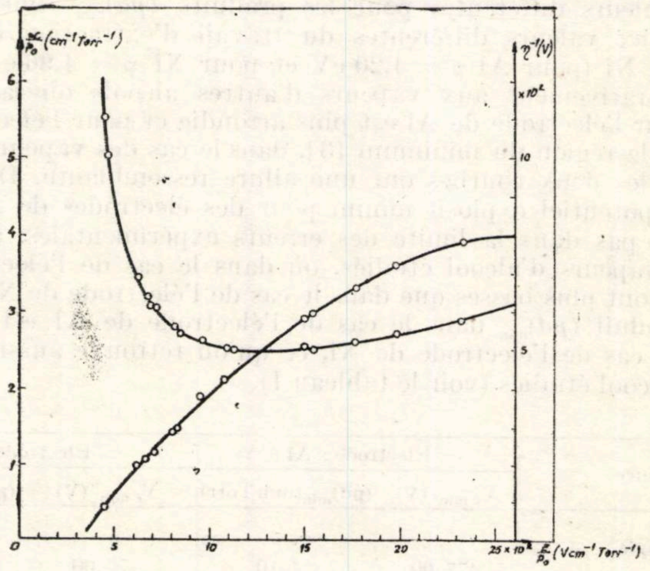

Fig. 2. Les courbes $\frac{\alpha}{p_0} = f\left(\frac{E}{p_0}\right)$ et $\eta^{-1} = f\left(\frac{E}{p_0}\right)$ pour l'électrode de Al.

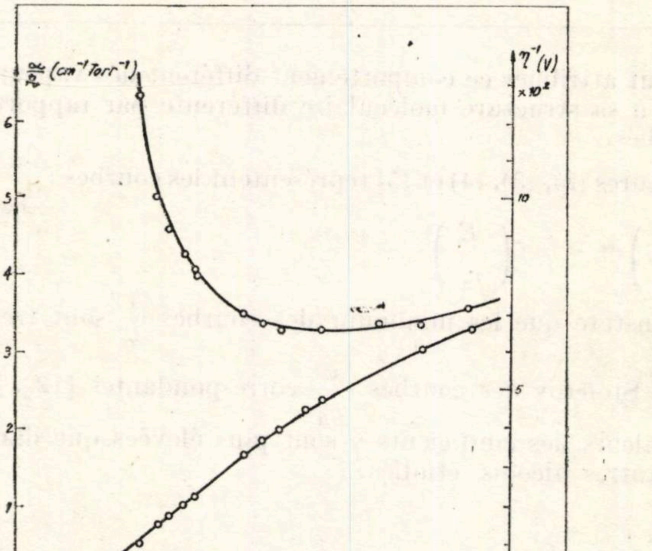

Fig. 3. Les courbes $\frac{\alpha}{p_0} = f\left(\frac{E}{p_0}\right)$ et $\eta^{-1} = f\left(\frac{E}{p_0}\right)$ pour l'électrode de Ni.

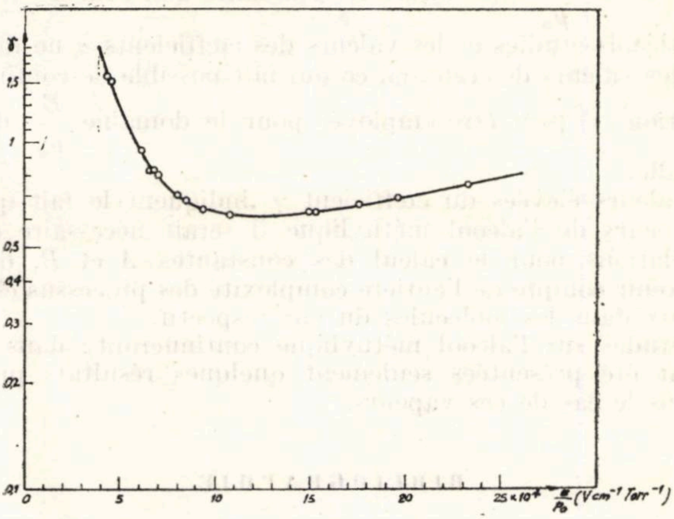

Fig. 4. La courbe $\gamma = f\left(\frac{E}{p_0}\right)$ pour l'électrode de Al.

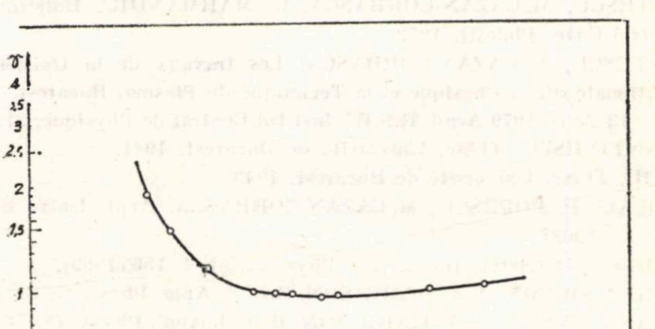

Fig. 5. La courbe $\gamma = f\left(\frac{E}{p_0}\right)$ pour l'électrode de Ni.

Les courbes $\frac{\alpha}{p_0}$ ont l'allure ressemblante aux courbes tracées pour les autres alcools étudiés et les valeurs des cœfficients α ne diffèrent pas beaucoup des valeurs des ceux-ci, ce qui fait possible de confirmer le fait que la relation (1) peut être employée pour le domaine $\frac{E}{p_0}$ dans lequel on a travaillé.

Les valeurs élevées du cœfficient γ ,indiquent le fait que dans le cas des vapeurs de l'alcool méthylique il serait nécessaire d'employer d'autres relations pour le calcul des constantes A et B, dans lequel on devrait tenir compte de l'entière complexité des processus élémentaires qui ont lieux dans les molecules du gas respectif.

Des études sur l'alcool méthylique continueront ; dans le présent ouvrage ont été présentées seulement quelques résultats préliminaires obtenus dans le cas de ces vapeurs.

BIBLIOGRAPHIE

1. A. T. NICOLAU, E. PASCU, M. CAZAN-CORBASCA, P. POPESCU, Studii şi Cercetări de Fizică, *20*, 799 (1978).
2. G. G. BRĂTESCU, M. CAZAN-CORBASCA, Anal. Univ. Bucureşti, Fiz. *27*, 11 (1978).
3. G. G. BRĂTESCU, M. CAZAN-CORBASCA, C. MARMANDIU, Buletinul Institutului Petrol-Gaze, Ploieşti, 1979.
4. G. G. BRĂTESCU, M. CAZAN-CORBASCA, Les travaux de la troisième Conférence Nationale sur la Physique et la Technique du Plasma, Bucarest. 12–13 Avril 1979 Acad. R.S.R., Institut Central de Physique, 31.
5. L. CONSTANTINESCU, Thèse, Université de Bucareşt, 1941.
6. M. VALERIU, Thèse, Université de Bucarest, 1943.
7. A. T. NICOLAU, P. POPESCU, M. CAZAN-CORBASCA, Anal. Univ. Bucureşti, Fiz., *17*, 53 (1968).
8. H. SCHLUMBOHM, Zeistch. fur Angew. Phys. *11*, nr. 4, 156 (1959).
9. M. NARAYANA SWAMY, J. A. HARRISON, Brit. J. Appl. Phys., *17*, 123 (1966).
10. M. NARAYANA SWAMY, J. A. HARRISON, Brit. J. Appl. Phys., *18*, 781 (1967).
11. A. E. D. HEYLEN., Brit. J. Appl. Phys., 179 (1968).
12. E. BĂDĂRĂU, I. POPESCU, *Gaze Ionizante*, Ed. Tehnică, Bucureşti, 1965, pg. 25.
13. G. G. BRĂTESCU, *Fizica Plasmei*, Ed. Didactică şi Pedagogică, Bucureşti, 1970, pg. 403, 410.

ANALELE UNIVERSITĂŢII BUCUREŞTI, FIZICĂ XXIX, 1980, PAG. 15–20

THE COHERENCE OF SIDEBANDS OF ELECTRICALLY INTENSITY MODULATED LIGHT

G. G. BRĂTESCU, T. TUDOR
Faculty of Physics, University of Bucharest *

G. NEMEŞ, M. RISTICI
Institute for Physics and Technology for Radiation Devices **

ABSTRACT

The coeherence of various spectral components induced by electrically modulating the intensity of a laser beam by means of a Pockels cell K.D.P. modulator, is analysed by the rotating disk method. Several records of moving fringes resulted from the interference of different modulation sidebands are presented.

Introduction

It is well known that two waves of different frequencies which are coherent one with the other give rise by superposition to moving interference fringes. Thus the interferometrical method may be extended in the analysis of the coherence of disturbances of different frequency too : The occurence of a moving fringes pattern, in a Young's interference arrangement for instance, indicates that the disturbances at the two slits are coherent different frequency disturbances.

Moreover, the visibility of this fringes, measured in a referential which moves together with them, is related to the coehrence degree of the two disturbances. Fischer [1] has introduced the generalized degree of coherence as a measure for the coherence of two disturbances of different frequencies in the laboratory reference frame :

$$\gamma_{12L}(\sigma, \tau) = \frac{< V_1\left(t+\frac{\tau}{2}\right) \cdot V_2^*\left(t-\frac{\tau}{2}\right) \cdot \mathrm{e}^{2\pi i\sigma t} >}{< |V_1(t)|^2 > \cdot < |V_2(t)|^2 >} \qquad (1)$$

---

[*] National Center of Physics, P.O. Box, 5211, Măgurele, Bucharest.
[**] National Center of Physics, P.O. Box, 5206, Măgurele, Bucharest.

In a previous paper [2] we have established that the value of the generalized degree of coherence of two disturbances of different frequencies in the laboratory system, L, is equal to the value of Wolf's degree of coherence [3] of the same disturbances in a reference frame in which this disturbances have the same frequency, i.e. in a frame M, which moves together with their interference pattern :

$$v = i \cdot \Delta\nu_L \qquad (2)$$

where $\Delta\nu_L$ is the frequency difference of the disturbances in the laboratory frame, and i is the fringe spacing of their interference pattern. Particularly,

$$|\gamma_{12L}(\sigma, \tau)| = |\gamma_{12M}(\tau)| = \mathcal{V}_M(\tau) \qquad (3)$$

where we have supposed that the two disturbances, have the same intensity. This relation is the ground for extending the interferometrical method in the analysis of the coherence of different frequencies.

Fields of coherent different frequencies are often encountered in optics : In any kind of optical modulation [4] side bands result [5] which are coherent one with the other and with the central frequency. Particularly in a supressed carrier single-sideband modulation [6], [7], the sideband is coherent with the initial line.

The mode – locking of the lasers [8] consist in imposing to the modes of the laser to oscillate in a fixed phase relationship. That is, the modes of a mode-locked laser are disturbances of different frequencies coherent with one another.

Any Doppler-shifted disturbance is coherent with the initial one. For instance the signal and the local oscillator beams in a laser Doppler velocimeter [9] are different frequency coherent beams.

In the following we shall apply the interferometrical method to test the different frequency coherence of the side-bands which result by an electrical modulation of the intensity of a laser beam.

Experimental arrangement. Results

The polarized light of a L.G. – 10 He. – Ne. laser was modulated by means of a longitudinal K.D.P. electro-optic modulator K (fig. 1) followed by a polarizer, P. The modulator consists of a z cut plate 10 mm × 10 mm × 8 mm, from an optical quality region of a K.D.P. single crystal. $K.H_2PO_4$ belongs to the tetragonal group 42 m at room temperature. It is uniaxial with the optic axis along the tetragonal axis. If the light travels along this axis, no phase difference is introduced

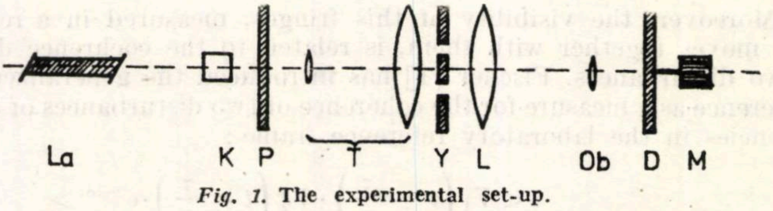

Fig. 1. The experimental set-up.

between two ortogonal polarized components of the light. But if an electric field is applied along this axis, the crystal symmetry becomes orthorombic and the optical symmetry becomes biaxial. The crystal introduces between the components of the light polarized along the electrically induced principal axes a phase difference :

$$\Gamma = \frac{2\pi}{\lambda_0} n_0^3 r_{63} V \tag{4}$$

where : r_{63} is the electro-optic coefficient for the electric field applied along the crystallographic z axis, n_0 is the unperturbed crystalline index of refraction and V is the voltage across the crystal in the direction of light propagation [4]. The voltage is applied by means of transparent electrodes coated on the end faces of the crystal. In this particular cut of crystal, the retardation along the normal is a function of the voltage rather than the field strength. The voltage required to make $\Gamma = \pi$, i.e. the half-wave voltage is $V_{\lambda/2} = 11$ kV at a wavelength of 0,63 μm.

The crystal is mounted with the electrically induced principal axes at 45° to the direction of polarization of the incident laser light and the polarizer P is set orthogonal to the laser polarization. Then the intensity of the transmitted light as a function of the retardation introduced by the crystal is :

$$I = I_0 \sin^2 \frac{\Gamma}{2} \tag{5}$$

where I_0 is the intensity of the incident light. If the crystal has a d.c. voltage impressed on it, as well as a harmonically – varying one,

$$V = V_0 + V_m \sin 2\pi\nu_M t \tag{6}$$

with :

$$\Gamma = \frac{2\pi}{\lambda_0} n_0^3 r_{63} \cdot V_0$$

$$\Gamma_m = \frac{2\pi}{\lambda_0} n_0^3 r_{63} \cdot V_m$$

and, from (5) it is shown that an intensity modulation of the incident beam is obtained, with the modulation frequency ν_M.

The spectrum of the light modulated in such a way is composed from a central line, with the frequency equal to that of the incident light, ν_0 and upper and lower sidebands at the frequencies $\nu_0 + n\nu_m$, [5]. The intensities of the various modulation sidebands as well as that of the central frequency are function of the bias voltage V_0 and of the modulating peak voltage V_m. In our experiment, V_0 and V_m were about 4 KV and 2 KV respectively.

BUDAPESTI MŰSZAKI EGYETEM KÖZPONTI KÖNYVTÁRA 1848

To test the coherence of different frequencies components of modulated light, a revolving disk on which photographic film is applied was mounted in a Young arrangement (fig. 1) : The modulated light expanded by a telescope, T, falls upon a double slit Y. In the focal plane of the lens, T, the diffraction patterns at the two slits are coincident and therefore the interference fringes have the greatest visibility, determined only by the coherence of disturbances at the two slits. But the interference pattern has the least spatial extent, it is concentrated around a focal line. For expanding the interference fringes to convenable dimensions, a microscope objective, Ob., is used, which projects a region from the neighbourhood of the focus of the lens L, on the a region disk D, on which the film is applied.

On the film are projected not only the fixed interference fringes, which arise from the interference of the pairs of disturbances of the same frequency from the two points, but also several systems of moving interference fringes :

An interference pattern which arises from the interference of the disturbances of frequencies $\nu_0 + n\nu_m$ from Y_1 with the disturbances of frequencies $\nu_0 + (n+1)\,\nu_m$ from Y_2. Using the relation (2), it follows that this pattern moves in the plane of the disk in a direction normal to the slits, with a speed :

$$v_{+1} = i\,\nu_m$$

A fringes pattern which corresponds to the interference of the components $\nu_0 + n\nu_m$ from Y_1 with the components $\nu_0 + (n-1)\,\nu_m$ from Y_2 respectively. This pattern move with the speed :

$$v_{-1} = -i\nu_m$$

A moving fringes pattern corresponding to the interference among the $\nu_0 + n\nu_m$ spectral components of the modulated light from Y_1 and the $\nu_0 + (n+2)\,\nu_m$ components from Y_2 and whose speed in the laboratory system is :

$$v_{+2} = i\cdot 2\,\nu_m$$

And so on.

For each interference pattern moving in the sense of rotation of the disk, there exists a circumference on the disk for which the linear speed of its points is equal to the speed of the pattern, as long as each point of the disk crosses a little central region of the arrangement. But the film is impressed only during each of its points travells such a little region, namely that of the central maximum of diffraction at the slits Y ; that is the region in which the interference fringes have an appreciable intensity. Thus for each moving interference pattern the fringes are recorded radially along a circle of radius determined by the condition $v_{\text{fringes}} = v_{\text{disk}}$.

$$in\nu_m = 2\pi r\cdot\nu_D$$

$$r_n = n\frac{i}{2\pi}\frac{\nu_m}{\nu_D} \tag{7}$$

On both sides of such a circle, the frigens speed differs from the speed of the disk and as each zone of the disk passes by the fringes, a certain shift of the fringes from their initial recording position on the disk takes place. The fringes are recorded outside the circles r_n too, as long as this shift is much smaller than the fringe spacing.

In order to avoid the blurring of the fringe pattern at the succesive passages of each point of the film in the fringes region during the exposure time, the modulating frequency ν_m must be an integer multiple of the disk frequency

$$\nu_m = N_0 \nu_D \tag{8}$$

We have achieved this synchronism condition by means of a synchro-loop between the motor, M, which rotates the disk, and the generator of modulating voltage ; in ours experiments $N_0 = 25$.

If this condition is fulfilled, the mean radius of the nth. ring may be written :

$$r_n = \frac{i}{2\pi} n N_0 = \frac{N_i}{2\pi} \tag{9}$$

One observes that $N = nN_0$ is then the number of fringes of the ring. In fig. 2 we present several such recordings of moving interference fringes which results from the interference of different modulation side-bands : By slighty varying the distance of the objective Ob from the focal plane of the lens L, the length of the fringes can be varied to contain either the first fringes ring only or all the other as well.

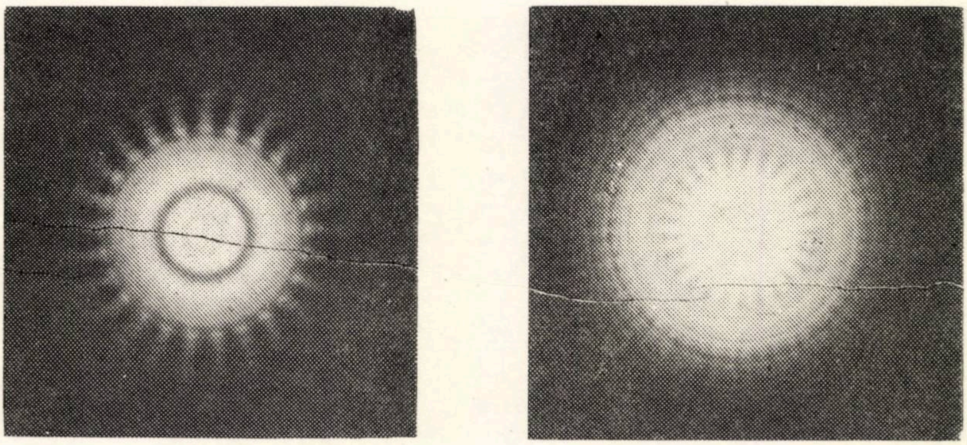

(a) *(b)*

Fig. 2. The fringes rings corresponding to several moving interference patterns :
a) $\Delta\nu_L = \nu_m$; $N = 25$,
b) $\Delta\nu_L = \nu_m, 2\nu_m, 3\nu_m$; $N = 25, 50, 75$.

Thus, in fig. 2 a, is recorded only the first ring, corresponding to the pairs of disturbances from the two slits whose frequencies differ, for all, by ν_m. In fig. 2 b are recorded the first three frings rings, resulting from the interference between all pairs of disturbances whose frequencies differ by ν_m, $2\nu_m$, $3\nu_m$, respectively.

REFERENCES

1. F. FISCHER, Zeit Physik., *199*, 541 (1967).
2. G. G. BRĂTESCU, T. TUDOR, Ann. Univ. Buc., *XX*, 29 (1971).
3. M. BORN, W. WOLF, *Principles of Optics*, Pergamon Press, Oxford, 1975.
4. F. S. CHEN, Proc. I.E.E.E., *58*, 1440 (1970).
5. J. HOPSON, I.E.E.E. Trans. Commun. Syst., *C.S. 11*, 464 (1963).
6. L. E. DRAIN, B. C. MOSS, Opto-Electr., *4*, 429 (1972).
7. A. DUMITRICĂ, T. TUDOR, Ann. Univ. Buc., *XXIX*, 31, (1980).
8. B. COUILLAND, A. DUCASSE, Revue Phys. Appl., *14*, 331 (1979).
9. B. M. WATRASIEWICZ, M. J. RUDD, *Laser Doppler Measurements*, Butterworths, London (1976).

Received, October 25, 1979

ANALELE UNIVERSITĂȚII BUCUREȘTI, FIZICĂ XXIX, 1980, PAG. 21-29

THE INFLUENCE OF THE HYPERFINE STRUCTURE ON THE PROFILE FINENESS OF RADIATIONS EMITTED BY MERCURY AND THE INTENSITY ANOMALY OF THE HYPERFINE COMPONENTS OF THE GREEN RADIATION

G. G. BRĂTESCU
Faculty of Physics, University of Bucharest *

F. GRUZSNICZKI
National Institute of Metrology Bucharest

ABSTRACT

Under certain conditions of excitation of the radiation produced into the mercury vapours lamps, the intensity distribution of the hyperfine components given by each isotope, is not proportional any more with its amount. This disproportionality is present too into the low pressure discharge lamps at minimum currents.

The hyperfine shape of the optical excitation of the $^3P_{0,1,2}$ triplet hyperfine levels has been studied.

Introduction

The Hg vapour lamp achieved by us made possible the study of the hyperfine structure of some mercury spectral lines emitted by these lamps, in comparison with the radiations emitted by a Hg vapour lamp at low pressure. The mercury radiations are-known to be very rich in hyperfine structures, the intensity and width of their components being enough to be attained by means of spectral aparata and interferometers of a high resolution power. We analysed three lines, 404,6 nm ; 435, 8 nm and 546,1 nm.

As it is known, the mercury contains seven stable isotopes with the abundence shown in table 1.

---

* National Center of Physics, P.O. Box 5211, Măgurele, Bucharest.

Table 1

Mass (A):	196	198	199	200	201	202	204
Abundence (%):	0,15	10,1	17,0	23,3	13,2	29,6	6,7
Nuclear spin (I):	0	0	1/2	0	3/2	0	0

Making use of the rules mentioned in [1], we caculated the number of level splittings and the hyperfine structure components for a few Hg radiations. The results are mentioned in table 2.

The isotopic abundence reveals that the abundence of all the even isotopes with spin $I = 0$, except for the Hg^{196} isotope, is high enough, four unsplit lines intense enough are resulting.

Table 2 points out the theoretical number of the hyperfine components of the three radiations dealt with. Thus, as a result of the splittng, the 404,6 line will supply 5 hyperfine components, beside the four isotopic shifting, while the 435,8 nm and 546,1 nm lines will supply 11 hyperfine components.

Experimental results

It was built a lamp of medium pressure in order to analyse the possibilities of using it as a standard spectral source.

The scheme of this lamp is shown in fig. 1. The lamp is a quartz tube (1) which contains two main electrodes (2) and (3) and an auxiliary electrode (4). The lamp contains some mercury drops which evaporate, while the lamp works, and thus a pressure of approximately 4 atm is created inside. In order to start the initial discharge, the lamp also contains a certain amount of argon at a pressure of 40 mm Hg. When the voltage is connected, a priming electric arc appears between the electrodes (2) and (4) which causes the evaporation of a part of the mercury, helping thus the start of the electric discharge between the electrodes (2) and (3). Onviously, after the start of the discharge, the priming arc disappears because of the fall of the disharge electric resistance under the value of he resistance R_p. In order to protect the lamp a limiting resistance R_l is introduced in the circuit.

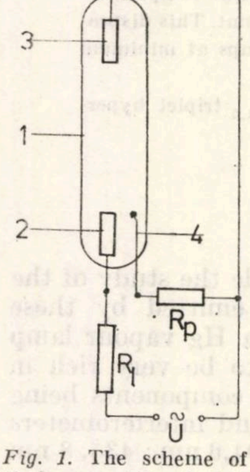

Fig. 1. The scheme of the lamp and the electric circuit

We registered the profile of the 404,6 nm; 435,8 nm and 546,1 nm lines emitted by the low pressure Hg lamp by means o the Fabry-Perot interferometer. The profiles are given in fig. 2, 3 and 4.

A thorough image of level splitting and isotopishifting for the green radiation (546,1 nm) is given in fig. 5, which also mentions, both distance between the respective components in mK and the procentual contribution of the intensity of every component.

Table 2

Level splitting and the hyperfine structure components of some radiations emitted by Hg

Wavelength (nm)	Transition	A	I	Number of levels and the F values after level splitting				
				Lower level		Upper level		Number of components
				No.	(F)	No.	(F)	
404, 656	$6\ {}^3P_0 - 7\ {}^3S_1$	199	1/2	1	(1/2)	2	(3/2 ; 1/2)	2
		201	3/2	1	(3/2)	3	(5/2 ; 3/2 ; 1/2)	3
407, 783	$6\ {}^3P_1 - 7\ {}^1S_0$	199	1/2	2	(3/2 ; 1/2)	1	(1/2)	2
		201	3/2	3	(5/2 ; 3/2 ; 1/2)	1	(3/2)	3
410, 805	$6\ {}^1P_1 - 9\ {}^1S_0$	199	1/2	2	(3/2 ; 1/2)	1	(1/2)	2
		201	3/2	3	(5/2 ; 3/2 ; 1/2)	1	(3/2)	3
433, 922	$6\ {}^1P_1 - 7\ {}^3D_2$	199	1/2	2	(3/2 ; 1/2)	2	(5/2 ; 3/2)	3
		201	3/2	3	(5/2 ; 3/2 ; 1/2)	4	(7/2 ; 5/2 ; 3/2 ; 1/2)	8
434,363	$6\ {}^1P_1^0 - 7\ {}^3D_1$	199	1/2	2	(3/2 ; 1/2)	2	(3/2 ; 1/2)	4
		201	3/2	3	(5/2 ; 3/2 ; 1/2)	3	(5/2 ; 3/2 ; 1/2)	7
434, 750	$6\ {}^1P_1^0 - 7\ {}^1D_2$	199	1/2	2	(3/2 ; 1/2)	3	(5/2 ; 3/2)	3
		201	3/2	3	(5/2 ; 3/2 ; 1/2)	4	(7/2 ; 5/2 ; 3/2 ; 1/2)	8
435, 833	$6\ {}^3P_1^0 - 7\ {}^3S_1$	199	1/2	2	(3/2 ; 1/2)	2	(3/2 ; 1/2)	4
		201	3/2	3	(5/2 ; 3/2 ; 1/2)	3	(5/2 ; 3/2 ; 1/2)	7
491, 607	$6\ {}^1P_1^0 - 8\ {}^1S_0$	199	1/2	2	(3/2 ; 1/2)	1	(1/2)	2
		201	3/2	3	(5/2 ; 3/2 ; 1/2)	1	(3/2)	3
504, 564	$6\ {}^1P_1^0 - 8\ {}^3S_1$	199	1/2	2	(3/2 ; 1/2)	2	(3/2 ; 1/2)	4
		201	3/2	3	(5/2 ; 3/2 ; 1/2)	3	(5/2 ; 3/2 ; 1/2)	7
546, 073	$6\ {}^3P_2^0 - 7\ {}^3S_1$	199	1/2	2	(5/2 ; 3/2)	2	(3/2 ; 1/2)	3
		201	3/2	4	(7/2 ; 5/2 ; 3/2 ; 1/2)	3	(5/2 ; 3/2 ; 1/2)	8

The three radiation profiles (fig. 2, 3 and 4) show that on the case of the 404,6 nm line, out of the five structural components, four are solved° For the 435,8 nm line, the number of the solved structure is smaller.

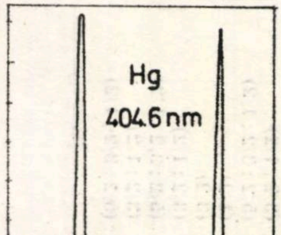

Fig. 2. The profile of the 404,6 nm line of Hg with hyperfine structure

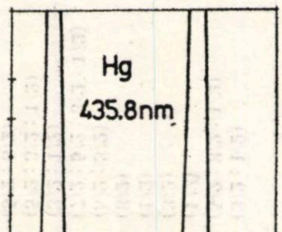

Fig. 3. The profils of the 435,8 nm line of Hg with hyperfine structure

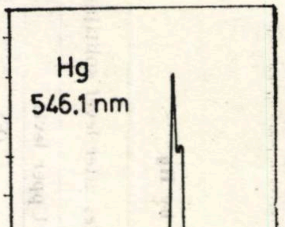

Fig. 4. The profile of the 546,1 nm line of Hg with hyperfine structure

Out of the 11 components only 5 were solved while for the 546,1 nm line, only 8 out of 11. The distances between the outermost components of these lines are given in table 3.

Table 3

Wavelength (nm)	Distance (mK)
404 ,6	1 440
435 ,8	1 480
546 ,1	1 380

Conveniently solving the 546,1 nm line structure, we could minutely study the width and intensity of the hyperfine components.

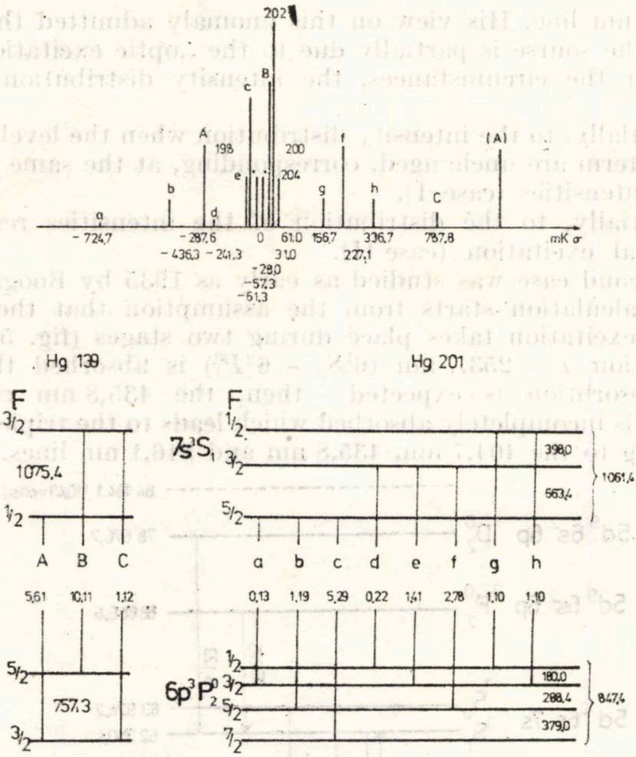
202
B
c
A
198
200
f
(A)
e
204
b
g
h
C
a
d
- 724,7
- 287,6
0
61,0
156,7
336,7
787,8
mK σ
- 436,3
- 241,3
31,0
227,1
- 28,0
- 57,3
- 61,3
Hg 139
Hg 201
F
F
3/2
1075,4
1/2
A
B
C
5,61
10,11
1,12
5/2
757,3
3/2
1/2
7s 3S1
3/2
398,0
1061,4
563,4
5/2
a
b
c
d
e
f
g
h
0,13
1,19
5,29
0,22
1,41
2,78
1,10
1,10
1/2
6p 3P0 2
3/2
180,0
5/2
288,4
847,4
379,0
7/2

Fig. 5. The scheme of level splitting and isotope shifting of the green radiation

Discussions

During these measurements, some anomalies appeared regarding the intensity relations of some components. Such alterations in the intensity of the hyperfine components were noticed for the first time by Schuler and Keyston [2] and then, by others, too [3], [4].

Bradley [5] noticed an abnormal alteration, with the 546,1 nm line, consisting in a general increase of the intensity of the hyperfine components of the odd isotopes in comparison with the even isotope components. This takes place in a hollow cathode lamp when the current intensity increases from 200 to 500 mA.

Considering the abundence of the mercury isotopes and the green radiation structure, one can notice that the intensities of the hyperfine components of the odd isotopes are, at least, with one order inferior to the intensities of the central components belonging to the even isotopes. For this reason, the increasing intensities of the odd components, as against the even ones, can be due to selfabsorption which is not abnormal. But selfabsorbtion may be excluded and the values of the intensity ratios among the various hyperfine components differ from their theoretical values, then anomaly is doubtlessly present. H. Chantrel [6] noticed this phenomenon out only with the green radiation, but also in the case of the 435,8 nm line. His view on this anomaly admitted that the light emitted by the sourse is partially due to the „optic excitation" at some levels. Under the circumstances, the intensity distribution would correspond,

— partially, to the intensity distribution when the level populations of the same term are unchanged, corresponding, at the same time, to the theoretical intensities (case I),

— partially, to the distribution of the intensities resulting of a purely optical excitation (case II).

The second case was studied as early as 1935 by Boogs and Webb [7]. Their calculation starts from the assumption that the absorption of the light-excitation takes place during two stages (fig. 5). The resonance radiation $\lambda = 253{,}7$ nm $(6^1S_0 - 6^3P_1^0)$ is absorbed the first — a thorough absorbtion is expected — then, the 435,8 nm radiation on the $3S_1$ level is incompletely absorbed which leads to the triple ${}^3S_1 - {}^3P^0_{0.1.2}$ corresponding to the 404,7 nm, 435,8 nm and 546,1 nm lines.

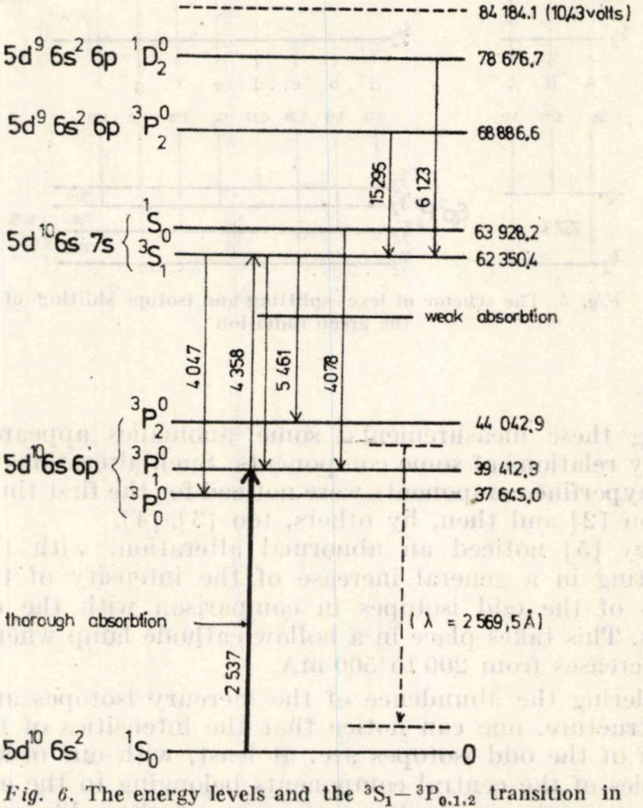
84 184.1 (10,43 volts)
5d⁹ 6s² 6p ¹D⁰₂
78 676,7
5d⁹ 6s² 6p ³P⁰₂
68 886,6
15295
6 123
5d¹⁰6s 7s
¹S₀
³S₁
63 928,2
62 350,4
weak absorbtion
4 047
4 358
5 461
4078
5d¹⁰6s 6p
³P⁰₂
³P⁰₁
³P⁰₀
44 042,9
39 412,3
37 645,0
thorough absorbtion
(λ = 2 569,5 Å)
2 537
5d¹⁰ 6s² ¹S₀
0

Fig. 6. The energy levels and the ${}^3S_1 - {}^3P_{0,1,2}$ transition in the case of the optical excitation of Hg. Weak absorbtion; thorough absorbtion.

According to Boggs and Webb's calculations for the optical excitation, table 4 points out the contribution of each Hg isotope to the total intensity of a radiation in the above mentioned triplet.

Table 4

Isotope	196	198	199	200	201	202	204
Percentual contribution in intensity	10^{-5}	5,7	6,1	33,06	2,3	50,1	2,74

For the odd isotopes, the contribution value mentioned in the table consists in the intensity sum of all the hyperfine components. This table shows that the contribution of the 202 isotope alone represents 50,1 % of the total intensity of the radiation, while the contribution of all the hyperfine components of the 201 isotope, for exemple, is not more than 2,3 % although its abundence is 13,22 %.

In the case of the optical excitation, therefore, the contribution of each Hg isotope to the whole radiation intensity is not thoroughly proportional with its abundence.

The intensity distribution of the hyperfine components of the 199 and 201 isotopes (case II) is completely modified as against the distribution corresponding to the excitation in case I, when all the hyperfine levels of a term are supposed to be equally populated. Table 5 provides the intensity values of the hyperfine structure components in the two possible excitation cases published by Boggs and Webb [7].

Table 5

Isotope	Upper level	Central component	Theoretical intensities	
			Excitation case I	Excitation case II
201	5/2	a	0,13	0,03
		b	1,19	0,29
		c	5,29	1,27
	3/2	d	0,22	0,024
		e	1,41	0,16
		f	2,78	0,30
	1/2	g	1,10	0,11
		h	1,10	0,11
199	1/2	A	5,60	0,98
	3/2	B	10,11	4,60
		C	1,12	0,51
196, 198 200, 202, 204		central components	70,00	91,62

Bradley underlines [8] that, when the optical excitation prevails, the 407,7 nm, 435,8 nm and 546,1 nm radiations resulting from the $3S_1-3P_{0\,1\,2}$ transitions do not correspond to the isotopic abundence measurement.

Thus, the optical excitation at work, the intensities of the hyperfine components are weakened, while the central components are intensified. With the 201 isotope, for example, the a, b, c components obtained at the $F = \frac{5}{2}$ level are nearly 4 times weakened, while the d, e, f, g, h, components obtained at the $F = \frac{3}{2}$ and $F = \frac{1}{2}$ levels are approximately 10 times weakened. Similarly, the B and C components of the 199 isotope at the $F = \frac{3}{2}$ level are 2,2 times weakened, while the A components at the $F = \frac{1}{2}$ level is 5 times weakened.

Considering four hyperfine components A, C a and b for example, the I_A/I_C, I_C/I_b proportions are noticed to vary considerably when the I case excitation is replaced by the one in case II, for a constant I_b/I_a relation, table 6.

Table 6

Relation	Case I.	Case II.
$\frac{I_A}{I_C}$	$\frac{5,60}{1,13}=5$	$\frac{0,98}{0,51}=1,9$
$\frac{I_C}{I_b}$	$\frac{1,12}{1,19}=0,94$	$\frac{0,51}{0,29}=1,75$
$\frac{I_b}{I_a}$	$\frac{1,19}{0,13}=9,15$	$\frac{0,29}{0,03}=9,66$

The above mentioned literature does not show that this anomaly would also be possible with the discharge lamps. Our study of the Hg green radiation effected in discharge lamps at low pressure and medium pressure points out the appearance of this anomaly in the case, too.

The Fabry-Perot interferometre registered the profile under three conditions: at the low pressure lamp ($i = 0,3$ A) and at our medium pressure lamp for two different current intensities ($i = 0,48$ A and $i = 0,51$ A) which revealed modifications in the hyperfine constituent proportions depending on the excitation conditions.

Abnormal aspects intensify if the low pressure lamps and the our lamp work at a 0,48 A current. Thus, the C component is stronger than the b component, with both lamps, although the contrary, should happen since the intensity contribution of these components is $I_c = 1,12\%$ and $I_b = 1,19\%$ (fig. 5).

The results of our measurements are reflected in table 7 including both the I_A/I_C, I_C/I_b, I_b/I_a relations measured at the three lamps and three theoretical values for the two types of excitation.

In the case of the medium-pressure Hg lamp, the relations measured for a 0,51 A discharge current are in accordance with Boggs and Webb's

Table 7

Relation	Theoretical values		Measured relations		
	Case I	Case II	Lamp INM 0,51 A	Lamp INM 0,48 A	Low pressure lamp
I_A/I_C	5	1 ,9	62/13=4 ,8	53/25=2 ,3	73/50=1 ,5
I_C/I_b	0 ,94	1 ,75	13/14=0 ,93	25/19=1 ,3	50/33=1 ,5
I_b/I_a	9 ,15	9 ,66	12/1 ,5=8	19/2 ,7=7	33/6=8 ,7

calculations. For more intense currents, the phenomenon cannot be studied, as the radiations effected by the our lamps broaden sp much that self-absorbtion appears and the profile alters.

Conclusions

The anomalies we noticed, therefore, that is the intensification of the hyperfine components obtained for higher values of F, under the discharge conditions of the low-and medium pressure Hg lamps for the optimum functioning intensity should be linked with the fact that the radiation emitted is partially due to optical excitation.

REFERENCES

1. M. A. ELIASEVICI, *Spectrscopia atomică și moleculară*, Ed. Acad. București (1966).
2. H. SCHULER, J. E. KEYSTON, Z. Phys., 71, 413 (1931).
3. S. MROKOVSKI, Phys. Rev., *67*, 161 (1945).
4. R. H. GARSTANG, J.O.S.A., *52* (8), 845 (1962).
5. D. J. BRADLEY, „Nature", 4832 (6), 967 (1962).
6. H. CHANTREL, „Thèse", Paris (1958).
7. E. E. BOGGS, H. W. WEBB, Phys. Rev., *48*, 226 (1935).
8. D. J. BRADLEY, Proc. Roy. Soc. A., vol. *262*, 529 (1961).

Received, October 25, 1979.

ANALELE UNIVERSITĂŢII BUCUREŞTI, FIZICĂ XXIX, 1980, PAG. 31–35

OPTICAL FREQUENCY TRANSLATOR USING TWO K.D.P. CRYSTALS IN TANDEM

T. TUDOR

Faculty of Physics, University of Bucharest *

A. DUMITRICĂ, D. APOSTOL

Institute for Physics and Technology for Radiation Devices **

ABSTRACT

An optical single sideband modulator has been constructed, which uses two K.D.P. crystals in tandem. The matrix treatment of this modulator and some experimental results are presented.

Theoretical considerations

The single – sideband suppressed carrier modulator which we have constructed and whose characteristics presents here is a tandem type modulator [1], [2] with longitudinal electro-optic effect in K.D.P. crystals [3]. The incident light is passed through a left-hand circular polarizer consisting of a linear polarizer P_1 and a quarter-wave plate, Q_1 (fig. 1) The circular polarized light so obtained, is passed through a system of two K.D.P. crystals, M_1, M_2, having the b axes [2] oriented 45 degrees apart. The modulating voltages applied to these crystals are in phase quadrature. Finally, the light passes through an other quarter-wave plate Q_2, and a linear polarizer P_2 which form a right-hand circular analyzer.

---

* National Center of Physics, P.O. Box 5211, Măgurele, Bucharest

** National Center of Physics, P.O. Box 5206, Măgurele, Bucharest

Knowing the matrixes of each element [4] the over-all matrix of the series of retarders $Q_1 - M_1 - M_2 - Q_2$ may be written, up to an unessential factor, as :

$$\begin{bmatrix} 1 & -i \\ -i & 1 \end{bmatrix} \begin{bmatrix} e^{i\Phi_2} & 0 \\ 0 & e^{-i\Phi_2} \end{bmatrix} \begin{bmatrix} \cos\Phi_1 & i\cdot\sin\Phi_1 \\ i\cdot\sin\Phi_1 & \cos\Phi_1 \end{bmatrix} \begin{bmatrix} 1 & i \\ i & 1 \end{bmatrix} = \tag{1}$$

$$= \begin{bmatrix} \cos\Phi_1\cdot\cos\Phi_2 - i\cdot\sin\Phi_1\cdot\sin\Phi_2 & i\cdot\sin\Phi_1\cdot\cos\Phi_2 - \cos\Phi_1\cdot\sin\Phi_2 \\ \cos\Phi_1\cdot\sin\Phi_2 + i\cdot\sin\Phi_1\cdot\cos\Phi_2 & i\cdot\sin\Phi_1\cdot\sin\Phi_2 + \cos\Phi_1\cdot\cos\Phi_2 \end{bmatrix}$$

The phase angle retardations Φ_1 and Φ_2 produced by the two crystals are proportional with the voltages accros the crystals [5]

$$\Phi = \frac{\pi}{\lambda_0} r_{63} n_0^3 V \tag{2}$$

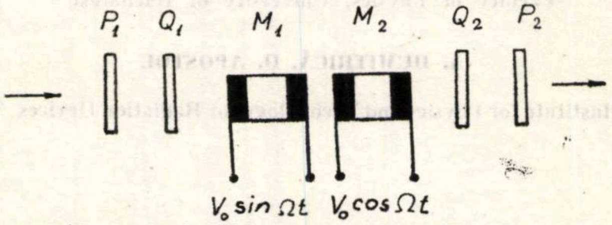

Fig. 1. Optical frequency ranslator. Notations

and, for the above mentioned phase quadrature of the modulating voltages, may be written :

$$\Phi_1 = \Gamma \sin \Omega t \tag{3}$$

$$\Gamma_2 = \Gamma \sin\left(\Omega t + \frac{\pi}{2}\right) \tag{4}$$

with :

$$\Gamma = \frac{\pi}{\lambda_0} r_{63} n_0^3 V_0 \tag{4}$$

where : λ_0 is the free-space wavelength of the incident light wave, r_{63} — the electro-optic coefficient for the electric field applied along the crystallographic c axis [2], n_0 — the unperturbed crystalline index of refraction and V_0 — the peak modulation voltage. Both crystals are modulated with the same modulation index, Γ, (4).

The effect of the retarders block $Q_1 - M_1 - M_2 - Q_2$ upon the x-linear polarized light incoming from P_1, is computed, in what it has essential, by applying the matrix of this block (1), on the standard normalized Jones vector [6] of the incoming light : $E_0 = \begin{bmatrix} 1 \\ 0 \end{bmatrix}$. The result is :

$$\begin{bmatrix} E_x \\ E_y \end{bmatrix} = e^{i\omega t} \begin{bmatrix} \cos\Phi_2\cdot\cos\Phi_1 - i\cdot\sin\Phi_2\cdot\sin\Phi_1 \\ \sin\Phi_2\cdot\cos\Phi_1 + i\cdot\cos\Phi_2\cdot\sin\Phi_1 \end{bmatrix} \tag{5}$$

The outcome of the whole tandem-modulator is, because of the polarizer P_2 (see fig. 1), only the y component of this vector, that is :

$$E_y = e^{i\omega t} (\sin \Phi_2 \cdot \cos \Phi_1 + i \cdot \cos \Phi_2 \cdot \sin \Phi_1) \tag{6}$$

With (3) it readily follows that this outcoming light vector may be put in the form :

$$\begin{aligned} E_y = e^{i\omega t} &\left\{ \frac{1+i}{2} \sin \left[\sqrt{2}\, \Gamma \cdot \sin \left(\Omega t + \frac{\pi}{4} \right) \right] - \right. \\ &\left. - \frac{1-i}{2} \sin \left[\sqrt{2}\, \Gamma \cdot \sin \left(\Omega t - \frac{\pi}{4} \right) \right] \right\} = \\ = \sum_{n=1}^{\infty} &J_{2n-1} (\sqrt{2}\, \Gamma) \cdot \sin \left[\left(2n - 1 \right) \frac{\pi}{4} \right] \cdot e^{i[\omega + (-1)^{n-1} \cdot (2n-1)\Omega] \cdot t} \end{aligned} \tag{7}$$

That is, the carrier and the even sidebands are suppressed. Also, some odd sidebands are missing. Choosing a suitable value for the argument of Bessel functions, i.e. for Γ, the other undesired sidebands can be well suppressed, so obtaining the great majority of the outcoming light power in the first upper sideband.

The construction of the modulator. Experimental results

The modular was constructed using two K.D.P. crystals, each opperating in longitudinal electro-optic effect. KH_2PO_4 belongs to the tetragonal group $\bar{4}2$ m, which lacks a center of inversion and exhibits a linear electro-optic effect. In the paraelectric phase, it is opticaly uniaxial, with the optic axis (c) along the tetragonal axis. The application of an electric field along c reduces the crystal symmetry to orthorombic and the optical symmetry to biaxial. So, the index of refraction for light propagating along c axis is different for light polarized in the two principal planes.

The voltages are applied to the crystals by means of electrods of a new form, namely stuck at the ends of the lateral faces of crystals. In order to obtain an omogen electric field, it is necessary that the length of the crystal be at least twice with respect to its transverse dimensions. Our samples, cut from optical-quality regions of K.D.P., have each 8 mm × 8 mm × 16 mm, with the length along the optical axis. To prevent a depolarizing effect it is necessary to assure a good optical finish of the crystal face. The end faces were polished with a planeity of one — fourth wavelength of light and a parallelism of 5″. In this way, we have obtained, an extinction ratio of 1000 : 1.

Each crystal was introduced in a body of plexiglass with coated glass windows (fig. 2).

The modulating voltages applied to crystals are obtained from a sinus wave high voltage generator. This voltages are in phase quadrature (fig. 3) peak modulating voltage is $V_0 = 0 \div 8$ KV, and frequency 100 Hz — 10 KHz.

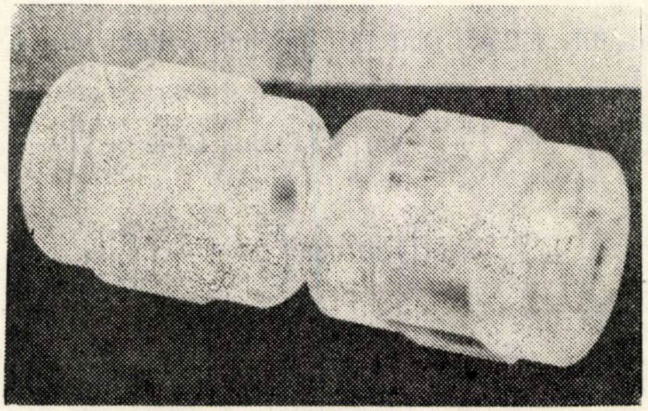

Fig. 2. K.D.P. crystals of the modulator

The optical translator has been tested by using it to shift the He.— Ne. laser frequency, ω, by frequency Ω. Fig. 4 shows the experimental arrangement.

The occurence of electrooptical frequency shifting was established by using optical mixing on a photocell area. The output from the frequency translator was combined with a reference beam obtained, by means of a beam-splitter, from same laser.

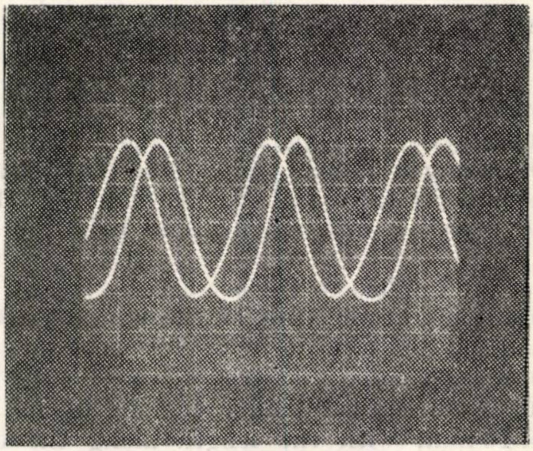

Fig. 3. The voltages on the crystals

The conversion efficiency to the desired $n = +1$ side-band is a function of the peak voltage, V_0. For peak voltage up to 4,5 kV, the intensity of first upper sideband ($n = +1$) is nearly linear with the peak voltage. For $V_0 = 7{,}2$ kV we have obtained the maximum conversion efficiency. In this case, the first upper sideband ($n = +1$) contains 64% from the incident light.

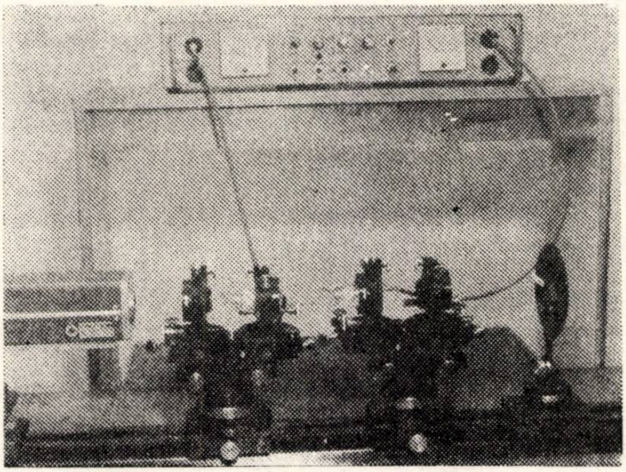

Fig. 4. Optical frequency translator. Experimental arrangement

REFERENCES

1. L. E. DRAIN, B. C. MOSS, Opto-Electronics, *4*, 429 , 1972.
2. C. F. BUHRER, V. J. FOWLER, L. R. BLOOM, Proc. I.R.E., *50*, 1827, 1962.
3. F. S. CHEN, Proc. I.E.E.E., *58*, 1440, 1970.
4. W. PRATT, *Laser Communication Systems*, J. Willey, N.Y., 1969.
5. I. P. KAMINOW, *An Introduction to Electrooptic Devices*, Acad. Press., N.Y., 1974.
6. W. A. SHURCLIFF, *Polarized Light*, Harvard Univ. Press, Cambridge, 1962.

Received, November 10, 1979

ANALELE UNIVERSITĂŢII BUCUREŞTI, FIZICĂ XXIX, 1980, PAG. 37–42

LONGITUDINAL MODE-LOCKING IN A HE.-NE. LASER BY NONLINEAR ABSORPTION IN NEON

M. RISTICI, A. I. CIURA

Institute for Physics and Technology for Radiation Devices *

T. TUDOR

Faculty of Physics. University of Bucharest **

ABSTRACT

An experimental arrangement for locking the longitudinal modes of a He – Ne. laser, using natural neon as saturable absorber is presented. The modifications of spectral mode distribution and temporal features of the laser output for the locked operation are pictured.

Introduction

The electromagnetic field of a laser, is, at any instance, a linear combination of some self-consistent field configurations – the modes of the laser. In a free-running state of a laser, the phase relationship between the oscillating electromagnetic fields comprising the modes is time dependent; the modes add incoherently and produce a laser output which varies as function of time in an erratic way. If the oscillating modes are forced to maintain a fixed phase relationship to each other, the modes add coherently and the laser output will be a well-defined function of time. The laser is then said to be „mode-locked" [1], [2]. The form of its output depends on which modes are oscillating and what phase relationship is maintained between themselves. If A_n, ω_n, and Φ_n are respectively the amplitude, the angular frequency and the phase of the nth. mode, the total laser output field is written

$$V(t) = \sum_n A_n e^{i\left[\omega_n\left(t-\frac{x}{c}\right)+\Phi_n\right]} \tag{1}$$

---

* National Center of Physics, P.O. Box 5206, Măgurele, Bucharest.
** National Center of Physics, P.O. Box 5211, Măgurele, Bucharest.

where we have denoted by x the traveling direction of the wave. If the spectral interval between any two adjacent modes is the same, say Ω, we can write $\omega = \omega_0 + n\,\Omega$ and (1) becomes :

$$V(t) = e^{i\omega_0\left(t-\frac{x}{c}\right)} \sum_n A_n e^{i\left[n\Omega\left(t-\frac{x}{c}\right)+\Phi_n\right]} \tag{2}$$

This represents a carrier wave of frequency ω_0, whose envelope depends on the values of A_n and Φ_n. In the case of a free-running laser, A_n, Φ_n and, consequently, this envelope, are erratic functions of time. For a mode — locked laser A_n and Φ_n are constant in time and the laser output envelope is a periodical function of time with the period $\Sigma = \frac{2\pi}{\Omega}\cdot$ For example if the modes are locked together so that there is a zero phase difference between one mode and the next and, idealised, the modes amplitudes are assumed to be equal, we have from (2) :

$$V(t) = A_0 e^{i\omega_0\left(t-\frac{x}{c}\right)} \sum e^{in\Omega\left(t-\frac{x}{c}\right)} = A_0 e^{i\omega_0\left(t-\frac{x}{c}\right)} \frac{e^{iN\Omega\left(t-\frac{x}{c}\right)}-1}{e^{i\omega\left(t-\frac{x}{c}\right)}-1} \tag{3}$$

This formula describes a train of pulses with repetition rate $\frac{\Omega}{2\pi}$ and width $\frac{2\pi}{N\Omega}$ where N is the number of oscillating modes of the laser. For the real distribution of the amplitudes A of the various modes of the laser, if all modes are locked in phase this result still holds but in an approximate form : The envelope of the laser output consists of a train of pulses with repetition rate T, the pulse width being approximately the reciprocal of the frequency range over which the A_n's have an appreciable value. Within the laser cavity, this corresponds to a pulse of light traveling back and forth between the mirrors with the velocity. For other sets of modes amplitudes and phases, the laser euvelope has other forms. For instance, if the alternate modes are π radians out of phase, the pulses have a repetition rate of $2\frac{\Omega}{2\pi}$ while the pulse width remain the same, $\frac{2\pi}{N\Omega}$.

Locking between the modes of laser, particularly between the modes of He-Ne lasers, has been induced in very different ways : One way is to force the locking by internal time varying perturbations at a frequency equal to the resonator mode-spacing frequency Ω. Hargrove, Fork and Pollack [3] made first observation of a forced locking in a 0,63 μm. He-Ne. laser, whose losses have been internally modulated by means of an acoustic diffraction cell. Harris and Targ [4], in a pioneering work too, reported the mode-locking induced by an intra-cavity phase perturbation obtained by means of a K.D.P. crystal phase modulator. Since then, numerous internal modulation mode-locking experiments have been performed using either acoustic, electro-optic loss modulators or electro-optic phase modulators [1], [2]. Huggett [5] has proposed a feedback arrangement for maintaining the mode-locking condition independent of cavity perturbations : he used the R.F. beat signal between the modes, to drive the internal modulators. Henneberger and Schulte [6] have obtained mode-locking by vibrating one of the resonator mirrors at $\frac{\Omega}{2\pi}$ rate ; the resonator length modulation is equivalent to that produced by an internal phase modulator driven at the same frequency. Simple ways to forcing the modes to lock is by translating the resonator end mirror at a constant velocity [7] or by low-frequency modulating the length of the cavity, for instance by means of a loud-speaker coil [8].

Under certain conditions, the nonlinearity of the interaction between the substance and the radiation within the laser may be such that mode locking occurs in absence of any other mode locking element ; the phenomenon, denoted by the term self-locking was very extensively investigated [1], [2], [9]. Finally, a relative simple way for coupling the modes is the use of a saturable absorber, for instance a pure neon discharge [10], [11], or of flowing dyes [12], inside the laser cavity.

In this paper we present the locking of longitudinal modes of a He-Ne laser, obtained by using a discharge tube filled with natural neon as a nonlinear element into the laser cavity.

Experimental arrangement. Results

The experiments were performed with a d.c. excited 160 cm. active length, 4 mm. bore laser tube (fig. 1), filled with a 10 : 1 mixture of He : Ne at a total pressure of 1,5 torr. The cavity consisted of a 250 cm. radius

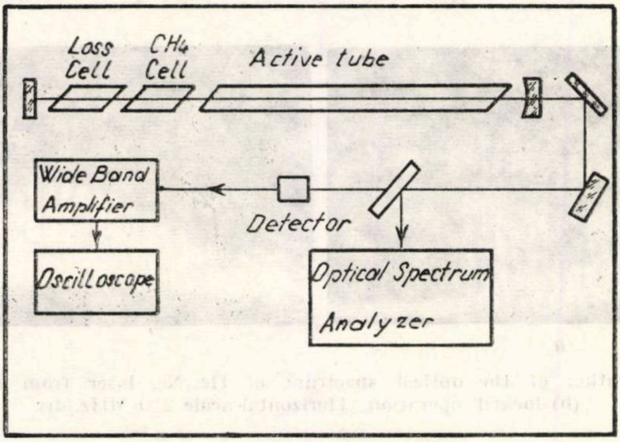

Fig. 1. The experimental set-up

focussing mirror and a flat mirror, spaced by 240 cm. Methane gas at atmospheric pressure was introduced into a small gas cell in the laser cavity to prevent oscillation on the high-gain 3,39 μ transition. The loss tube, 22 cm. discharge length, with a 2 mm. bore, was filled with natural Ne, to a pressure of 3 torr. and placed inside the cavity, near the flat mirror, in the waist of the beam. The geometry of the arrangement impose fundamental transverse mode operation only.

The output of the laser as a function of time, was observed by a Monsanto type D1, PIN photodiode, whose output was fed into a S 7 — 10 A oscilloscope, via a P.R.D. 7835 Harris amplifier. The rise time of the photodiode is ~ 0,5 ns., with 50 Ω load. The oscilloscope has the bandwidth of 1,2 GHz., the vertical sensitivity 0,7 V/cm. and the input impedance 50 Ω. The amplifier has a bandwidth of 550 MHz., gain 40 dB. and input and output impedances 50 Ω. Since both the amplifier and oscilloscope have fixed gain and sensitivity respectively, for adjusting the puls heigth on the oscilloscope screen, matched calibrated attenuators were used. The combined rise-time of the detection system is about 0,80 ns. The frequency spectrum of the laser output was monitored by a Spectra Physics Model 420 Optical Spectrum Analyzer.

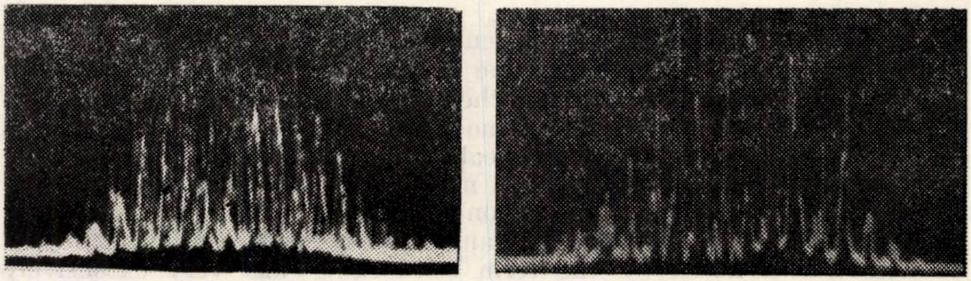
a b

Fig. 2. Typical frequency spectrumal of the free-running laser (a) exposure time $\frac{1}{30}$ s. (b) exposure time 1 s

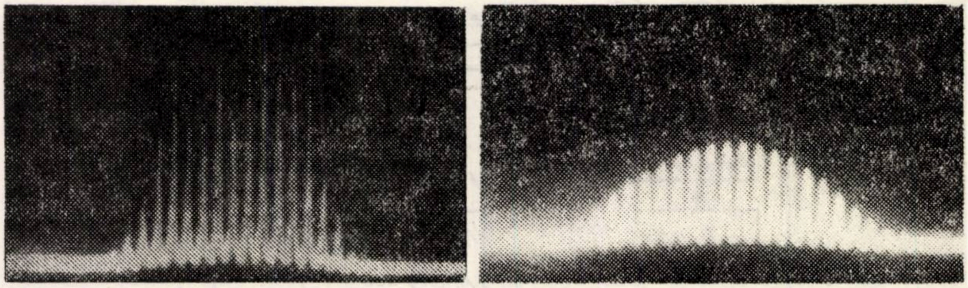
a b

Fig. 3. Modification of the optical spectrum of He.-Ne. laser from (a) unlocked to (b) locked operation. Horizontal scale 250 MHz./div

If the loss cell is not supplied, the laser operated in a free-running state. The modes are in competition, fluctuations of the mode amplitudes and frequencies occur. Fig. 2 presents Optical Spectrum Analyzer displays of such fluctuations, recorded with different exposure time. These fluctuations are responsible for the low frequency noise present in the laser output during unlocked operation. The ouput as a function of time has a d.c. component although some signs of pulsing are present. When the loss cell discharge is on, the optical spectrum changes from rapidly fluctuating mode intensities to a stationary spectrum (fig. 3). Also one may observe the broadening of the oscilating bandwidth. For a more accurate measurement of the mode spacing, fig. 4. presents an enlarged view of the Spectrum Analyzer display (125 MHz./div.). As it is shown the frequency spacing between oscillating longitudinal modes is about 60 MHz corresponding to $C/2L$ for our cavity. In the time domain the laser output consists of equally spaced short pulses (fig. 5). Fig. 6 presents more detailed views of the pulses. The horizontal scale in fig. 6 a. is 5 ns./div.;

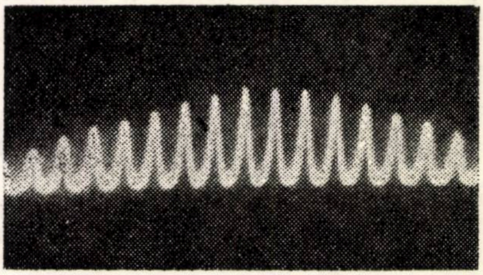

Fig. 4. Expanded view of the optical spectrum in the mode-locked operation. Horizontal scale 125 MHz/div

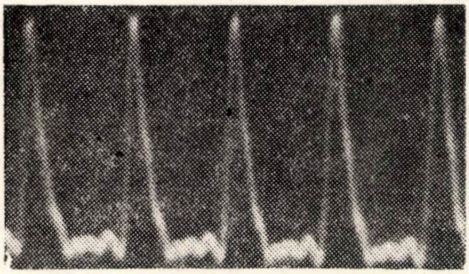

Fig. 5. Output pulses with repetition rate c/21, of the mode-locked laser. Horizontal scale 10 ns./div

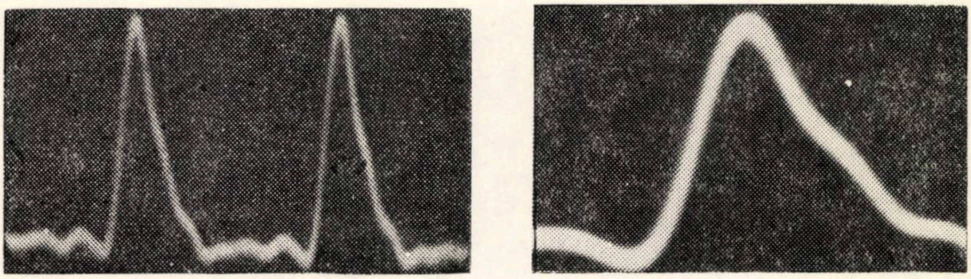

a *b*

Fig. 6. Expanded view of the pulses (a) Horizontal scale 5 ns./div. Pulse-spacing 16 ns. (b) Horizontal scale 1,25 ns./div. Pulse width 1,3 ns

thus the pulse spacing is about 16 ns. The asymmetry of the pulses is contributed by the photodiode. The observed rise-time in fig. 6 b. (scale 1,25 ns.) permitts, after retaining the contribution of the electronics, to estimate the full-width at half-maximum of the laser pulses to be about 1,3 ns.

Thus the locking of the He.-Ne. laser modes by a loss cell filled with natural neon constitutes a relatively simple way to obtain stable short pulses. Such a laser output is a very useful tool for determining the response time of high-speed detectors and the life-time of atomic levels.

REFERENCES

1. L. ALLEN, D. G. C. JONES, *Mode-locking in Gas Lasers*, in *Progress in Optics*, vol. IX, ed. E. Wolf, North-Holland Publs. Comp., (1971).
2. P. W. SMITH, M. A. DUGUAY, E. P. IPPEN, *Mode-locking of Lasers*, in *Progress in Quantum Electronics*, vol. III, ed. J. H. Sanders, S. Stenholm, Pergamonn Press, Oxford, (1975).
3. L. E. HARGROVE, R. L. FORK, M. A. POLLACK, Appl. Phys. Lett., *5*, 4 (1964).
4. S. E. HARRIS, R. TARG, Appl. Phys. Lett., *5*, 202 (1964).
5. G. R. HUGGETT, Appl. Phys. Lett., *13*, 186 (1968).
6. W. C. HENNEBERGER, H. J. SCHULTE, J. Appl. Phys., *37*, 2189 (1966).
7. P. W. SMITH, Appl. Phys. Lett., *10*, 51 (1967).
8. A. BAMBINI, P. BURLAMACCHI, J. Appl. Phys., *39*, 4864 (1968).
9. A. I. CIURA, M. RISTICI, V. VASILIU, St. Cerc. Fiz., *30*, 785 (1978).
10. A. G. FOX, S. E. SCHWARZ, P. W. SMITH, Appl. Phys. Lett., *12*, 371 (1968).
11. V. P. CHEBOTAYEV, I. M. BETEROV, V. N. LISITSYN, J. Quant. Electron., QE−4, 788 (1968).
12. P. K. RUNGE, Optics Commun., *3*, 434 (1971).

Received, December 20, 1979

ANALELE UNIVERSITĂŢII BUCUREŞTI, FIZICĂ, XXIX, 1980, PAG. 43–46

DEPOSITION AND STUDY OF SOME PROPERTIES OF TIN OXIDE FILMS

B. LOGOFĂTU, A. DAFINEI
Faculty of Physics, University of Bucharest *

I. DAFINEI
Secondary School, Bucharest

ABSTRACT

Tin oxide films were prepared using three different methods ; sputtering, evaporation and pyrolysis. The electrical conductivity and optical transmission of the films are presented here.

Introduction

The transparent conducting films (tcf) have two important properties : high electrical conductivity and high transparency in the visible spectrum. That's why tcf are required in many opto-electronic devices. There are already some review articles about these materials [1, 2]. Physics and chemistry involved in deposition processes and behaviour of tcf are complex. For film deposition are widely used : tin oxide and indium oxide as materials and chemical vapour deposition (hydrolysis, pyrolysis), evaporation and sputtering as deposition techniques.

The films with good electrical conductivity are oxygen deficient and contain donor impurities. There is an optimum concentration of these defects in crystalline lattice for which the resistivity is minimum. The oxygen vacancies are created during the film deposition ; for conduction to be efficient one must controle the temperature of the substrate and the amount of oxygen in deposition chambers. Antimony for tin oxide and tin for indium oxide are frecvently used as dopants.

---

* National Center of Physics, Măgurele, Bucharest, P.O. Box 5211.

The post-deposition heat treatment modifies the electrical conductivity ; these modifications depend on the temperature and the ambient ; the annealing in an oxiding ambient produces an decrease in conductivity while annealing in reducing ambient (H_2) or in inert gas (Ar) produces an increase in conductivity.

In this work are presented some experimental results concerning preparation and investigation of some electrical and optical properties of tin oxide films.

Materials and methods

We have applied three methods to deposit tcf of tin oxide :

a) dc Sputtering. We used the UBH-75P-1 equipment. The tin oxide for target was prepared by oxiding tin (set A) or SnO (set B), in air at 800°C. The doping was performed with antimony oxide in 10, 20, 30% weight percent (or 11, 26, 44 atoms of Sb for 100 atoms of Sn).

b) Oxidation. Sn was evaporated in vacuum, $p < 10^{-2}$ Torr, simultaneously with Sb as dopant. The layers obtained in this manner were subjected to heat treatment in air, at 200 –500°C.

c) Pyrolysis. A solution containing 30 ml $SnCl_4$ + 10 ml CH_3COOH + + 30 ml C_2H_2OH was heated at 100°C, in a furnance (fig. 1). The vapours are thermaly decomposed on the substrate, maintained at 400 –500°C ; the result is a tin oxide film. The rotation of the substrate helps to obtain films with uniform thickness.

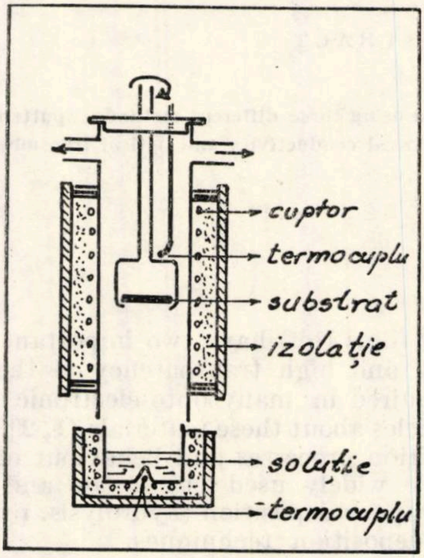

Fig. 1. Schematic of the apparatus for pryolytic deposition

Electrical and optical properties

An interferometric method was used to measure the film thickness. The conduction electron concentration (n) was found from typical Hall measurements, while for the electrical resistivity (ρ) a conventinal four-point probe was used. The transmission spectrum (T) was measured with a UVVIS-Zeiss spectrophotometer.

a) dc Sputtering. The as deposited coatings exhibit n-type conductivity, with $n \simeq 10^{18}$ cm^{-3} and high resistivity $\rho \simeq 10^3\ \Omega$ cm. Annealing the film in air at 500°C produces a decrease in resistivity with about four order of magnitude (fig. 2). Probably there are water vapours in the deposition chamber which favour the formation of hydrates of the oxide; these compounds have higher resistivity than pure oxide and they are decomposed at 500°C. That's why the annealing produces a decrease in resistivity, in this case. As we see the impurification is not so efficient for our samples.

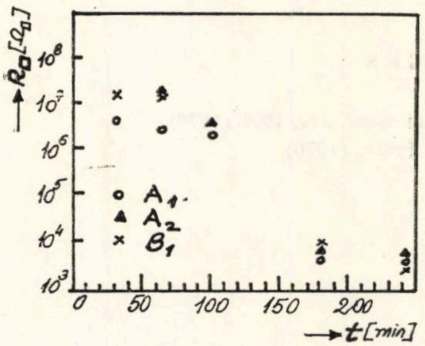

Fig. 2. The effect of the annealing for three samples: A_1(10%); A_2 (20%); B_1 (10%).

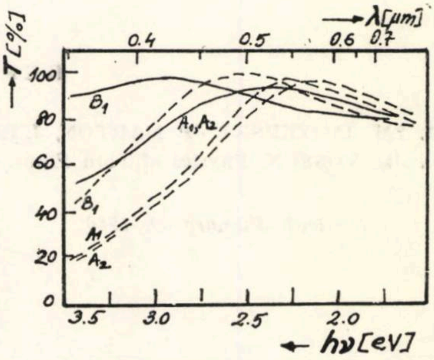

Fig. 3. Transmission spectra of the films: (---)before, (—) after the annealing.

The films have high optical transmission throughout the visible spectrum (fig. 3); the modification of transparency is caused by a decrease in film thickness during the annealing. The variations of T are principally due to interference phenomena; on the basis of well known relation: $\lambda = (nb/k)$, where n is refractive index, k is order of interferece, λ is wavelength for extrema k, one may calculate film thickness.

b) Oxidation. The temperature at which the oxidation is performed was found to be critical: at 200°C the film are dark in appearance, which poor transparency; above 300°C the transparency is high but the resistivity is too high, because the oxidation process is complete (stoechiometric compounds).

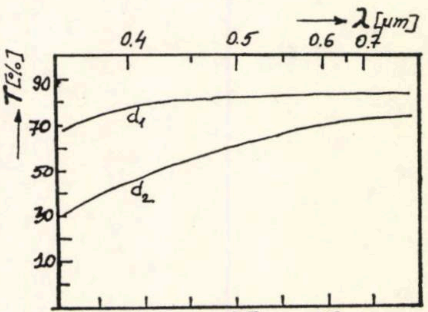

Fig. 4. Transmission spectra for two films with thickness $d_1 = 200$ Å, $d_2 = 300$ Å.

Transmission spectrum is given in fig. 4, for two samples.

c) Pyrolysis. The SnO_2 films obtained by this method have thickness between 1–1,5 μm, good electrical ($\rho \simeq 10^{-3}\ \Omega$ cm) and optical ($T = 80\%$) properties, but they are not uniform and reproductible.

Conclusions

The results we have presented here were obtained using three methods of deposition. The most promising techniques is pyrolysis, wich has the advantage of simplicity and low cost apparatus.

One major limitation of this process is related to the film uniformity.

REFERENCES

1. ZM. JARZEBSKI, JP. MARTON, J. Electrochem. Soc., *123*, 199C (1976).
2. JL. VOSSEN, Physics of Thin Films, *9*, Acad. Press, (1970).

Received, January 30, 1980

ANALELE UNIVERSITĂȚII BUCUREȘTI, FIZICĂ XXIX, 1980, PAG. 47–50

SOME INDIUM ARSENIDE PHOTOCONDUCTIVE PROPERTIES

MICHAELA LOGOFĂTU, B. LOGOFĂTU
Faculty of Physics, University of Bucharest *

M. F. LĂZĂRESCU
Institut of Physics and Technology of Materials

M. T. DUMITRIU
University of Craiova

ABSTRACT

In this work, some experimental results concerning the InAs photoconductivity spectral distribution in 3– 4 μm range at 300 K are presented.

The measurements were made on n-type mono- and polycrystalline material.

Introduction

The electrical and optical properties of indium arsenide indicate that it is a suitable material for infrared detectors, operating in photoconductive mode in the 3–4 μm region, at 300 K.

The simplest detector is based on the photoconductivity associated with intrinsic absorption in a photoconductor. When a semiconductor is illuminated with light of wavelengths lying in the fundamental absorption region, nonequilibrium electrons and holes are generated [1]

$$\Delta n = \frac{\tau g(0)\, L}{\alpha(L + s\tau)\, w} \qquad (1)$$

This relation is satisfied for n-type samples, in the fundamental absorption edge region, only when the carriers are generated in a very thin surface layer with a thickness of about $1/\alpha$ much les sthan the sample

---

* National Center of Physics, Măgurele, Bucharest, P.O. Box 5211.

thickness. ω. Consequently, the excess (nonequilibrium) conductivity $\Delta\sigma$ appears.

The spectral distribution of the photoconductivity $\Delta\sigma(\lambda)$ is determined by the absorption coefficient $\alpha(\lambda)$, the surface recombination velocity$s$ and by the geometry of the sample, ω/L [2]. The fundamental absorption edge of n-type InAs at 300 K and its dependence upon carrier concentration is given in fig. 1 [3]. It can be seen that the addition of donor impurities moves the absorption edge to higher energies and changes its shape in agreement with Burstein's theory.

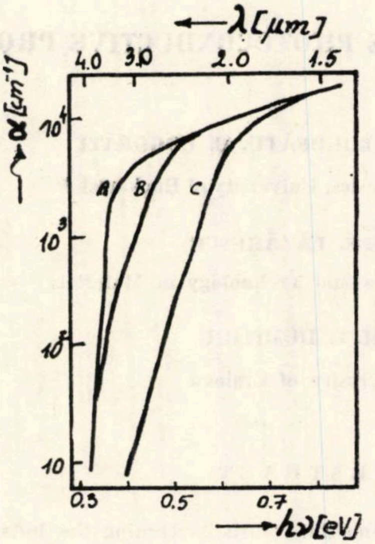

Fig. 1 [3]
The fundamental absorbtion edge of n-type InAs at 300 K
A : $n = 3{,}6 \times 10^{16}$ cm^{-3}
B : $n = 6{,}0 \times 10^{17}$ cm^{-3}
C : $n = 3{,}8 \times 10^{18}$ cm^{-3}

In order to prepare InAs photoconductors, the photoconductivity $\Delta\sigma$ was measured at 300 K, for n-type material with different carrier concentrations.

Experimental results and discussion

The n-type samples studied were polycrystalline although they contained large single crystal regions, prepared by Bridgman horizontal method [4], [5].

At 300 K, the carrier concentration ranges from 3.8×10^{16} to 1.0×10^{17} cm^{-3} and electron Hall mobility varies from 3.0×10^{3} to 1.8×10^{4} cm^{2} V^{-1} s^{-1}.

The samples were prepared under the form of rectangular parallelepipeds, their thickness varying from 1 mm to 0.3 mm. The lengthwas made relatively long to reduce the significance of end effects. Ohmic contacts have been achieved by alloying with metallic indium under vacuum conditions. The electrodes were masked to eliminate possible photovoltaic effects. Low recombination velocity surfaces were obtained by treatment with CP-4 etchant.

Light from a 600 Watt halogen lamp was chopped and was used to illuminate the samples. The lamp has been calibrated previously by means of a VTh-5 model vacuum-thermoelement.

The resulting low-level a.c signal was passed to a Keithley model 103 A preamplifier after which it was amplified by a Keithley model 840 amplifier.

Spectral measurements were made using a SPM 2 spectrometer with a NaCl prism.

The electric field varies from 25 to 150 V/m.

Generally, the relationship between the signal v received at the amplifier input and the photoconductivity $\Delta\sigma$ is nonlinear and quite complex. In some special cases this relationship is simpler : for example, in the case of weak relative photoconductance $\Delta\sigma/\sigma < 1$ a linear relationship is obtained for any load resistance [6]

$$v = \text{cst}\,\frac{\Delta\sigma}{\sigma} \tag{2}$$

i.e the signal v is proportional to the relative change of the conductance on illumination.

In order to determine the relative change of the conductance $\Delta\sigma/\sigma$ we have measured the signal v which ranges from 10^{-2} to 10 V.

The results, given in relative units are presented in fig. 2 ; the $_4$ per curve is for an imported single-crystal material having $n = 7.5 \times 10^{15}$ cm^{-3}.

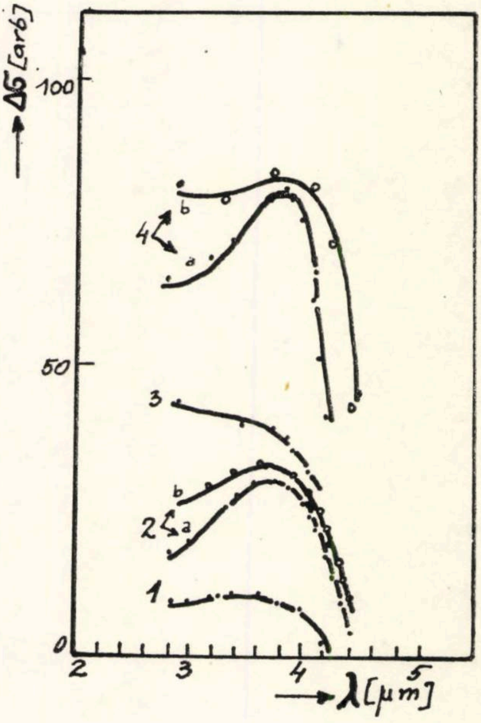

Fig. 2
The photoconductivity spectral distrbution, in relative units
1 : n = $1{,}2 \times 10^{17}$ cm^{-3}
2 : n = $6{,}7 \times 10^{16}$ cm^{-3} (pollycryst)
3 : n = $3{,}4 \times 10^{16}$ cm^{-3} (single cryst)
4 : n = $7{,}5 \times 10^{15}$ cm^{-3}
a : before etcjing
b : after etching

We can see that as the carrier concentration increases, the signal v and consequently $\Delta\sigma/\sigma$ reduces.

By etching, the surface recombination velocity decreases and the signal v increases. Also, the peak is broadening for the etched samples. The influence of the surface states on photoconductivity is presented in [7].

As expected, the photoconductivity of single crystal samples is greater than that of polycrystalline samples with the same carrier concentration.

REFERENCES

1. A. AMBROZIAK, *Semiconductor Photoelectric Devices*, London, 1970.
2. C. CONSTANTINESCU, A. GLODEANU, *Stări locale în semiconductori*, București, 1968.
3. J. R. DIXON, J. M. ELLIS, Phys. Rev., *123*, 1560, 1961.
4. M. LĂZĂRESCU, M. GEORGESCU, M. DUMITRIU, Congresul Național de Chimie, București, 11–14 sept. 1978, vol. I, pag. 123.
5. C. CONSTANTINESCU, M. LĂZĂRESCU, M. GEORGESCU, M. DUMITRIU, Rev. Roum. Phys., *24*, 705, 1979.
6. S. M. RYVKIN, *Photoelectric effects in semiconductors*, New York, 1964.
7. M. LOGOFĂTU, B. LOGOFĂTU, M. LĂZĂRESCU, Simpozionul național de fizica și chimia fenomenelor interfaciale, Baia Mare, 5–6 oct. 1979.

ANALELE UNIVERSITĂŢII BUCUREŞTI, FIZICĂ XXIX, 1980, PAG. 51–56

THE STUDY OF DEFECTS IN THE ADP SINGLE CRYSTALS BY THE X-RAY TOPOGRAPHY METHOD

H. V. ALEXANDRU, Z. CSIKI AND G. BACIU

Faculty of Physics, University of Bucarest*

ABSTRACT

In this paper the structure defects of the statically grown ADP single crystals are studied by the X-ray topographic (Lang) method. The defects produced by the growing mechanism acting on the prismatic and pyramidal faces of the crystals are shown.

Introduction

The study of the defects which appear during the growth of crystals have a special importance. By knowing the nature of these defects one can try to find the cause of their appearence. Thus one could learn how to optimize the crystal growth conditions in order to diminish these defects.

The purpose of the prezent work is to prezent the experimental results obtained in studying the defects by using the X-ray topography in the case of the static growth of the ADP single crystals.

Experimental results

The ADP crystals (ammonium dihydrogen phosphate) hase been grown in a static regime by slow evaporation of the solvent in vessels containing about-21 solution. The growing lasted one year at the steady temperature of 30 ± 0,2°C in a termostatic room of about 8 m^3. The solution has been prepared from the p.a. substance with an impurity contents given with tolerances of 10 p.p.m. (clorides); 50 p.p.m. (sulphates); 20 p.p.m. (iron); 10 p.p.m. (heavy metals). The solution pH has been

---

* National Center of Physics, P.O.Box 5211, Măgurele, Bucharest.

adjusted to 2.5 by addition of P_2O_5 (the solution pH is normally 3.5). The solution heated at a temperature above 40°C has been double filtered and placed in the growing vessel in the thermostatic room. The employed germ have been *Z* section slabs cut form a previously grown crystal and introduced by a nylon thread within the growing solution. (fig. 1). Because of their bounding type, there is a high probability for the crystals to form on slab side two ends which can grow independently for a long period of time (see the right hand side of fig. 1), and by slow sideways growth (along the X direction) the two parallel ends come in touch with each other, the crystals rapidly set up a single pyramidal end, after which the normal growth goes on. [1].

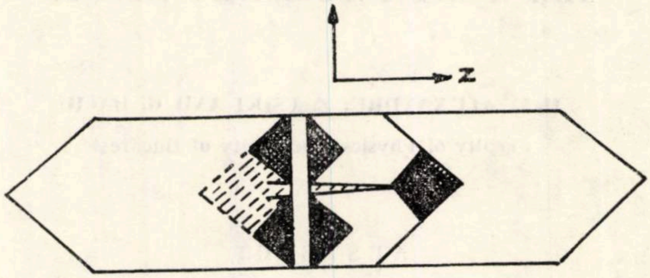

Fig. 1. The ADP single crystal and its germ and growth pyramids.

Optical single crystals (growing slightly thinner) of 6 –10 cm length and 2 cm 2 cm section have been obtained. *Z* section samples taken from the appropriate regions of these single crystals have been used for measurements of electrooptic coefficients. The dispersion of the coefficient r_{63} measured in the region optic showed values comparable to those given in the literature [2]. Samples of diferent characteristic sections have also been cut by the method of the wet cotton thread, polished and used in the prezent work for X-ray topography.

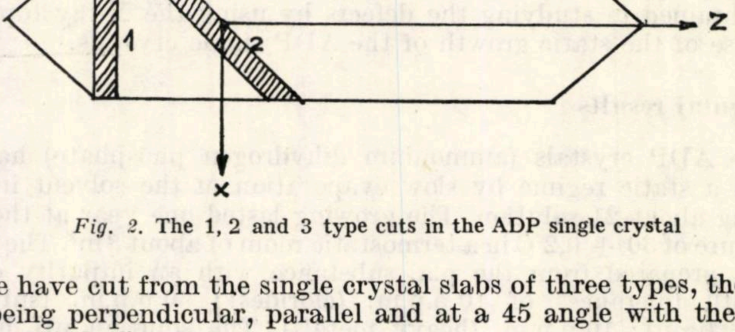

Fig. 2. The 1, 2 and 3 type cuts in the ADP single crystal

We have cut from the single crystal slabs of three types, the cutting planes being perpendicular, parallel and at a 45 angle with the growing direction [001] (fig. 2).

The thickness of the slab was between 1.5 mm and 2 mm. In order to distinguish among them we shall label them with 1.2 and 3 as shown on fig. 2. We have used the MoKα X-ray wave length. The topographs have been obtained with a topographic chamber of original construction. The topographs have been magnified 10 times.

Discussions

The most important impurities responsibl for the changes on the crystal habitus and the growth speed along the Z axis of the crystal are the trivalent metals in the following sequences : Cr^{3+}, Fe^{3+}, Al^{3+}. Although the segregation coefficients are very small, the impurity concentration may be several orders of magnitude smaller in the crystal then in the solution, their influence on the growth is already studied in the literature [3]. For usual growth supersaturation in dynamic regime $\sigma = 8\%$ and $CrCl_3$ impurity concentrations of about 70 p.p.m., Mullin [3] could decelate large oscillations of the growth speed along the Z axis with a time period of about two ours. For smaller impurity concentrations the period of the oscillations rises drastically.

In our case the presence of Fe^3 impurities in concentrations up to 20 p.p.m. (compared to the ground substance) may, for extremely small growth rates show oscillations, though possibly of lessen growth rate amplitudes at much larges time intervals. The temporary fall in the growth rate of the crystal along the Z axis and the growth of the {(011)} faces can be explained by the gradual accumulation within the adsorbed layer of impurities which attain very high concentrations, blocking up the growth. Their incorporation in the lattice within a definite zone can bring about the alteration of the lattice parameters. The practically free fourther growth takes place until a new impurity accumulation in the adsorbed layer takes place and so on.

For the very small growth rates employed by us the jumpstages are spaced in time and also along the length of the crystal. The absence of specific colouring (green) in the region of the (100) faces indicates that the Me^{3+} impurity concentration in the crystal is unimportant. In the high impurity concentration crystals, they are usually located along the line of the displacement edge of the (100) and (101) faces, that is incorporated by the layers traveling towards the pyramidal ands on the prismatic (100) faces.

With the type 1 slabs we have obtained topographs from the planes {200{ in two perpendicular directions. All topographs obtained with this type of slabs show practically identical defect types, the contrast being also conserved.

The most characteristic defect is the one produced on the intersection lines of the pyramidal faces which divide the topograph in 4 triangles. The regions at the face interactions being distorted, they give defects appearing less black on the magnified topographs. The intersection lines of the pyramidal faces do not coincid with the diagonals of the rectangle, a fact which shows that the growth rate are not equal over the pyramidal faces (101) and (101) [4].

Because these stresses appear on the magnified topographs indepently of the orientation of the diffraction vector, we may conclude that there exist stresses in at least too directions.

As seen on topograpvic images the left han side triangle (pyramidal face (011) shows different blackenings in different zones of the triangle, the zones being parallel with one another and vertical. The fact that these zones do not appear any more on topograph obtained after a 90° rotation of the direction of the diffraction vector, indicates that they appear due to unidirectional stresses produced by the variation of the lattice parameters due to the impurity concentration variations during the growth of the pyramidal faces. This variation is possible if only the growth rate, namely the growth rate parallel to the concerned faces, is not constant. By examining the topographic images obtained with the diffraction vectors g_{200}, $g_{\bar{2}00}$, g_{020} and $g_{0\bar{2}0}$, it follows that the tangent growth rate of the respective faces are correlated on the 4 faces as the zones of larger or lesser blackening coincid on these faces. On the topographic image 1 one may see the exist places of dislocations making an angle very near to 90 with the cutting plan of the slab.

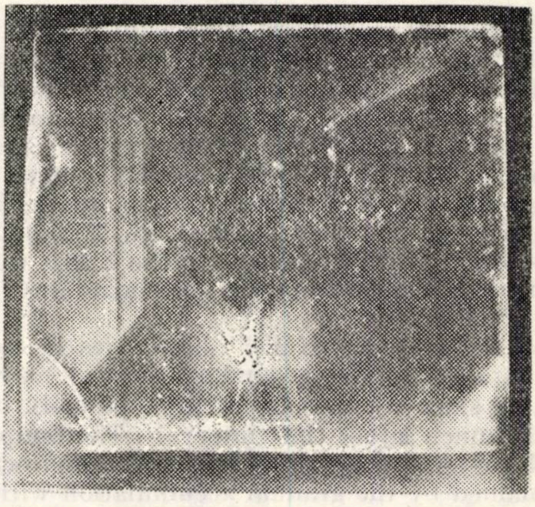

Top. 1. The topographyc image obtained on the type 1 cut. The Mo K radiation, the reflexion (200) the magnification 10

On the topograph 2 (diffraction vector (020) it may be seen the defects in a type 2 slab. The white contrast vertical region on thistopograph is due to the distorsion of the ADP crystal produced by the prismatic and pyramidal growth of the single crystal. The two growth have different rates, fact that leads to the modification of the impurity concentration on the 2 crystal faces. The shown defect indicates also unidirectional stress of the lattice in the direction [010], because the defect vanishes at a 90° changing of the direction of the diffraction vector.

The V-shape defect of lesser blackening on the toporgaph 2 shows in fact the variation of the advancing speed of two oppozite pyramidal faces. During the growth at given time intervals, the impurities gather on the pyramidal faces, their concentration becoming so important that the crystal practically loses its single crystal character in the concerned zone. The produced stress is bidimensional because the defect remains visible while rotating the diffraction vector at an angle of 90° [5].

On the topograph 3 obtained on a type 3 slab (the diffraction vector g_{200}) one can see the inclusions in the strongly distorted region around the germ (where the growth takes place following two pyramids because of the suspension thread). Alongside of the slab may be seen some defects of diminishing blacking, which are parallel to the identical pyramidal faces. These defect reflect in fact the same unsteadiness of the vertical growth rate of the crystal, therefore the variation of the impurity concentration during the growth.

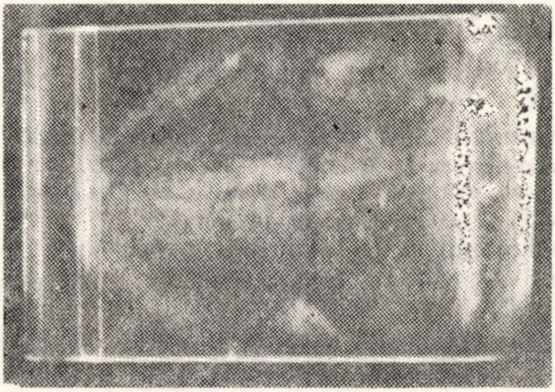

Top. 2. The topographyc image obtained on the type 2 cut. The Mo K radiation, the reflexion (200) the magnification 10

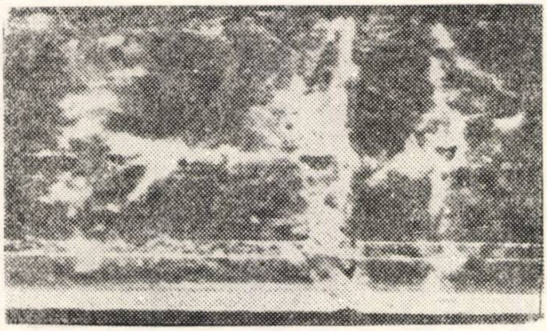

Top. 3. The topographyc image obtained on the type 3 vut. The Mo K radiation, thee (reflexion (200) the magnification 10

By examining the topograph 1, 2 and 3, we conclude that there are few defects in the volume of the crystal formed through prismatic growth of ADP crystal. This fact can be explained by assuming a high groth rate in the direction parallel to the groth direction [001]. Thus the impurity concentration vary very little during the groth a and defects leading to strong stresses in the lattice cannot appear.

We think that a further clarification of the nature of the observed defects and of their causes needs the examination of the stresses produced on asymetric reflections [6].

REFERENCES

1. H. V. ALEXANDRU, Doctoral Thesis, Bucharest University, 1974.
2. D. DRĂGOI, Batchelor Thesis, Bucharest University, 1977.
3. R. J. DAVEY, J. W. MULLIN, J. Cryst. Growth., *23*, 1974 (189).
4. Y. M. FISHMAN, Phys. stat solidi (a), *18*, 1973, (1).
5. P. PENNING, D. POLDER, Philips Res. Reports, *16*, 1961, (419).
6. Y. M. FISHMAN, V. G. LUTSAU, Phys. stat solidi (a), *3*, 1970, (829).

Received, January 24, 1980

ANALELE UNIVERSITĂŢII BUCUREŞTI, FIZICĂ XXIX, 1980, PAG. 57–62

DIELECTRIC PROPERTIES OF PLASTICIZATED ELASTOMER MIXTURES

I. C. PETREA, C. A. STĂNESCU, M. COJOCARU, E. BARNA

Faculty of Physics, Bucharest University *

ABSTRACT

We have investigated the dielectric properties of elastomers having permanent dipoles in macromolecules comparatively with polymers without permanent dipoles. We obtained a plasticizer like effect for additional polymers (as well as for plasticizer substances). We suppose carbon black produces the same effect.

Introduction

Dielectric studies can supply pieces of information concerning the polymer structure. In the present study we have started from the hypothesis of a solid solution model which implies its verification as well as an effect of internal plasticizing of the investigated elastomers.

Imediat consequences of such a model may by the polymer internal viscozity lowering. The value of dielectric constant can be determinated by means of the size of electric dipoles existing in the system, by their density and also by their mobility at different working frequencies.

As a plasticizing effect we expect the permanents dipoles to gain supplementary mobility at low frequencies and to extend the ligh values domain for the dielectric constant.

We still have to examine to what an extend the permanent dipole dilution can lower the dielectric constant values and which is the influence of their growing mobility. Knowing similar studies (1, 2) and knowing that the dielectric constant raises with the temperature (3), we have tried to obtain elastic dielectrics with high performances for the dielectric constant values.

Within the condition of the suggested model we expected a similar behaviour for the nonpolar polymers, having only a grater influence

---

* National Center of Physics, P.O. Box 5211, Măgurele, Bucharest.

the dielectric behaviour at relatively higher frequencies. We should notice that the polydispersion of used polymer evident a relaxation time spectre-the values of the dielectric constant continuously decreasing on a large frequencies interval (fig. 2 and 3 –5).

We have investigated the complex dielectric constant for polar and non polar elastomers. The research was performed for industrialy made polymers having practical applications.

For some of our compositions we have studied the effect of crosslinking and that of crosslinking period.

The investigations were made at room temperature for a large domain of frequencies (audio and radiofrequencies). The aim of the paper was to determine the plasticizing effect upon the elastomers by means of different components as well as the crosslinking effect associated with plasticization.

The materials

For rendering obvious the specifical properties of the high elastomers we have chosen polar and nonpolar (or slightly polar) materials. Out of the polar materials used we have selected data concerning the nitrylic rubber (NBR) Krynac 801 with 38% acrilonitryl in copolymer.

We have also selected the data on this vulcanized rubber having the formula as in the table 1.

component	D	E (percent)
nitrylic medium	46.35	46.46
zinc oxide	22.32	2.30
stearic acide	0.46	0.46
sulphur	0.10	0.10
plasticizer	9.00	10.00
carbon black	35.23	34.73
other components	6.54	5.95

The materials were vulcanized from 5 to 120 minutes and labeled as D_i or E_i the index being the vulcanization time. As samples we used squares having 20 mm sides or cercles having 30 mm diameter.

For the nonpolar samples we had selectionated mixturea from polyizoprenic rubber (PI) and polyacrilonitryl (PAN).

The izoprenic rubber was Al/Ti catalyzated, the PE was a low pressure one, made at Petrochemical Work Brazi, the PS was produced at the Chemical Work Borzești and the PAN at UFS Săvinești. We added as an index the rubber percentage in the respective compositions.

The experimental instalation and the method used

For dielectric constant and dielectric loss we used *Q*-meter measurement ; in the domain 1,8 kHz –70 kHz a Ferissol *Q*-meter typ M 803·A, with a supplementary generator C903T and a power amplificator CA301 was used, for the 16 MHz –30 MHz domain, the Tesla BM 3091 E *Q*-meter.

We used more apparata for reconfirmation of data, in the high frequencies domain, especialy because the polar materials had high dielectric losses and very low quality factors (Q-values). These losses make the experiments dificult particularly at high frequencies.

The sample thickness was micrometric determined. As a result the maximum error was of 0.001 mm for the thickness and of 2 mm² for the sample area. The maximum relative error for the dielectric constant has been estimated as lower than 5%. As we had used samples with an area smaller than the measurement cell area, we imagined an equivalent schema presented in fig. 1, and we obtained the relations :

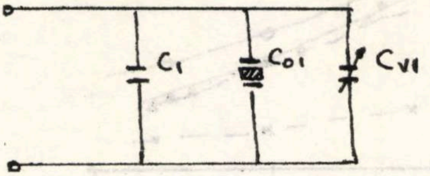

Fig. 1

$$\varepsilon' = \frac{\Delta C}{C} + 1$$

$$\operatorname{tg} \delta = \frac{Q_0 - Q}{Q_0 \cdot Q} \; \frac{C_{V0} + C}{\Delta C' + \varepsilon' C_2 + C_a}$$

with the notations :

$$C_a = \frac{\varepsilon_0 S_p}{d} \qquad \Delta C = C_1 - C_0$$

$$C_1 = \frac{\varepsilon_0 (S - S_p)}{d} \qquad \Delta C' = C_{V0} - C_{V1}$$

and : S_p the sample area, ε_0 vacuum dielectric constant, d the sample thickness, C_{01} the measurement cell capacity with sample within, C_0 the capacity of the same cell without sample, S cell electrodes area, Q_0 the quality factor without sample, Q the quality factor with sample in the cell, C_{v0} variable condenser capacity without sample, C_{v1} its capacity with the sample inside.

The experimental results

In fig. 2 we presented the frequency dependence of the dielectric constant for the polar mixtures indicated while in fig. 3 and 5 the obtained values for the nonpolar mixtures. We separately emphasised the vulcanization influence upon materials in fig. 6.

The results obtained and presented in this study indicate a remarkable rise of the dielectric constant in rubberlike polymer mixtures in the presence of added auxiliaries.

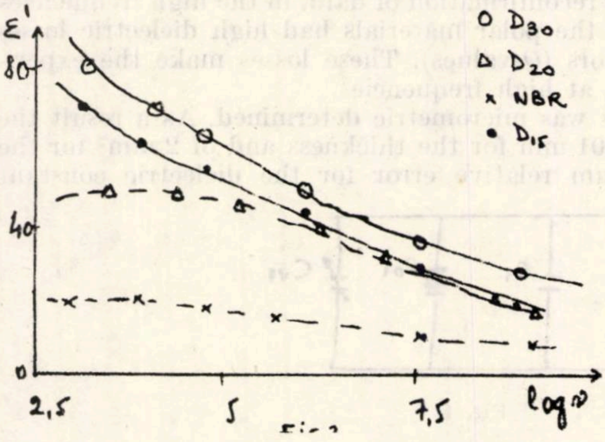

Fig. 2

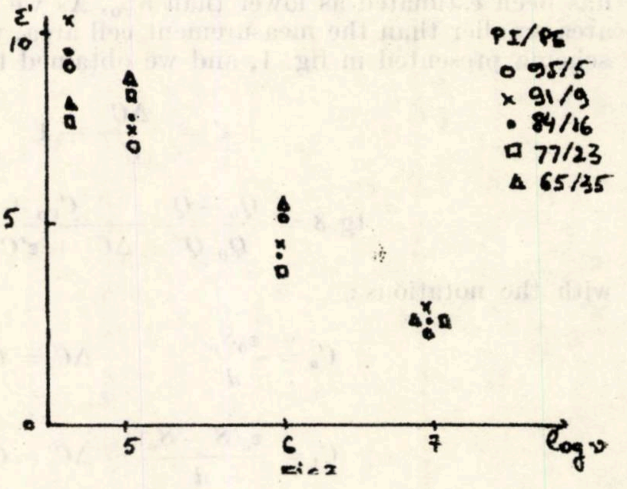

Fig. 3

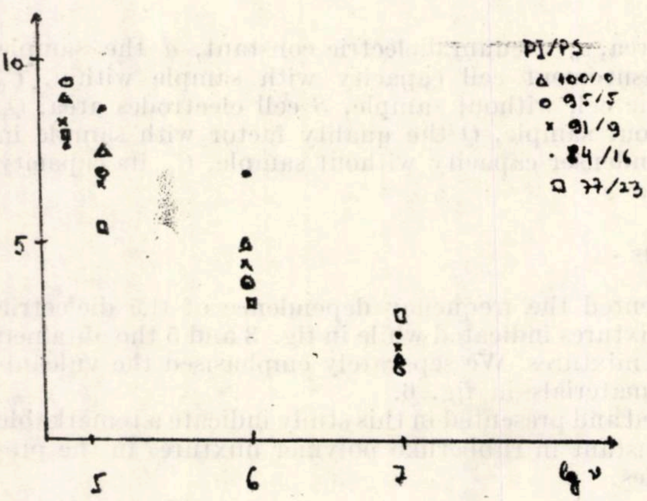

Fig. 4

The authors consider this effect as being linked to the plasticization of the elastomers and it consequence, the diminishing of the interaction energies between the polymer chains by means of a solvation effect. This allows an easyer orientation of the polymer within the electric field, especialy at low frequences (for the permanent dipoles). Similar effect are made evident (4 –6) by heating the PE, PVC and other polymers.

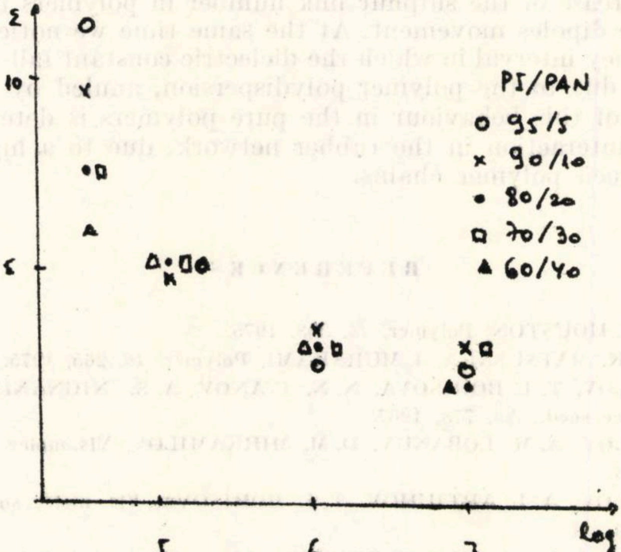

Fig. 5

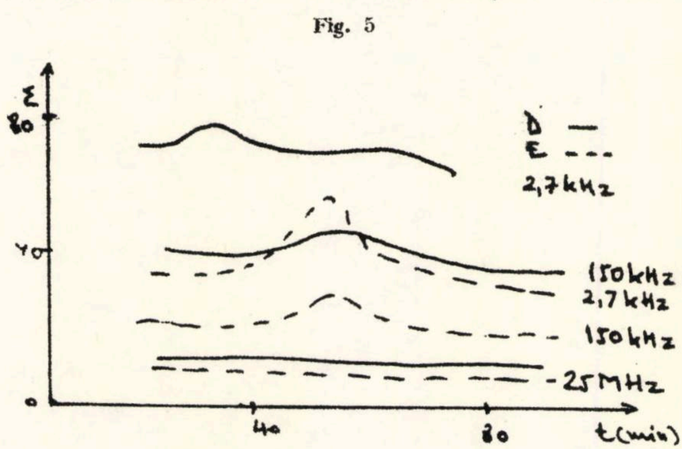

Fig. 6

We notice that a polymeric excess as plasticizer diminishes the. dielectric constant of the mixtures and remarkes the rigid structure

This way we underlined an optimum existence for the plasticizer proportion reprezenting the maximum orientation liberty for macromolecules dipoles.

This optimum composition obviously depends upon the mechanical and thermal sample treatment conditions but we can locate this optimum between 18 –20%, for the studied materials.

The similar behaviour for the NBR emphasised the validity of the given model.

The increase of the sulphur link number in polymers imply a limitation of the dipoles movement. At the same time we notice a decrease of the frequency interval in which the dielectric constant falls. This means this effect is due to the polymer polydispersion, anuled by crosslinking. The absence of this behaviour in the pure polymers is determined by a high energy interaction in the rubber network, due to a higher contact number between polymer chains.

REFERENCES

1. M. BAIRD, E. HOUSTON, Polymer, *16*, 308, 1975.
2. Y. KIHIRA, K. MATSUSAKA, I. MURAKAMI, Polymer, *16*, 265, 1975.
3. S. P. MIHAILOV, T. I. BORISOVA, N. N. IVANOV, A. S. NIGNANHODJAEV, Vis. molec. soed., A9, 778, 1967.
4. S. P. MIHAILOV, A. M. LOBANUV, D. M. MIRKAMILOV, Vis. molec. soed. A10, 836, 1968.
5. S. P. MIHAILOV, A. I. ARTIUHOV, T. I. BORISOVA, Vis. molec. soed., A10, 1755, 1968.
6. E. I. RIUMTEV, F. M. ALIEV, V. N. TVETCOV, Vis. molec. soed, A17, 1712, 1975.

ANALELE UNIVERSITĂŢII BUCUREŞTI, FIZICĂ XXIX, 1980, PAG. 63–67

MESURE DE RÉSISTENCE SPÉCIFIQUE ET ÉVALUATION D'UNE TRANSITION ISOTROPE-SMECTIQUE C

E. BARNA, L. M. IONESCU, I. C. PETREA

Faculté de Physique, Université de Bucarest

RÉSUMÉ

Les mesures électriques de résistence spécifique effectuées sur un système mésogène révèlent, dans certaines conditions, alignements et associations moléculaires spécifiques pour la phase smectique, ayant en vue le système savon-eau caractérisé par des domaines amphiphiliques.

Par la suite de l'étude expérimentale de la smectophase lyotrope et thermotrope d'un détergent indigène, les auteurs ont mis en évidence et évalué pour ce cas la transition isotrope-smectique C.

Remarques sur le polymésomorphisme des smectiques

Toutes les phases smectiques présentent une structure en couches. Les études par diffraction de rayons X indiquent un arrangement régulier des molécules à l'intérieur de ces couches. L'épaisseur d'une couche dans la mésophase smectique est généralement plus grande ou égale à la longueur des molécules, et dépasse de loin la dimension de la maille élémentaire du réseau cristallin. Les molécules ne sont pas toujours perpendiculaires au plan de la couche smectique [1, 2].

Le polymorphisme des smectiques peut être expliqué par le changement de l'angle d'inclinaison des molécules dans la couche smectique : la diffraction des rayons X sur les mésophases smectiques a confirmé l'idée de l'arrangement des smectiques en couches, remarqué au début d'après les modifications dans les propriétés optiques [3]. L'ordre et la symétrie d'arrangement dans une couche smectique subit des modifications lorsque la température augmente.

Dans un smectique C, l'axe longue de la molécule est inclinée par rapport à la normale aux couches. Si l est la longueur de la molécule et θ-l'angle d'inclinaison, l'épaisseur de la couche sera $d = l. \cos \theta$.

Les composés amphiphiliques, lyotropes ou thermotropes, peuvent avoir un comportement mésomorphe, soit en présence d'un solvant sélectif (par exemple savon dans l'eau), soit comme phase pure (certains bloccopolymères) [4 –6].

Les savons et les détergents non-ioniques montrent de mésophases remarquables. Les systèmes organisés de ce genre correspondent à une phase lamellaire avec des couches de l'eau et de mésogène. Pratiquement les souscouches sont assez épaisses (20 –30 Å).

La dissociation électrolitique des savons, qui sont des sels des acids gras avec les métaux alcalins, dépend entre autres de la nature et la concentration du savon et du solvant.

En solution coexistent des ions de dimensions différentes et des molécules nondissociées, leur quantité et le mode d'association étant fonction, tout d'abord, de la concentration qui détermine ainsi les propriétés électriques du système. Pour les basses concentrations la dissociation est presque totale, tandis que les valeurs élevées impliquent un degré de dissociation plus réduit, ce qui favorise l'apparition d'associations micellaires d'ions, l'aspect de la solution étant celui d'une solution colloïdale.

La structure en couches du liquide où les molécules sont disposées parallèlement, mène à une augmentation de l'anisotropie électrique déjà existente ; les dipôles des molécules situées dans les couches parallèles donneront une polarisation en couche, formant de petits essaims, avec des orientations différentes et polarisation propre (pareils aux domaines ferromagnétiques).

L'étude des propriétés électriques du système peut être effectuée à l'aide d'un champ électrique généré par une tension soit continue, soit alternative ; afin d'éliminer l'effet de conduction, l'usage d'un champ électrique alternatif est préféré. La période du champ doit être beaucoup plus petite que le temps de relaxation des molécules susceptibles d'orientation ; si les valeurs sont comparables, les phénomènes sont beaucoup plus complexes. Pour des périodes suffisamment basses, l'effet d'orientation des dipôles dépend seulement du carré du vecteur champ électrique, et ne depend donc pas de son signe.

Dans le cas d'une mésophase smectique, les couches de liquide avec deux dimensions rendent équivalentes deux directions du plan de la couche, ainsi que le tenseur de la résistance électrique a seulement deux composantes distinctes $\rho_{||}$ et $\rho_{\perp}$, parallèle respectivement perpendiculaire à la couche. Elles se trouvent dans la relation $\rho_{||} \ll \rho_{\perp}$, à cause de la différence de section efficace lors du déplacement des porteurs de charge.

Lorsqu'on établit la direction de la couche par rapport au champ, donc celle de $\rho_{||}$ et $\rho_{\perp}$, un rôle important revient à l'angle formé par la direction du dipôle électrique et la direction de la couche.

Technique expérimentale

La substance smectique étudiée est un détergent indigène, dont la composition est : 23% stéarate de potassium, 1% hydroxyde de potassium, 0,5% glycérine, 0,5% alcool méthylique, 75% eau.

Le produit a été concentré par déshydratation dans l'étuve. Les concentrations obtenues ont été comprises entre 55–95% produits principaux dans l'eau.

Pour préparer les échantillons, nous avons utilisé une technique spéciale, compte tenue que par agitation et éboulition le produit devient mousseux. Au dessus de 85°C le produit se dégrade. L'échantillon a été mis dans un tube en verre, ayant une forme de U, long de 40 cm et avec une section transversale de 3 cm de diamètre. Les électrodes étaient en cuivre, étant „lavée" par la solution sur une longueur de 10 cm.

La résistance électrique de l'échantillon a été mesurée en champ électrique alternatif à une fréquence de 1000 Hz, à l'aide d'un pont RLC „Tesla" BM 498 et une précision de 1%.

Le domaine de température étudié a été compris entre 1°C et 60°C, la thermostation étant assurée avec une précision de 0,1%.

Résultats et discussions

La résistence électrique a été mesurée à une fréquence du champ électrique extérieur beaucoup plus grande que la fréquence de résonnance. Comme nous l'avons déjà remarqué, le phénomène d'orientation ne dépend pas de sens du champ et les phénomènes de transport sont négligeables.

Afin d'éliminer certaines erreurs systématiques et pour une bonne mise en évidence de la transition, nous avons examiné les différentes valeurs de la résistance rapportées à la résistence de l'échantillon à 60°C, température pour laquelle l'échantillon se trouve en dehors du domaine de mésomorphisme.

Tableau 1

T°C	Echantillon 1 c=94%	Echantillon 6 c=72%	Echantillon 8 c=64%	Echantillon 12 c=59%
	R (KΩ)			
14,5	13,00	12,00	10,60	4,52
19,9	11,80	13,40	9,8	4,06
25,5	11,07	16,20	7,86	3,62
32,5	12,60	14,3	6,95	3,28
39,5	10,80	12,08	5,56	2,75
55,0	7,90	9,15	4,14	2,19
60,0	7,40	8,45	3,41	2,05
6,0		21,09	6,44	6,06
4,3		25,50	5,62	7,70
1,0		35,7	3,38	9,19

Dans le tableau 1 sont rassemblés les résultats expérimentaux concernant cette étude.

Sur la figure 1 nous avons représenté la variation du rapport R/R_0 en fonction de la température, pour concentrations différentes. Les échantillons présentés ont les concentrations indiquées dans le tableau 1.

On peut voir que l'augmentation de la concentration du système lyotrope a pour résultat l'élargissement du domaine des températures spécifiques pour la phase smectique ; la position même de ce domaine sur l'échelle des températures est fonction de la concentration. Ainsi il est évident que pour l'échantillon 1, de concentration 94%, le domaine d'existence du smectique est compris entre 25 –31°C, tandis que pour l'échantillon 8, de concentration plus petite (64%) le même domaine est deplacé vers les températures plus basses. Mais en même temps, l'intervalle de température dans lequel se manifeste la mésophase smectique est plus large.

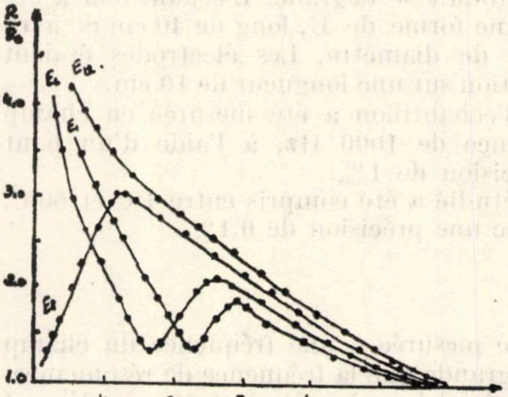

Fig. 1. La résistance électrique relative R/R_0 en fonction de la température, pour des échantillons de diverses concentrations : échantillon 1 (c = 94%), échantillon 6 (c = 72%), échantillon 8 (c = 64%), échantillon 12 (c = 58%)

Sur la figure 2 nous avons représenté l'influence de la température sur la largeur du domaine d'existence de la mésophase.

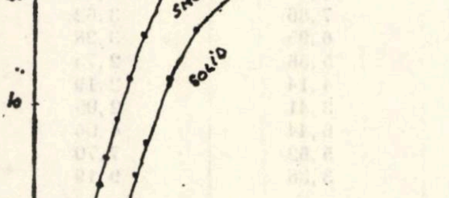

Fig. 2. La largeur du domaine d'existence de la mésophase en fonction de la température.

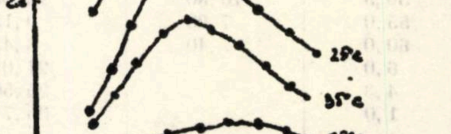

Fig. 3. La variation de la résistence relative R/R_0 avec la concentration, en conditions isothermes.

En même temps, la diminution de la concentration mène à une augmentation du saut de la résistance électrique lors de la transition de la phase solide à celle isotrope.

Pour les échantillons ayant une concentration en dessous de 60% il n'est plus possible de mettre en évidence une mésophase smectique dans le domaine de températures étudié. La variation de la résistence avec la température est celle connue pour les cas où l'angle formé par la direction du champ électrique avec la couche nématique est 0°.

Sur la figure 3 nous avons représenté les variations de la résistence relative en fonction de la concentration, dans des conditions isothermes. Le comportement est semblable à celui rencontré aux transitions de phase continues.

Connaissant l'orientation du dipôle permanent, perpendiculaire à l'axe de la molécule, nous pouvons conclure que l'orientation moyenne des molécules est normale à la couche. L'ensemble des résultats présentés plus hauts et les conclusions qui en découlent semblent indiquer que le système est un smectique qui, étudié par voie microscopique, montre un type C.

REFERENCES

1. G. W. GRAY, *Molecular Structure and Properties of Liquid Crystals*, Academic Press, New York, 1962.
2. L. GEORGESCU, I. C. PETREA, D. BORSAN, *Fizica stării lichide*, E.D.P., București, 1977.
3. I. C. PETREA, L. GEORGESCU, Analele Universității București (Fizică), vol. XXVI, 37, 1977.
4. P. G. De GENNES, *The Physics of Liquid Crystals*, Clarendon Press, Oxford, 1974.
5. A. SKOULIOS, *Advances in Liquid Crystals*, vol. 1 (C), 169, 1975.
6. L. M. IONESCU, Analele Universității București (Fizică), vol. XXVII, 35, 1978.

ANALELE UNIVERSITĂȚII BUCUREȘTI, FIZICĂ XXIX, 1980, PAG. 69–74

DEDUCTION OF FLORY AND HUGGINS FORMULA FOR MACROMOLECULAR SOLUTIONS OF THE BASIS OF ISING'S MODEL

L. GEORGESCU and C. A. STĂNESCU

Faculty of Physics, University of Bucharest *

ABSTRACT

Ising's model is applied to a macromolecular binary solution and the chemical potential expression is calculated both in one-dimensional and two-dimensional variants. For the two cases the well known expression is obtainedif solution is a concentrated one. In the two-dimensional case variant a supplementary term may be obtained if it is considered the interaction between the neighbouring chains, equivalent to an external field.

1. Introduction

The chemical potential for an athermal macromolecular binary solution has been calculated by Flory [1] and Huggins [2] using as model a pseudoreticular lattice (the lattice model proposed by Bethe [3]). The calculus has been latter resumed by Miller [4] and Guggenheim [5] and after that the interaction forces between the molecules of solvent-solvent, solvent-solute and solute-solute were taken into account by Orr [6] and Guggenheim [7] for neregulat solutions. Other details about the theory of Flory and Huggins can be found in Tompa and Petrea monographies [8].

The chemical potential for macromolecular solutions has as well been calculated on the basis of Ising model in the case of the binary athermal solutions [9], the general model of Montroll [10] being adopted for binary mixtures.

The obtained results cannot be directly compared with the formula given by Flory and Huggins because the interaction terms are given in a different transcription. Because of that Ising's model for the macromolecular binary solutions has been remade so that a correspondence with

---

* National Center of Physics, Măgurele, Bucharest, Romania, P.O. Box 5211.

Flory lattice it is possible to introduce either a solvent molecule or a monomer unit of the macromolecules. In the language of Ising's model we may say that a state j of the lattice can be represented by a quantity σ_j that can take two values only ± 1. In the event when $\sigma_j = 1$ the lattice cell j is occupied by a particle of type 1 (a solvent molecule) and when $\sigma_j = -1$ the lattice j is ocupied by a particle of type 2 (a monomer unit of the macromolecule).

The quantity $\left(\frac{1+\sigma_j}{2}\right)$ that also takes the values 1 may be defined if the lattice cell j is occupied by the particle of type 1, and the quantity $\left(\frac{1-\sigma_j}{2}\right)$ that also takes the value 1 if the particle of type 2 is present in the j lattice cell. In this manner the number of type 1 and 2 is

$$N_1 = \frac{1}{2}\sum_{j=1}^{N}(1+\sigma_j), \tag{1}$$

$$\sigma N_2 = \frac{1}{2}\sum_{j=1}^{N}(1-\sigma_j), \tag{2}$$

with $N = N_1 + \sigma N_2$, where σ is the polymerisation degree.

The way of calculus for the chemical potential is the following: starting from the partition function conveniently chosen the free energy of mixture is calculated and further by derivation with respect to the number of the moles, the chemical potential of the solvent or of the macromolecular component is obtained. The calculation is made both for one-dimensional and two-dimensional variants of Ising model.

2. General formulation of the theory

We consider an athermal molecular binary solution where the component 1 is the solvent molecules and component 2 the macromolecular monomer unites, into each cell existing a single particle. We choose the partition function of the binary solution in the following form [10]

$$Z = \sum_{N}\sum_{m}\exp\left(N_1 \ln \Phi_1 + N_2 \ln \Phi_2 - \frac{E_m}{kT}\right), \tag{3}$$

where

$$\Phi_1 = \frac{n_1}{n_1 + \sigma n_2}, \quad \Phi_2 = \frac{\sigma n_2}{n_1 + \sigma n_2}$$

are the molar fractions and E_m the system energy in the state m. In order to be able to pass directly from the partition function (3) to the mixture free energy it is more convenient to calculate first the system energy, considering the existence of 1–1, 1–2 and 2–2 type interactions. In this case the system energy can be written as

$$E_m = \varepsilon_{11} n_{11} + \varepsilon_{22} n_{22} + \varepsilon_{12} n_{12}, \tag{4}$$

where ε_{ij} is the interaction energy between the particles i and j and n_{ij} the number of interactions of i and j type.

If we replace the expressions of the interaction number and we take into account that $\Phi_1 + \Phi_2 = 1$, we obtain the following simplified relation for the mixture energy,

$$\frac{E_m}{kT} = z\varepsilon N_1 \Phi_2, \tag{5}$$

where z is the coordination number and ε Flory and Huggins [8] interaction parameter. Considering the relation (5), (1) and (2) ones the expression (3) can be also written as :

$$Z = \sum_{\sigma_1=\pm1} \dots \sum_{\sigma_N=\pm1} \exp\left\{-\frac{N}{2}\left[\ln\Phi_1 + \frac{1}{\sigma}\ln\Phi_2 + z\varepsilon\Phi_2\right] - \frac{1}{2}\left[\ln\Phi_1 - \frac{1}{\sigma}\ln\Phi_2 + z\varepsilon\Phi_2\right]\sum_j \sigma_j\right\}. \tag{6}$$

If we introduce Ising's classical notations

$$\alpha = -\frac{1}{2}\left[\ln\Phi_1 + \frac{1}{\sigma}\ln\Phi_2 + z\varepsilon\Phi_2\right],$$

$$J = 0, \tag{7}$$

$$B = -\frac{1}{2}\left[\ln\Phi_1 - \frac{1}{\sigma}\ln\Phi_1 + z\varepsilon\Phi_2\right],$$

the relation (6) for the mixture quantities can be condensed as

$$Z_m = e^{N\alpha} \sum_{\sigma_1=\pm1} \dots \sum_{\sigma_N=\pm1} \exp \sum_j \sigma_j \tag{8}$$

or

$$Z_m = e^{N\alpha} Z_I, \tag{9}$$

where Z_I is the partition function in Ising's model. This partition function can be expressed either in the one-dimensional, or in the two-dimensional one, in the form

$$Z_I = \lambda^N, \tag{10}$$

where λ is the maximum eigenvalue of matrix P, that is connected to the partition function through the relation $Z_I = \mathrm{Sp}\, P^N$ [11]. The maximum eigenvalue λ can be explained as a function of the adopted model, which may be one or two-dimensional.

3. Chemical potential of a macromolecular solution in Ising's one dimensional model

In the case of Ising's one-dimensional model, the maximum eigenvalue has the form

$$\lambda = e^{J}\,[\mathrm{ch}\,B + (\mathrm{ch}^2\,B - 2e^{-2J}\,\mathrm{sh}^2\,2J)^{\frac{1}{2}}], \tag{11}$$

and the macromolecular partition function, according to relations (7) will be

$$Z_m = e^{\alpha N}\,[e^{B} + e^{-B}]^{N}. \tag{12}$$

If we consider the macromolecular solution as concentrated, what gets into the frame of the work hypothesis of Flory and Huggins theory then it can be done the approximation $[2\,\mathrm{ch}B]^N \simeq e^{B(2N_1-N)}$. With this approximation the relation (12) can be written in the form $Z_m = e^{N\alpha}\,e^{B(2N_1-N)}$, or

$$\ln Z_m = -\frac{N}{2}\left[\ln \Phi_1 + \frac{1}{\sigma}\ln \Phi_2\right] - \frac{1}{2}\left[\ln \Phi_1 - \frac{1}{\sigma}\ln \Phi_2\right](2N_1 - N) - z\varepsilon N_1 \Phi_2, \tag{13}$$

hence it results the mixture free energy $\Delta F_m = -kT \ln Z_m$, or

$$\Delta F_m = RT\,[n_1 \ln \Phi_1 + n_2 \ln \Phi_2 + z\varepsilon n_1 \Phi_2], \tag{14}$$

where $N_i = n_i N_A$ (N_A is the Avogadro number). From relation (14) it can be imediately obtained the expression of the chemical potential of the solvent by derivation of this relation with respect to n_1. Finally we obtain:

$$\Delta\mu_1 = \frac{\partial \Delta F_m}{\partial n_1} = RT\left[\ln(1 - \Phi_2) + \Phi_2\left(1 - \frac{1}{\sigma}\right) + z\varepsilon\Phi_2^2\right], \tag{15}$$

that is representing the well known Flory and Huggins formula for the chemical potential of the solvent. If the solution is not concentrated, the approximation made can be no more used and we must use directly the relation (12). On the basis of this relation we obtain for the chemical potential of the solvent, the expression

$$\begin{aligned}\Delta\mu_1 = RT\Bigg\{&\frac{1}{2}\left[\ln \Phi_1 + \frac{1}{\sigma}\ln \Phi_2 + \left(\frac{\Phi_2}{\Phi_1} - \frac{1}{\sigma}\right)\right] - \ln\left[\exp\left(-\frac{1}{2} < \ln \Phi_1 - \right.\right.\\ &\left.\left.- \frac{1}{\sigma}\ln \Phi_2 + z\varepsilon\Phi_2 >\right) + \exp\frac{1}{2} < \ln \Phi_1 - \frac{1}{\sigma}\ln \Phi_2 + z\varepsilon\Phi_2 >\right] - \\ &- \frac{1}{2}\left(\frac{\Phi_2}{\Phi_1} + \frac{1}{\sigma} - z\varepsilon\Phi_2\right)\mathrm{th}\,\frac{1}{2}\left(\ln \Phi_1 - \frac{1}{\sigma}\ln \Phi_2 + z\varepsilon\Phi_2\right)\Bigg\}.\end{aligned} \tag{16}$$

If the numerical data obtained on the basis of the relations (15) and (16) are compared, for a binary mixture (for instance polystyren in benzene), the results are very different over a wide range of concentrations. This fact explains on one hand that Flory and Huggins formula can be applied to concentrated solutions only, and on the other it demonstrates that the one-dimensional model is an enough simplist one to be able to describe a macromolecular binary solution, fact imposing the use of the two-dimensional variant.

4. Chemical potenial of a macromolecular solution in Ising's two dimensional model

In the frame work of the two-dimensional model in the absence of external fields, the eigenvalue λ has the form

$$\lambda = \frac{1}{2} \ln (2\mathrm{sh}2J) + \frac{1}{2} \ln \frac{2\mathrm{ch}^2 2J}{\mathrm{sh}^2 J} + I. \tag{17}$$

where

$$I = \frac{1}{2\pi} \int_0^{\pi} \mathrm{d}\varphi \ln \frac{1}{2} \left[1 + (1 - k^2 \sin^2 \varphi)^{\frac{1}{2}}\right], \tag{18}$$

with

$$k = \frac{1}{\mathrm{ch}2J\mathrm{cth}2J}.$$

The free energy per particle may be expressed as

$$\beta F = \alpha - \ln(\mathrm{ch}2J) - I, \tag{19}$$

or as

$$\beta F = \alpha + \frac{1}{2} \ln(2\mathrm{sh}2J) + \frac{1}{2} \ln \frac{2\mathrm{ch}^2 J}{\mathrm{sh}2J} + I, \tag{20}$$

with $\beta = 1/kT$.

If we consider the relation (7), $J = 0$, and from the relation (19) taking into account the compound of the field of the matrix $V_3 = \exp(B \sum_j \sigma_j)$, we have

$$\beta F_m = N\alpha + B \sum_j \sigma_j. \tag{21}$$

As $\sum_j \sigma_j = 2N_1 - N$, the relation (21) can also be written under the form :

$$\beta F_m = N\left[-\frac{1}{2} \ln \Phi_1 + \frac{1}{\sigma} \ln \Phi_2 + z\varepsilon\Phi_2\right] - \frac{1}{2}\left[\ln \Phi_1 - \frac{1}{\sigma} \ln \Phi_2 + z\varepsilon\Phi_2\right] \cdot (2N_1 - N), \tag{22}$$

relation equivalent to the expressions (13) or (14) that are finally to Flory and Huggins formula (15). We can reach to the conclusion that in the frame of Ising's model, the two-dimensional variant, the same result is obtained as that obtained by Flory and Huggins.

Ising's model in the two-dimensional variant may be improved, considering in the relation (7) $J \neq 0$, which implies $I \neq 0$ too. The fact that $J \neq 0$ puts into evidence the existence of some external fields, in the present case these being possibly created by the interactions of superior order given by the interaction between the monomer units frome neighbour chaines fact ignored in the first approximation. This case will be considered in a further work.

REFERENCES

1. P. J. FLORY, J. Chem. Phys., 10, 51, 1942.
2. M. L. HUGGINS, J. Phys. Chem., 46, 151, 1942.
3. H. A. BETHE, Proc. Roy. Soc. (A), 150, 552, 1935.
4. A. R. MILLER, Proc. Cambridge Phil. Soc., 39, 54, 151, 1943.
5. F. A. GUGGENHEIM, Proc. Roy. Soc., (A), 183, 203, 1944.
6. W. J. C. ORR, Trans. Faraday Soc., 40, 320, 1944.
7. F. A. GUGGENHEIM, Proc. Roy. Soc. (A), 183, 213, 1944.
8. H. TOMPA, *Polymer Solutions, Butterworths*, London, 1956 ; I. PETREA, *Termodinamica statistică a macromoleculelor*, E.D.P., Bucharest, 1968.
9. L. GEORGESCU, Polymer, 16, 355, 1975.
10. F. N. GORDON and E. W. MONTROLL, Rev. Mod. Phys., 25, 353, 1953.
11. KERSON HUANG, *Statistical Mechanics*, John Wiley, New York, 1963.

Received, January 24, 1980

ANALELE UNIVERSITĂŢII BUCUREŞTI, FIZICĂ XXIX, 1980, PAG. 75–80

APPLICATIONS OF DECORATED LATTICES TO SOLUTIONS.

I. EQUILIBRIUM POLYMERISATION IN A DECORATED LATTICE MODEL

C. A. STĂNESCU

Faculty of Physics, Bucharest University *

ABSTRACT

We attempted to obtain a formula suggesting Mayo's result on the degree of polymerization using a latticeal method, namely, a decorated lattice method at thermal equilibrium.

Introduction

Studies of thermodinamic polymeric functions using latticeal methods were initiated by P. J. Flory and M. L. Huggins but in all cases the methods were approximate. In the present paper we would like to start from an exact soluble model [6] and yield to a so called „exact result" concerning the equilibrium average polymerisation degree and the polymer concentration in a solution. The model is about polymerisation from monomers in solution – without initiator or catalyst (for simplification). The solvent is supposed to be a good solvent. The resulting solution is composed by polymer, monomer and the solvent. The polymerisation can be either thermally initiated or by chain transfer [1, 2, 9]. For this system description we have adopted a decorated lattice used to the ternary systems by Wheeler, Widom, Neece [4, 7] and to the polymeric systems by the author [8]. In the last section we will discuss the motivation of this choice.

We would like to consider the monomer completely surrounded by z possible solvent molecules. We also consider the resulted polymer deprived of only those solvent molecules which are excluded by poly-

---

* National Center of Physics, P.O. Box 5211, Măgurele, Bucharest.

merisation links. We assume that polymer and monomer have the same interaction energies with the solvent. A supplementary simplificatory hypothesis arises from the supposition that polymerisation does not modify the interaction energies and the coordination number z in the system.

Model description

Suppose we have N lattice sites, every site with z nearest neighbours. On each vertex in this primary lattice a site from a secondary lattice can be placed. There are $\frac{zN}{2}$ primary vertices and certainly $\frac{zN}{2}$ secondary sites.

In the primary lattice we assume to have initially the monomer filling all the sites. The polymer is obtained by polymerisation after a time.

In the secondary lattice the solvent is in quantitative equilibrium with the primary components. It is not necessary for it to fill all the sites.

Let's suppose initially $n_{10} = N$ monomer molecules, and n_3 solvent molecules.

For the partition function estimation is it necessary to write the lattice energies. Let w_1 be the energy per link between primary components and w_2 the energy between primary — secondary components. Interactions in the secondary lattice can be neglected — being not essential.

Let us further suppose that, by a polymerisation process, the monomer can form liniar polymeric chains, transforming one of his neighbours into a succeeding polymeric unit. This will be achieved by transforming a Van der Waals link into a polymerisation valence link. (without perturbing the whole frame of the lattice).

We certainly assume that a polymeric segment (occupying a cell) can not have more than two other neighbours from the same chain all the monomers being at most bifunctional. The monofunctional monomers are necessarily two times the number of the polymeric chains.

Our problem is to determine the number of ways to constitute a microcanonical state, by different polymerisation sequences, performing the same energy, but including the various distinct ways in which the solvent molecules can be placed into the secondary lattice.

We express :

$$x = \sum_i n_i(p - 1) \tag{1}$$

the number of valence links — n_i being the number of chains with p_i segments (the exmonomer molecules), and try to write the number of ways to complete the lattice with x polymerisated links. This should be done because the one state energy depends only on x — according to the relation (4). It will be the product of the ways to place the solvent by the number of ways to construct the primary lattice. For the solvent there are $\frac{zN}{2} - x$ disponible places and n_3 molecules to be placed. The number of ways is :

$$g_2\,(n_3, x, N) = C^{n}_{\frac{zN}{2}-x} = \frac{\left(\frac{2N}{2} - x\right)!}{n\,!\left(\frac{zN}{2} - n - x\right)!} \tag{2}$$

For the primary lattice it will be the number of ways to choose the x links from the $\frac{zN}{2}$ possible links.

$$g_1(n_1, x) = C^{x}_{\frac{zN}{2}} \tag{3}$$

n_1 being the remaining number of monomer molecules.

We ought to include a multiplicative factor g_3 describing the limited possibilities of only pne or two links for a single cell.

Noticing that the energy is :

$$E_x = \frac{zN}{2} w_1 - w_1 \sum n_i(p_i - 1) + 2n\, w_2 \tag{4}$$

we can write the partition function as follows :

$$Z = \sum_{E} g_3 \cdot g_2 \cdot g_1 \exp\left(-\frac{E}{kT}\right) \tag{5}$$

or :

$$Z = \sum_{x} g_3 C^{n}_{\frac{zN}{2}-x}\; C^{x}_{\frac{zN}{2}} \exp\frac{x w_1}{kT} \exp\left[-\frac{1}{kT}\left(\frac{zN}{2} w_1 + 2n\, w_2\right)\right] \tag{6}$$

but :

$$C^{n}_{\frac{zN}{2}-x}\; C^{x}_{\frac{zN}{2}} = C^{n}_{\frac{zN}{2}}\; C^{x}_{\frac{zN}{2}-n} \tag{7}$$

And neglecting the g_3 dependance on x :

$$Z = g_3 \exp\left[-\frac{1}{kT}\left(\frac{zN}{2} w_1 + 2n\, w_2\right)\right] C^{n}_{\frac{zN}{2}} \sum_{1}^{\frac{zN}{2}-n} C^{x}_{\frac{zN}{2}} \left(\exp\frac{w_1}{kT}\right)^{x} \tag{8}$$

But because the sum in (8) is a binomial development we get finally :

$$Z = \frac{\left(\frac{zN}{2}\right)!}{n!\left(\frac{zN}{2}-n\right)!} \exp\left[-\frac{1}{kT}\left(\frac{zN}{2}w_1 + 2n w_2\right)\right]\left[1+\exp\frac{w_1}{kT}\right]^{\frac{zN}{2}-n} \tag{9}$$

with the supplementary condition :

$$n \leqslant \frac{zN}{2} - \sum p_i n_i + \sum n_i \tag{10}$$

Noticing that $\bar{p} = \frac{\Sigma p_i n_i}{\Sigma n_i}$ is the average polymerisation degree and remarking that :

$$x = (\bar{p} - 1) \sum n_i \approx \bar{p} \sum n_i \tag{11}$$

we obtain x at equilibrium from the partition function by a generating function method :

$$x = z^{-1}\, C^{n}_{\frac{zN}{2}} \exp\left[-\frac{1}{kT}\left(\frac{zN}{2}w_1 + 2nw_2\right)\right] \sum_x x\, C^{x}_{\frac{zN}{2}} \exp\frac{xw_1}{kT} \tag{12}$$

equivalent with :

$$x = \frac{\partial}{\partial\left(\frac{w_1}{kT}\right)} \ln\left[1+\exp\frac{w_1}{kT}\right]^{\frac{zN}{2}-n} = \left(\frac{zN}{2}-n\right)\frac{\exp\frac{w_1}{kT}}{1+\exp\frac{w_1}{kT}} \tag{13}$$

Using the notations :

$$C_{10} = \frac{N}{n+N} \tag{14}$$

for the initial monomer concentration,

$$C_1 = \frac{N}{n+N} - C_p \tag{15}$$

for the remaining monomer concentration :

$$C_p = \frac{\Sigma p_i n_{i_\infty}}{n+N} \tag{16}$$

for the polymer concentration,

$$C_s = \frac{n}{n+N} \tag{17}$$

for the solvent concentration; we can write (13);

$$\left(1-\frac{1}{p}\right)C_p = \left(\frac{z}{2}C_{10} - C_s\right)\frac{\exp\frac{w_1}{kT}}{1+\exp\frac{w_1}{kT}} \tag{18}$$

and (10) using the relations (11) and (14–17)

$$C_s \leqslant \frac{z}{2}C_{10} - C_p \tag{19}$$

which is a condition for a non-negative polymerisation degree.

Complementary remarks

(a) The (10) or (19) conditions must be interpreted as not having a very low monomer concentration comparative to that of the solvent. That is we should not have solvent molecules in excess after polymerisation, except for those solvating the primary components. Experimentally [1, 2, 9] it has been proved how slowly the polymerisation with this kind of transfer agents develops.

(b) The g_3, not x-dependent, is an hypothesis which yields to eliminate ring formation, but accepts ramificated polymers. If we neglect completely this factor we admit ring polymer formation but we will obtain the same result.

The g_3 is a combinatorial factor:

$$g_3 = C^1_{\Sigma n_i p_i}\, C^2_{\Sigma n_i p_i - \Sigma n_i} = \frac{x(x-1)}{2}\sum n_i \tag{20}$$

which complicates the partition function but does not make the summing up impossible and finally includes an unessential factor.

(c) We can adopt another manner, namely to consider the remaining monomers like $p = 1$ — polymers and to reconsider the average degree of polymerisation. This method is not normally used.

Concluding remarks

To some extent we can justify the placement of monomer into the primary lattice using a model in which we assume that polymer and monomer molecules can not exist in solution without being solvated, namely surrounded by enough solvent molecules.

Having in mind a supplementary hypothesis on different energies in screened or unscreened cases — we thus adopt a point of view in which the model is more elastic and which corresponds to different energies for various solvated molecules.

We have also made the assumption that polymerisation does not modify the energies between the new formed polymer and the lattice It is a restrictive hypothesis — which from the demonstration developed so far is obviously not essential. [11, 12].

Including new parameters would complicate the expressions concerning energies and maybe would make more accurate a relation which only hopes to describe an exact soluble model.

Limiting polymerisation to some types of reactions we look for the elimination of a real complication — the presence of the initiator or catalyst. This will constitute the aim of a future paper.

The relation (18) is close to Mayo's formula which has experimental verifications. However there are differences which have to be elucidated. In our case we deal with the equilibrium between the monomer and the polymer, indicating high concentrations for the polymer, while in the experimental verifications the polymer leaves partially the solution not participating in establishing the equilibrium with its whole quantity. We can find experimental confirmations in the dependence on temperature and in those experiments corelated to the coordination parameter (1).

REFERENCES

1. P. J. FLORY, *Principles of Polymer Chemistry*, Cornell Univ. Press Ithaca N.Y. 1953.
2. B. VOLMERT, *Grundniss der Mmacromolecularen Chemie*, Springer Verlag, Berlin, 1962.
3. C.A. STĂNESCU to be published.
4. B. WIDOM, J. Chem. Phys. 46, 3324, 1967.
5. R. K. CLARK, J. Chem. Phys. 48, 741, 1968.
6. G. NEECE, J. Chem. Phys., 47, 4112, 1967.
7. J. C. WHEELER, R. B. GRIFFITH, Phys. Rev. 170, 249, 1968.
8. C.A. STĂNESCU, to be published.
9. C. SIMIONESCU, C. V. OPREA, *Tratat de chimia compușilor macromoleculari*, E.D.P., București, 1972.
10. F. R. MAYO, J. Am. Chem. Soc., 65, 2324, 1943.
11. M. L. HUGGINS, J. Phys. Chem. 75, 389, 1971.
12. M. L. HUGGINS, Polymer 12, 389, 1971

ANALELE UNIVERSITĂŢII BUCUREŞTI, FIZICĂ XXIX, 1980, PAG. 81–87

ETUDE DES INTERFACES DES MICRODOMAINES DE SEGREGATION D'UN COPOLYMERE SEQUENCE ORGANISE

LIVIA IONESCU, I. C. PETREA, E. BARNA

Faculté de Physique, Université de Bucarest

RÉSUMÉ

Les copolymères séquencés sont des systèmes capables, dans certaines conditions, de mésomorphisme. La ségrégation des séquences, caractéristique essentielle des copolymères séquencés, mène à l'apparition des interfaces à l'échelle moléculaire. La ségrégation est associée à la tendence des copolymères séquencés à l'état organisé d'adopter quelques structures bien définies : lamellaire, à cylindres, à sphères.

La diffraction des rayons X aux petits angles de Bragg, appliquée au copolymère polystyrène-polyisoprène à structure lamellaire, a permis tout d'abord de caractériser la conformation des chaînes macromoléculaires à l'interface des phases et ensuite d'évaluer avec précision l'épaisseur des interfaces diffuses. On a trouvé ainsi qu'à l'équilibre, les interfaces sont nettes, ce qui indiquairait une ségrégation prononcée des séquences.

I. L'état mésomorphe de la matière

Les composés chimiques capables de mésomorphisme peuvent être partagés, sauf quelques exceptions, en deux grands groupes. Le premier contient des substances comme le paraazoxyphénétole (1), dont les molécules filiformes sont constituées d'une partie rigide et polarisable prolongée, d'habitude, par des chaînes paraffiniques. Le deuxièmeme groupe réunit des systèmes comme le stéarate de sodium (1), ayant une structure identique aux savons et dont les molécules possèdent une chaîne paraffinique terminée par un groupe ionique.

Généralement on admet que le premier groupe appartient aux systèmes mésomorphes de type thermotrope, réalisés par la variation de la température des substances mésogènes ; l'autre groupe comprend les systèmes appelés mésophases lyotropes, obtenus par la variation de la concentration de certaines solutions. L'étude comparative des caractéristiques physiques-structurales des systèmes thermotropes et lyotropes est compliquée par les nombreuses similitudes rencontrées au niveau de la configuration et de l'organisation moléculaire ; l'alignement, l'ordre de position et d'orientation des molécules sont des caractéristiques primordiales.

---

* Centre National de Physique, Măgurele, Bucarest, P.O.Box. 5211.

En 1922 Friedel (2) distinguait parmi les mésophases, la phase smectique semblable par structure et comportement aux savons (σμηγμα = = smegma en greque signifie savon).

Les propriétés des smectiques sont dues essentiellement à leur caractère amphiphilique. Leurs molécules sont constituées de deux parties distinctes : une chaîne paraffinique, longue et hidrophobe, et un groupe terminal polaire, hidrophile et généralement ionique. Ces deux parties sont chimiquement différentes, ainsi que leur incompatibilité (elles sont insolubles l'une dans l'autre) mène à une ségrégation en microdomaines distinctes ; ceux-ci sont capables, dans certaines conditions, de conserver leurs propriétés et leur comportement spécifiques. Dans certaines circonstances ils peuvent cristalliser, ou rester à l'état amorphe, peuvent se dissoudre, ou rester insolubles dans un solvant ajouté au système. Etant donnée la liaison covalente qui réunit cependant les microdomaines au sein d'une même molécule, la ségrégation mène tout simplement à l'apparition d'interfaces qui délimitent les microdomaines de ségrégation, les molécules se disposant de part et d'autre de ces interfaces. La diffraction des rayons X par ces systèmes (3) a montré qu'en présence de l'eau, les interfaces ont des formes géométriques bien précises : plane, cylindrique, sphèrique, les microdomaines étant distribués périodiquement dans l'espace.

Les copolymères séquencés sont des systèmes constitués d'entités structurales chimiquement différentes et réunies dans de grandes séquences (blocs), tel qu'il résulte de la représentation schématique usuelle :

A ..... AAAAAAABBBBBBB . . . .B ;

les séquences sont réunies par des liaisons covalentes. Cette représentation appartient à un copolymère biséquencé contenant une chaîne macromoléculaire A liée par une covalence à une chaîne B.

La structure moléculaire des copolymères séquencés se ressemble, de plusieurs points de vue, avec la structure des smectophases. Les études de diffraction des rayons X aux petits angles de Bragg effectuées sur le copolymère sequencé polystyrène-polyethilèneoxyde, montrent que la structure de tels systèmes est similaire à celle des savons (4).

II. Proces et effets d'interface associés à la segregation et à l'organisation des copolymères séquencés

II.1 — Incompatibilité et ségrégation.

La caractéristique essentielle des copolymères séquencés réside dans le fait que leurs séquences, chimiquement différentes (donc incompatibles), se repoussent et se séparent spontanément, pour former des microdomaines distinctes. Reunies cependant au sein de la même molécule par des liaisons covalentes, celles-ci ne conduisent pas à une démixtion véritable, avec apparition de phases macroscopiques ; les microdomaines, ayant des dimensions comparables avec celles des chaînes macromoléculaires, assurent une certaine homogénéité macroscopique du système. Pareil au cas des smectiques, la ségrégation des copolymères séquencés mène à l'apparition des interfaces à l'échelle moléculaire.

Les données expérimentales confrontées par différentes techniques de laboratoire confirment ce fait. Ainsi, la diffraction des rayons X sur les copolymères séquencés révèle la localisation préférentielle du phénomène de diffraction dans le domaine des petits angles, où devienent visibles les interactions se manifestant à l'échelle 100 – 500 Å (4). Cela montre que la densité d'électrons dans l'échantillon a des fluctuations à l'échelle moléculaire et donc le système est ségrégé.

II.2 – Organisation des copolymères séquencés.

La ségrégation est cert la plus importante propriété des copolymères séquencés, étant l'expression la plus simple de la constitution chimique particulière de ce type de matériaux et, en même temps, la conséquence imédiate de l'incompatibilité fondamentale de leurs constituents. En même temps, elle est responsable de leur comportement spécifique, de leur originalité, ainsi que de leur utilité dans le domaine des applications techniques.

La ségrégation est d'habitude accompagnée d'une autre propriété caractéristique, à savoir, la tendence des copolymères séquencés de s'organiser. Les microdomaines sont juxtaposés régulièrement et périodiquement dans l'espace (4), donnant lieu exactement au même type de cristaux liquides que ceux rencontrés chez les mélanges binaires savons-eau.

Les diagrammes de rayons X montrent que, dans la région des petits angles qui contient toutes les informations concernant les fluctuations de la densité des électrons dues à la ségrégation, la reflexion des rayons X apparaît dans un domaine angulaire étroit, autour de quelques directions caractéristiques définies par la loi de Bragg. Ces diagrammes peuvent contenir jusqu'à 15 (quelquefois même plus de 15) raies de diffraction, indiquant des structures qui peuvent être décrites complètement et comentées dans les termes cristallographiques usuels.

Ainsi, l'organisation des copolymères séquencés est decrite par trois types de reseaux cristallines. Le type unidimensionnel consiste d'un système de points équidistants situés sur une droite ; il correspond aux diagrammes de rayons X contenant des raies dont les distances réciproques dans l'espace Bragg se trouvent dans le rapport 1 : 2 : 3. Le reseau bidimensionnel hexagonal est caractérisé par des raies de diffraction dont les distances réciproques sont dans le rapport $1 : \sqrt{3} : \sqrt{5} : \sqrt{7}$. Le troisième type est un réseau cubique classique tridimensionnel caractérisé par des raies de diffraction dont la distance réciproque se trouve dans le rapport $1 : \sqrt{2} : \sqrt{3} : \sqrt{4}$.

Ces réseaux correspondent à des structures bien définies. La première est lamellaire ; la seconde est un assemblage, selon un réseau bidimensionnel hexagonal, de cylindres de longueur indéfinie ; le troisième type de structure correspond à l'assemblage de sphères suivant un réseau cubique.

La position angulaire des raies de diffraction sur les diagrammes de rayons X, fournit des informations concernant la symétrie et la façon d'assemblage des éléments structuraux ; elle permet également le calcul des distances qui séparent ces éléments, de leurs dimensions et surtout, elle rend possible l'évaluation de la densité d'empaquement des chaînes macromoléculaires à l'interface des microdomaines.

II.3 — La structure des copolymères séquencés.

La structure lamellaire constitue un exemple typique de cristal liquide smectique. Elle consiste en deux types de couches juxtaposées périodiquement et alternativement dans l'espace (5) (figure 1). Une des couches contient des séquences A de copolymère, tandis que l'autre contient des séquences B. Par diffraction des rayons X on peut déterminer directement lépaisseur totale $d = d_A + d_B$ des deux couches juxtaposées, et qui forment une lamelle. Lorsque les solvants sont présents dans le système, ils se localisent, en fonction de leur affinité pour les blocs, soit dans les couches A, soit dans les couches B, soit éventuellement dans les deux blocs A et B avec un coefficient de partage p_A (la fraction du solvant localisé dans les couches A).

La diffraction des rayons X permet également de calculer les épaisseurs respectives d_A et d_B des deux souscouches, et avec celles-ci un troisième paramètre, la surface moléculaire spécifique S, fréquement utilisée pour décrire la conformation des chaînes macromoléculaires à l'interface des microdomaines de ségrégation (6). Ce paramètre représente la surface moyenne que l'occupe une macromolécule au niveau de l'interface : plus S est grande, plus les chaînes macromoléculaires sont étendues parallèlement aux interfaces et, par contre, plus S est petite, plus l'extension des blocs dans le sens de l'épaisseur des lamelles est importante.

Pour effectuer un tel calcul, il est nécessaire de connaître quelques paramètres tels que ;

— la composition chimique x_A du copolymère (la composition en masse des blocs A) ;

— la masse moléculaire moyenne en nombre M_A des blocs A ;

— les volumes spécifiques $\bar{v}_A$, $\bar{v}_B$, $\bar{v}_s$ des constituents A, B et respectivement du solvant ;

— la fraction en masse du solvant dans le système 1-c et son coefficient de partage p_A.

En admetant l'hypothèse sur l'additivité des volumes spécifiques partiels des entités dans le système et en s'apuyant sur certaines considérations géomètriques simples. devient évidentes (6, 7) les expressions suivantes :

$$d_A = d\left[1 + \frac{c(1 - x_A)\cdot\bar{v}_B + (1 - c)\,(1 - p_A)\cdot\bar{v}_s}{cx_A\,\bar{v}_A + (1 - c)\,p_A\bar{v}_s}\right]^{-1} \tag{1}$$

$$d_A = d - d_A \tag{2}$$

$$S = \frac{2\,M_A\bar{v}_A}{Nd}\left[1 + \frac{1 - x_A}{x_A}\cdot\frac{\bar{v}_B}{\bar{v}_A} + \frac{1 - c}{c}\cdot\frac{\bar{v}_s}{\bar{v}_A}\cdot\frac{1}{x_A}\right] \tag{3}$$

où N est le nombre d'Avogadro.

Le deuxième type de structure adoptée par les copolymères séquencés, la structure à cylindres, consiste d'un système de microdomaines cylindriques contenant un des blocs, insérés dans la matrice continue formée par l'autre type de blocs, orientés parallèlement les uns par rapport aux autres et assemblés selon un réseau bidimensionnel hexagonal (5) (figure 2). Pareil au cas de la structure lamellaire, un solvant présent dans le système se distribue entre les microdomaines et la matrice continue, d'après son affinité pour les deux blocs.

Dans ce cas, à nouveau, en plus de l'espacement d des axes des deux cylindres voisins, fournie directement par la diffraction des rayons X, peuvent être calculés encore deux paramètres qui caractèrisent la structure, à savoir le rayon R des cylindres et la surface spécifique S (6,7) :

$$R = d\left(\frac{\sqrt{3}}{2\pi}\right)^{1/2}\left[1 + \frac{c(1 - x_i)\cdot\bar{v}_e + (1 - c)\,(1 - p_i)\cdot\bar{v}_s}{c_i\,\bar{v}_i + (1 - c)\,p_i\bar{v}_s}\right]^{-1/2} \tag{4}$$

$$S = \frac{2M_i\bar{v}_i}{Nd}\left[\frac{2\pi}{\sqrt{3}}\left(1 + \frac{1-x_i}{x_i}\cdot\frac{\bar{v}_e}{\bar{v}_i} + \frac{1 - c}{c}\cdot\frac{\bar{v}_s}{\bar{v}_i}\cdot\frac{1}{x_i}\right)\left(1 + \frac{1 - c}{c}\cdot\frac{\bar{v}_s}{\bar{v}_i}\cdot\frac{p_i}{x_i}\right)\right]^{1/2} \tag{5}$$

Dans ces expressions, les indices i et e montrent les blocs qui se trouvent à l'intérieur, respectivement è l'extérieur des cylindres.

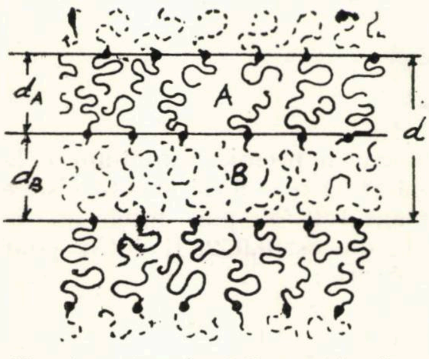

Fig. 1 — Représentation schématique de la structure lamellaire.

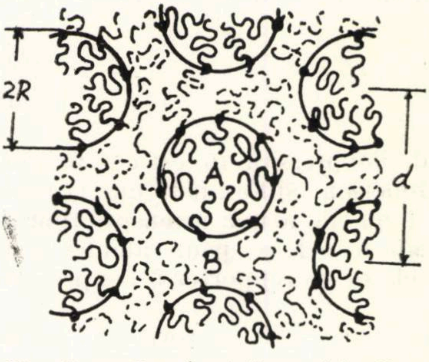

Fig. 2 — Représentation schématique de la structure à cylindres.

La dernière structure observée correspond aux domaines sphériques distribués dans l'espace selon un réseau cubique. Comme précédemment, la diffraction des rayons X permet de déterminer directement l'espacement des centres des sphères a ; ensuite, par calcule, on peut obtenir le rayon R des sphère et la surface moléculaire spécifique (8,9).

III. Caractérisation des interfaces des microdomaines d'un copolymère séquencé à structure lamellaire

Lorsqu'on essaye de caractériser avec précision la structure d'un copolymère séquencé présentant des particularités de smectique ordonné, il est nécessaire de savoir si l'interface des microdomaines est parfaitement nette ou, au contraire, floue et diffuse, autrement dit, si la ségrégation des séquences est totale ou partielle.

La diffraction des rayons X est une technique qui convient pour l'étude de ce problème. Pour illustrer ses possibilités, prenons l'exemple du copolymère biséquencé polystyrène-polyisoprène (PS–PI), de masse moléculaire globale $M_w = 108\,000$, étudié (10, 11) par cette méthode cristallographique.

De structure lamellaire, ce copolymère résulte de la superposition alternée de couches de PS et de PI dont l'épaisseur est respectivement $d_{PS} = 265$ Å et $d_{PI} = 310$ Å. Son paramètre Φ, qui représente la fraction volumique occupée par un des deux types des microdomaines de ségrégation du système, est égale à 0,465.

Dans la radiocristallographie des structures lamellaires, l'intésité I(n) correspondant au n-ième ordre de diffraction est (12) :

$$I(n) = \left[\frac{\sin\, n\pi\Phi}{n\,\pi\Phi} \cdot \frac{\sin n\pi\Phi\,(X/d_{ps})}{n\pi\Phi\,(x/d_{ps})} \right]^2 \tag{6}$$

ici X represente l'épaisseur de l'interface diffuse.

Revenant au copolymère PS-PI étudié, on observe que l'intensité des raies de diffraction décroît de façon monotone à mesure que l'ordre n de diffraction augmente, ce qui signifie que l'intervalle exploré du terme :

$$\frac{\sin n\pi\Phi(X/d_{ps})}{n\pi\Phi\;(X/d_{ps})}$$

de l'expression (6) est compris entre l'origine et le premier minimum de la fonction. Si l'on note que la raie correspondant à n = 9 est encore visible et qu'elle a une intensité approximativement 100 fois plus faible que la raie n = 1, on peut calculer la valeur X/d_{ps} qui est 0,052. Il suffit pour cela de se repporter à l'expression (6) et d'écrire :

$$\frac{I(9)}{I(1)} = \frac{\sin^2[9\pi 0{,}465\,(X/d_{ps})]}{9^4 \sin^2[\pi\cdot 0.465(X/d_{sp})]} \simeq \frac{1}{100} \tag{7}$$

Connaîssant $d_{PS} = 265$ Å, on trouve pour l'épaisseur de l'interface diffuse la valeur $X = 14$ Å. Cela signifie que l'épaisseur des interfaces diffuses est, dans le cas présent, extremment faible, puisqu'elle ne dépasse pas la dimension des motives monomères des séquences. On peut constater donc, qu'à l'équilibre, les interfaces des microdomaines sont très nettes.

REFERENCES

O. LEHMANN, Z. Kristallogr., *18*, 464 (1890).
G. FRIEDEL, Ann. Phys. (Paris), *18*, 273 (1922).
A. SKOULIOS, Advan. Colloid Interface Sci., *1*, 79 (1967).
A. SKOULIOS, G. FINAZ, and J. PARROD, C.R. Acad. Sci., *251*, 739 (1960).
A. SKOULIOS and G. FINAZ, C.R. Acad. Sci., *252*, 3467 (1961).
A. SKOULIOS and G. FINAZ, J. Chim. Physicochim. Biol., *59*, 473 (1962).
P. GROSIUS, Y, GALLOT and A. SKOULIOS, Makromol. Chem., 127, 94 (1969).
G. TSOULADZE and A. SKOULIOS, J. Chim. Physicochim. Biol., *60*, 626 (1963).
P. GROSIUS, Y. GALLOT and A. SKOULIOS, Makromol. Chem., 132, 35 (1970).
L. M. IONESCU, A. SKOILIOS, Makromol. Chem., 177, 257 (1976).
L. M. IONESCU, Thèse. Université de Strasbourg, (1976).
A. GUINIER, *Théorie et technique de la radiocristallographie*, Editions Dunod, Paris (1956).

ANALELE UNIVERSITĂŢII BUCUREŞTI, FIZICĂ XXIX, 1980, PAG. 89–98

NOISE REJECTION BY DISCRETE RESTORATION OF SIGNAL SPECTRUM

V. GHEORGHE and S. I. SPÂNULESCU

Faculty of Physics, University of Bucharest *

ABSTRACT

In this paper a general principle for noise rejection and two methods for it's applying are given. For each of them the theoretic considerations are made in a mathematical form, and the main relations necessary for the equippement design are obtained.

1. Introduction

The amplifying and measuring of low signals with a high level of noise represent an important problem in many experiments. For some particular kind of signals several methods have developed, concerning both the amplifying part and the signal from input and in many cases very complex numerical equippement is involved [2, 4].

This problem may be solved sometimes rather easy by the investigation of the signal spectrum and selecting the informations related only to it's harmonic content, followed by the signal restoration, noiseless. Each harmonic component and the noise also presents a time evolution, so the amplitude of the signal is a two variables function $\psi(\omega, t)$ that we will name the spectral body (Fig. 1). The proposed principle for noise rejection involves the selection of the crests from the spectral body by using a chopper that is opened only in the areas with enough great amplitude, above the level of white noise (valleys level). In this way only the important harmonics are selected, and the noise is practically complete rejected.

---

* National Center of Physics, Bucharest, Măgurele, P.O. Box, 5211.

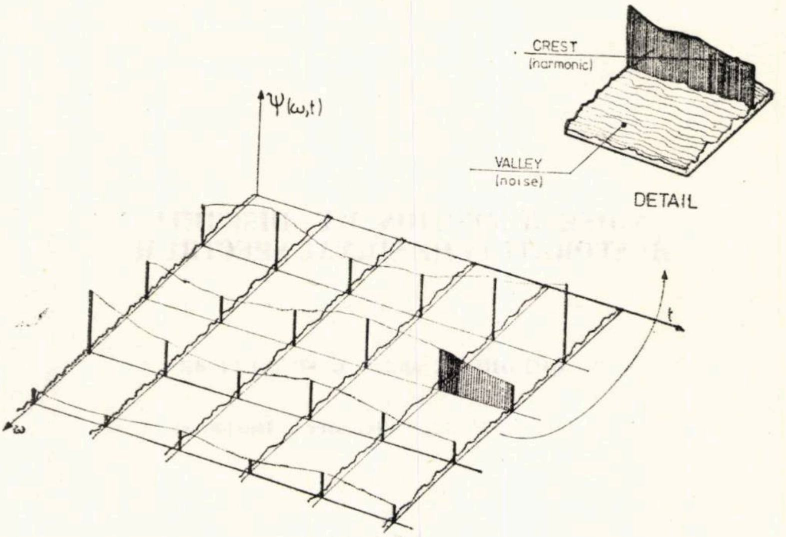

Fig. 1.

2. Spectral body sampling method

Introducing the input signal in a voltage controlled bandpass filter whose central frequency is moved through the spectrum with a sawtooth generator, the output signal will have the form given in figure 2. It can be observed that every harmonic is investigated for a certain period and

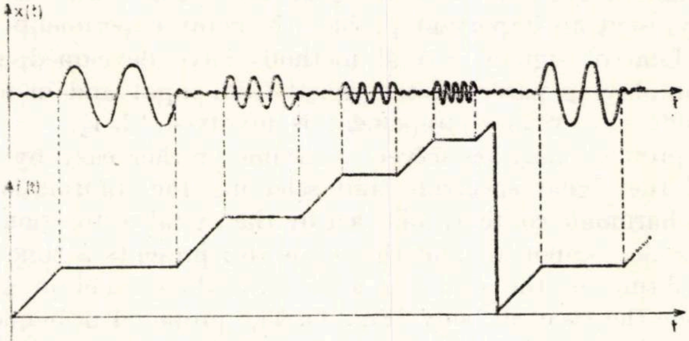

Fig. 2.

samples from each of them may be obtained (Fig. 3). The samples of the harmonics are not sinchronised for the restauration of the spectrum body and that is why they are introduced through a delay line with several inputs, the first harmonic beeing the most delayed and the last is not. The general form of the circuit is given in figure 4.

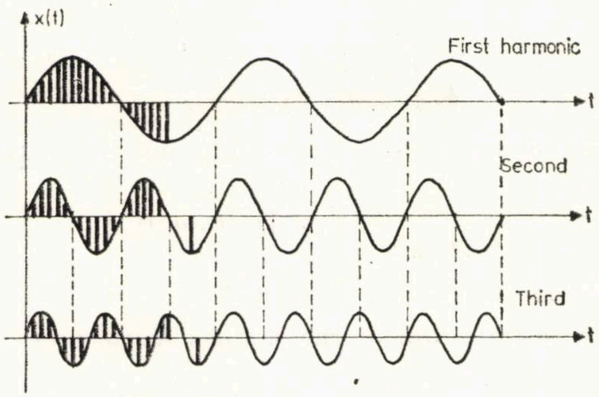

Fig. 3.

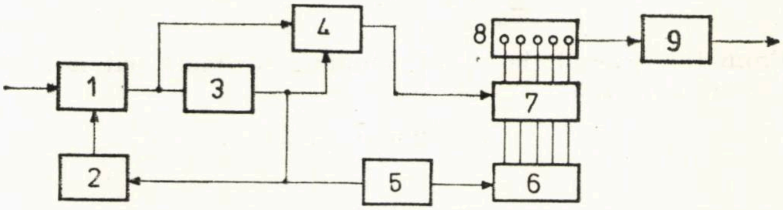

Fig. 4.

1. Voltage controlled filter ; *2.* Control generator ; *3.* Peak detector ; ***4.*** **Sampling circuit ;** *5.* Counter ; *6.* Decoder ; *7.* Gates ; *8.* Delayline ; *9.* **Low-pass filter.**

The spectral function may be written as :

$$\psi(\omega, t) = \begin{bmatrix} \varphi_1 \, [\omega_1(t). \ a_1(t)] \\ \varphi_2 \, [\omega_2(t), \ a_2(t)] \\ \vdots \\ \varphi_m \, [\omega_m(t), \ a_w(t)] \end{bmatrix}$$

with

$$\varphi_i[\omega_i(t), a_i(t)] = a_i(t) \, e^{j[\omega_i(t) \cdot t + \alpha_0^i} \tag{1}$$

The samples are amplitude modulated pulses, so their Fourier series is :

$$\varphi_i^* \, [\omega_i, \ a_i] = \sum_{n=-\infty}^{\infty} C_n^i(t) \cdot a_i(t) \cdot e^{jn\omega_e t} \cdot e^{j\omega_i(t)t} \tag{2}$$

with

$$\mathrm{C}_n^i = \frac{1}{T} \int_0^{Te} \varphi_i[\omega_i(t),\ a_i(t)]\, \mathrm{e}^{jn\omega_e t}\, \mathrm{d}t \xrightarrow[t_0 \to 0]{} z \frac{t_0}{T_e}$$

(t_0 is the durate of the pulse and z its amplitude). The sampled spectral body is

$$\psi^*(\omega,\ t) = \begin{bmatrix} \varphi_1^*\ [\omega_1(t),\ a_1(t)] \\ \vdots \\ \varphi_m^*[\omega_m(t),\ a_n(t)] \end{bmatrix}$$

The Fourier transform of the sampled harmonics

$$F[\varphi_i^*[\omega_i(t),\ a_i(t)]] = \sum_{n=-\infty}^{\infty} \mathrm{C}_n^i \int_{-\infty}^{\infty} a_i(t)\, \mathrm{e}^{j\omega_i t}\ \mathrm{e}^{jn\omega_e t}\, e^{j\omega t}\, \mathrm{d}t =$$

$$= \sum_{u=-\infty}^{\infty} \mathrm{C}_n^i\, A_i(\omega_i - n\,\omega_e + \omega_i) \tag{3}$$

From the general theory of sampling we must put now the well-known condition [1, 3]

$$\omega_e \geqslant 2 \max_{i \in N} (\omega_i(t)) \tag{4}$$

and introducing a low-pass filter with a transfer function

$$H_i(\omega_i) = \begin{cases} \dfrac{T_e}{zt_0} & |\omega_i| \leqslant \omega_f \\ 0 & |\omega_i| > \omega_f \end{cases}$$

the spectral body will be restorated from it's samples.

The demonstration involves the following steps :

We will write $\psi(\omega, t)$ as a vector, considering $\omega_i = \text{const.}$, because ω_e is high

$$\psi(t) = \sum_{i=1}^{m} a_i(t)\, \mathrm{e}^{j\omega_i t} \varkappa_i = \frac{1}{2\pi} \sum_{i-1}^{m} \left\{ \int_{-\infty}^{\infty} A_i\, (\omega + \omega_i(t)) \cdot \mathrm{e}^{j\omega t} \mathrm{d}t \right\} \varkappa_i =$$

$$= \frac{1}{2\pi} \sum_{i=1}^{m} \left\{ \int_{-\infty}^{\infty} F_i^*(\omega + \omega_i(t))\mathrm{e}^{j\omega t}\, H(\omega)\, \mathrm{d}t \right\} \varkappa_i$$

$$\psi(t) = \sum_{i=1}^{m} \left\{ \int_{-\infty}^{\infty} \varphi_i^*(\tau)\, h(t - \tau)\, \mathrm{d}\tau \right\} \varkappa_i \tag{5}$$

where $h(t)$ is the Fourier transform of $H(\omega)$

$$h(t) = \frac{1}{2\pi} \int_{-\infty}^{\infty} H(\omega)\, e^{j\omega t} d\omega = \frac{2T_e}{T_f t_0} \frac{\sin \omega_f t}{\omega_f t}$$

$$\psi(t) = \sum_{i-1}^{m} \left\{ \int_{-\infty}^{\infty} \varphi_i^*(t)\, a_i(t)\, e^{j\omega_i(t)\cdot\tau} \cdot \frac{2T}{T_f t_0} \frac{\sin \omega_f(t-\tau)}{\omega_f(t-\tau)}\, d\tau \right\} \varkappa_i \qquad (6)$$

For $zt_0 = 1$ the samples have the Dirac function form

$$\varphi_i^*(t) \rightarrow \delta_{T_e}(t) = \sum_{n=-\infty}^{\infty} \delta(t - nT_e)\,; \quad C_n = \frac{1}{T_e}$$

Finally the spectral body is obtained from it's samples that go through a low-pass filter

$$\psi(t) = \frac{2T_e}{T_f} \sum_{i=1}^{m} \left\{ \sum_{n=-\infty}^{\infty} \varphi(nT_e) \frac{\sin \omega_f (t - n T_e)}{\omega_f(t - nT_e)} \right\} \varkappa_i \qquad (7)$$

3. Average values cuantizing method

The presented method allows the exactly restoration of the spectral body excepting the noise parts of it, but the complexity of the electronic circuits is rather high. It is necessary a very strictly sincronisation of the samples, which involves the use of precise delay lines, peak detectors and high speed devices. To overcome these dificulties, it is possible to use a method of indirectly restoration of the spectral body with a number of voltage controlled oscillators preceded by sample and hold circuits and followed by voltage controlled amplifiers. The whole system approximates the amplitude and frequency of every harmonic component as a cuantization of them (Fig. 5).

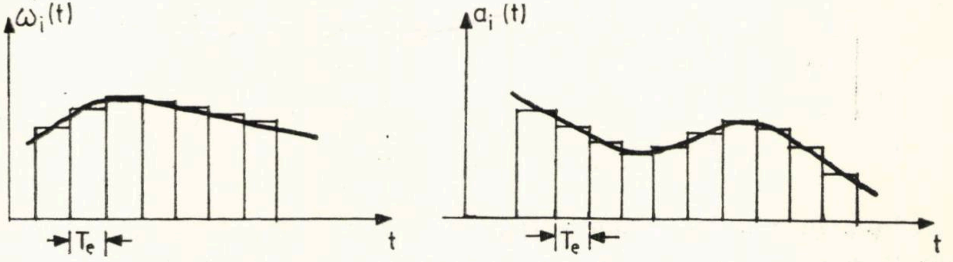

Fig. 5.

The information necessary for this process is given by frequency and amplitude detectors, each driven by a band-pass filter locked on a certain harmonic in the spectrum. Such a circuit is shown in a general form in figure 6. It is not necessary to use as many filters and detectors as the harmonics are. It is enough to drive a voltage controlled filter with sawtooth waves and at each maximum in the amplitude detector to give that information to a certain oscillator.

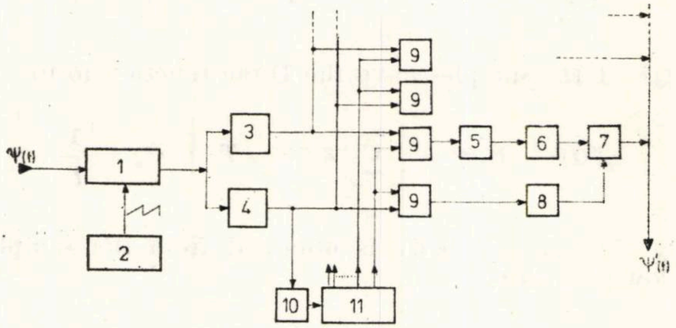

Fig. 6.

1. Voltage controlled filter; *2.* Sawtooth generator; *3.* Frequency detector; *4.* Amplitude detector; *5.*, 8. Sample and hold circuits; *6.* Voltage controlled oscillator; *7.* Voltage controlled amplifier; *9.* Analog gates; 10. Peak detector; *11.* Shift register.

This principle does not involve high quality circuits working too precisely for correct response. But it can be observed that systematic errors occurs as a noise due to the cuantizing process. This noise is given by the difference between the continuous and the step approximated signals and it is a sawtooth with slow variable amplitude as is shown in figure 7.

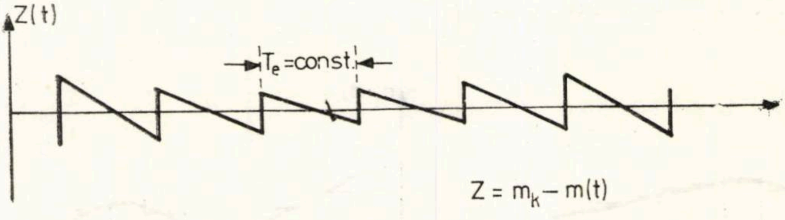

Fig. 7.

We used in the whole period $[kT_e, (k+1)\,T_e]$ the same value of the frequencies and amplitudes that exists in the moment $kT_e + \theta_k T_e$ with $0 < \theta_k < 1$, so, $t \rightarrow kT_e + \theta_k T_e$ and $m_k = m(kT_e + \theta_k T_e)$.

As it may be seen, the detectors will give the information as an average value over a period of each harmonic, so the total information will be the average of the whole spectrum

$$m(t) = \int_{t}^{t+T_e} \psi(t)\,\mathrm{d}t \tag{8}$$

$$m_k = \int_{kT_e}^{(k+1)\,T_e} \psi(t)\,\mathrm{d}t \tag{9}$$

The probability for $t \in [kT_e, (k+1)\,T_e]$ is known from the analog to digital converters, so we calculated the noise from the general relations [1, 4]

$$P(m_k) = \int_{kT_e}^{(k+1)\,T_e} w\,[m\,(t)] \cdot \mathrm{d}m\,(t)$$

$$W(z) = \omega[m(t)] \cdot \frac{1}{\left(\frac{dz}{dt}\right)} \quad \text{— density of probability}$$

$$\Phi z(u) = \int_{-\infty}^{\infty} \mathrm{e}^{juz}\, W(z)\,\mathrm{d}z \quad \text{— characteristic function}$$

$$M(z) = -\,j\,\left.\frac{\partial \Phi_z(u)}{\partial u}\right|_{u=0} \quad \text{— average value of the noise}$$

$$M(z^2) = -\left.\frac{\partial^2 \Phi_z(u)}{\partial u^2}\right|_{u=0} \quad \text{— square average value}$$

$$\sigma = \sqrt{M\,(z^2)} \quad \text{— effective value of noise}$$

By applying them to our problem, we obtain

$$W_k(z) = \omega[m(t)] \cdot m'(t) \cdot \mathrm{rectg}\,\frac{z}{T_e}\,m'(t)$$

$$W(z) = \sum_{k=-\infty}^{\infty} W_k(z) = \sum_{k=-\infty}^{\infty} \frac{1}{2\pi} F_z\left\{\Phi^*\,(u) \cdot \mathrm{e}^{jum\,[(k+\theta_k)T_e]}\right\} \cdot$$

$$\cdot\; m'(t) \cdot F\left\{\frac{T_g}{2\pi}\,\frac{\sin\frac{n\;T_e}{2}}{\frac{n\;T_e}{2}}\right\} \tag{10}$$

where we used some general known relations, in the form

$$\operatorname{rectg}\frac{z}{T_e}=F\left\{\frac{T_e}{2\pi}\,\frac{\sin\dfrac{n\,T_e}{2}}{\dfrac{n\,T_e}{2}}\right\}.$$

$$\omega(x-z)=\frac{1}{2\pi}\,F_z\{\Phi^*(u)\,\mathrm{e}^{jux}\}^2.$$

Taking for $m'(t)$ the value $[\psi(t+T\ )-\psi(t)]$ we obtain

$$W(z)=\frac{T_e}{4\pi^2}\sum_{k=-\infty}^{\infty}[\psi((k+1)\,T_e)-\psi(kT_e)]\cdot F_z\left\{\int_{-\infty}^{\infty}\Phi^*(\lambda)\cdot\right.$$

$$\left.\cdot\ e^{j\lambda m[(k+\theta_k)T_e]}\cdot\frac{\sin(\mu-\lambda)\dfrac{T_c}{2}}{(u-\lambda)\dfrac{T_e}{2}}\,\mathrm{d}\lambda\right\} \tag{11}$$

The characteristic function will be

$$\Phi_z(u)=\frac{T_e}{4\pi^2}\int_{-\infty}^{\infty}\sum_{k=+\infty}^{\infty}[\psi((k+1)\,T_e)-\psi(kT_e)]\cdot\mathrm{e}^{-jum(t)}\,\cdot$$

$$\cdot\,2\pi\,\Phi_m^*(\lambda)\,\mathrm{e}^{j(\lambda+u)m[(k+\theta_k)T_e]}\cdot\frac{\sin(u-\lambda)\dfrac{T_e}{2}}{(u-\lambda)\dfrac{T_e}{2}}\,\mathrm{d}\lambda. \tag{12}$$

where :

$$\Phi_m^*(\lambda)=\frac{1}{2\pi}\,\frac{\displaystyle\int_{-\infty}^{\infty}\Phi^*(\lambda)\cdot\mathrm{e}^{j(\lambda+u)m[(k+\theta_k)T_e]}\,\frac{\sin(u-\lambda)\dfrac{T_e}{2}}{(u-\lambda)\dfrac{T_e}{2}}}{\mathrm{e}^{j(\lambda+u)m[(k+\theta_k)T_e]}\cdot\dfrac{\sin(u-\lambda)\dfrac{T_e}{2}}{(u-\lambda)\dfrac{T_e}{2}}}$$

Introducing $\textcircled{H}_k$ by the relation

$$m[(k+\theta_k)T_e] = km_0 + \textcircled{H}_k T_d = km^* T_e + \mathrm{H}_k T_e \tag{13}$$

the characteristic function is

$$\Phi_z(u) = \sum_{k=-\infty}^{\infty} \frac{1}{m^*}[(\psi((k+1)\,T_e) - \psi(kT_e)]\Phi_m\left(\frac{2k\pi}{m^* T} - u\right)\cdot \mathrm{e}^{jum(t)} \cdot$$

$$\cdot\, \mathrm{e}^{-j2k\pi\frac{H_k}{m^*}} \cdot \frac{\sin\left(uT_e - \dfrac{k\pi}{m^*}\right)}{uT_e - \dfrac{k\pi}{m^*}} \tag{14}$$

The average value of the noise is

$$M(z) = T_e \sum_{k=-\infty}^{\infty} \frac{1}{k\pi}\Phi_m\left(\frac{2k\pi}{m^* T_e}\right)[\psi((k+1)\,T_e - \psi(kT_e)]\cdot \mathrm{e}^{j2k\pi\frac{H_k}{m^*}} \cdot$$

$$\left\{j\left[\sin\frac{k\pi}{m^*} + \frac{m^*}{k\pi}\cos\frac{k\pi}{m^*}\right] - \frac{m(t)}{T_e}\sin\frac{k\pi}{m^*}\right\}. \tag{15}$$

The square average value can be written as

$$M(z^2) = \sum_{\partial=-\infty}^{\infty} \frac{1}{k\pi}\,[\psi((k+1)\,T_e) - \psi(kT_e)]\mathrm{e}^{-j2k\pi\frac{H_k}{m^*}} \cdot$$

$$\Phi_m\left(\frac{2k\pi}{m^* T_e}\right)\cdot\left\{\sin\left(\frac{k\pi}{m^*}\right)\left[\frac{m^*}{k\pi}\cdot jm(t)\,T_e - m^2(t) + \right.\right.$$

$$\left.\left. + T_e^2\left(\frac{m^*}{k\pi}\right)^2 - T_e^2 + T_e\cos\left(\frac{k\pi}{m^*}\right)[(1+j)\,m(t) - T_f]\right\} \tag{16}$$

For an enough low T_e we can consider that the amplitude of the cuantization noise is slowly varying in time, so

$$\psi((k+1)\,T_e) - \psi(kT_e) \approx \Delta\psi(T_e)$$

and we obtain the relation

$$(u) = \Delta\psi\,(T_e)\cdot\frac{\mathrm{e}^{-jum(t)}}{m^*}\sum_{k=-\infty}^{\infty}\Phi_m\left(\frac{2k\pi}{m^*} - u\right)\cdot$$

$$\cdot\, e^{j1k\pi\frac{Hk}{m^*}} \cdot \frac{\sin\left(uT_e - \frac{k\pi}{m^*}\right)}{uT_e - \frac{k\pi}{m^*}} \tag{17}$$

The relation (17) has a formal resemblance with the known characteristic function from the analog to digital convertor, where the effective value of the noise is [1]:

$$\sigma_y = \frac{T_e}{\sqrt{3}}$$

In our case the problem is more complicated, so the effective valul of the noise is

$$\sigma = \frac{T_e}{\sqrt{3}}\, \Delta\psi\,(T_e)\, \frac{dm(t)}{du}\bigg|_{u=0} \cdot \frac{m(t)}{m^*} \tag{18}$$

This is the minimum of the noise, that we obtained for a null characteristic function of the input signal $\Phi_m\left(\frac{2k\pi}{m^*} - u\right)$ which involves a frequency limited distribution of it (this is the real physical case) [1].

The formula (18) can be used in the design of the circuits giving the maximum value of sample period for an imposed cuantizing noise.

4. Conclusions

Two methods of restoration the spectrum of a signal rejecting it's noise are presented, and the calculus for their implementing are given. According to the necessities of the system performances a practical project with the requirements given by the final relations can be made with the commonly electronic technics.

REFERENCES

1. E. POP, V. STOICA, *Principii și metode de măsurare numerică*, Timișoara, Ed. Facla, 1977
2. O. RADU, GH. SĂNDULESCU, *Filtre numerice*, București, Ed. Tehnică, 1979.
3. I. MARGHESCU, GH. BĂDESCU, *Transmiterea discretă a semnalelor*, București, Ed. Tehnică, 1978.
4. I. ANGHELOIU, E. OANCEA, *Informație și semnal*, București, Ed. Militară 1966.

Received, January 31, 1980

ANALELE UNIVERSITĂŢII BUCUREŞTI, FIZICĂ XXIX, 1980, PAG. 99–106

TRANSMEMBRANE POTENTIAL MEASUREMENT THROUGH A COLLAGEN MEMBRANE

SILVIA INDREI, V. GHEORGHE

Faculty of Physics, University of Bucharest *

GABRIELA ANGEL

Institute for Biological Sciences Bucharest

ABSTRACT

Membranes with a large content of collagen are used, in vitro, as a model of electric charged membranes. We measured the transmembrane potential in case of spontaneous diffusion of ions. We used a simplified theory of Teorell, Meyer and Sievers [1] to compute the diffusion potential and the efective fixed electric charge density. The computed electric charge density was negative and the mobilities of two different cations (Na^+ and K^+) were almost the same through the membrane. So, we concluded that the membrane has pores with a diameter larger than that of the ions in study.

Introduction

Collagen utilization on a large extent in medicine and bioengineering, as a biomaterial, led to the necessity of knowledge of the effective electric charge of both collagen fibers and membranes. By effective fixed electric charge we understand the electric charge associated with the material in its natural chemical medium. This electric charge is reflected in measurable macroscopic properties, as electrical resistance, transport properties, membrane potential and mechanical response to applied electrical stimuli Such informations are necessary in applications connected with its electrochemical and electromechanical properties, so as in the study of other chemical properties (crosslinks density) which involves charged groups.

---

* National Center of Physics, P.O. Box 5211, Măgurele, Bucharest.

The present paper proposes a relatively simple technique of characterization of fixed charge and transport properties of a synthetic collagen membrane. The technique is based on the measurement of transmembrane potential in case of spontaneous diffusion. Measured transmembrane potential, V_0, for different gradients of concentration and pH are presented. With a simplified form of Teorell-Meyer-Sievers theory (1) we compute the diffusion potential $\Delta\Phi_{diff}$ and the effective fixed electric charge density $\bar{\rho}_m$ on collagen membrane. Thes evalues present a practical importance in comparing the same material subjected to different chemical processes, or distinct polyelectrolitic materials in the same experimental conditions.

Materials and Methods

The membranes under study consisted of collagen and glycerine, 1 : 1 w/w, 20 μm dry thickness.

The experiments were performed in a Ussing-like cell with two compartments (figure 1). The electrodes were placed at the ends of the cell, 5 cm from the membrane. The membrane was situated between the two compartments, protected by one pair of rubber rings. The useful area of the membrane was about 0,78 cm^2, and the compartments volumes of 27 ml, respectively 24 ml.

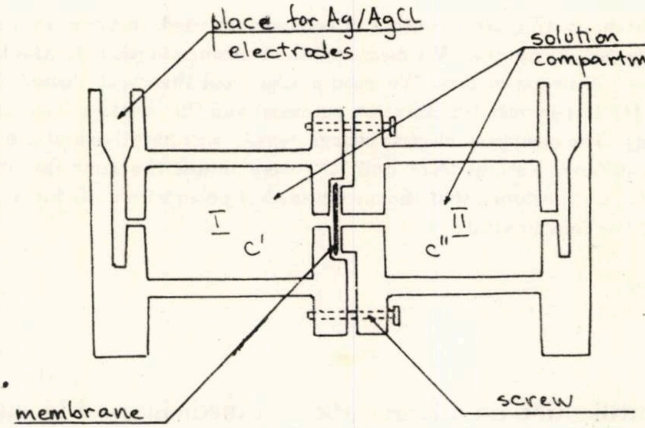

Figure 1. Transverse section through the Ussing-like cell utilized in determinations of transmembrane potential.

We used reversibile Ag/AgCl electrodes freshly clorurated before each set of determinations. Cloruration was made for 30 min at a current intensity of 2,5 mA, in a 0,75 HCl solution [2]. The electrodes asymmetry was less than 2 mV for a good cloruration ; that potential of asymmetry was subtracted from the measured one to obtain V_0. A Sephram-Graphispot II (internal resistance 1 MΩ) instrument was used to measure and record potentials. V_0 was measured always after reacing the equilibrium potential; the durate of stabilization was 15–20 min.

The measured potential V_0 involves the contribution of electrode-electrolite reaction, such as membrane potentials:

$$V_0 = -\,\Delta_{Nernst} + \Delta_{memb}$$

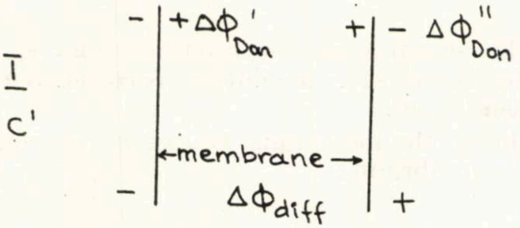

Figure 2. The components of membrane potential: Donnan and diffusion potentials (the membrane has a finit thickness, and the two interfaces are in contact with different concentrations).

The contribution of electrode-electrolite reaction to the potential, that is the Nernst potential [1], in each determination with Ag/AgCl electrodes, represents more than half of the measured potential.

To verify the calculated membrane potential, we emploied a pair of calomel electrodes in saturated KCl solution, bound to the cell by 2% agar bridges. The calomel electrodes were connected to a Corning model 12 pH-meter. It is considered that these reference electrodes give directly the membrane potential, without the influence of the electrolite. The results obtained with the two types of electrodes on tested solutions coincide untill ± 1 mV. All the determinations were made at room temperature, 25°C.

We measured the transmembrane potential for different gradients of concentration between the two compartments. We also measured biionic potential, between NaCl and KCl solutions, 10 mM, at the same pH.

The pH correction was carried out using NaOH, respectively HCl solutions and measured with a Radiometer PHM 63 pH meter, with the precision of ± 0,01 pH units. The increase in the concentration of the ionic solutions was less than 2%, then it was considered negligible in the calculus.

The diffusion potential $\Delta\Phi_{diff}$ and the effective fixed electric charge density $\overline{\rho}_m$ was calculated in a simplified form of Teorell-Meyer-Sievers theory [1]:

$$V_0 = \Delta\Phi_{diff} + (\Delta\Phi'_D - \Delta\Phi''_D) - \frac{RT}{F}\ln\frac{a''_{Cl}}{a'_{Cl}}, \tag{1}$$

where $\Delta\Phi'_D$ and $\Delta\Phi''_D$ are the Donnan potentials at the two interfaces (figure 2) and a'_{Cl}, a''_{Cl} the activities of Cl^- in bulk solutions. The later term represents the Nernst potential $\Delta\Phi_{Nernst}$.

From the theory mentioned above, and with the Henderson conditions :

$$\Delta\Phi_{diff} = \frac{RT}{F}\,\frac{\sum\limits_i \left(\frac{\bar{u}_i}{z_i}\right)(\bar{a}_i'' - \bar{a}_i')}{\sum\limits_i \bar{u}_i(\bar{a}_i'' - \bar{a}_i')}\ln\frac{\sum\limits_i \bar{u}_i\bar{a}_i''}{\sum\limits_i \bar{u}_i\bar{a}_i'}, \tag{2}$$

where $\bar{a}_i'$. $\bar{a}_i''$ are the activities at the interfaces and $\bar{u}_i$ the mobility of ion i within the membrane. (The mobility u_i is considered the same inside and outside the membrane).

On the left side of the membrane we can write, considering instantaneously Donnan equilibrium :

$$r' = \frac{\bar{a}_{i+}'}{a_{i+}'} = \frac{a_{i-}'}{\bar{a}_{i-}'} \tag{3}$$

$$\Delta\Phi_D' = -\frac{RT}{F}\ln r' \tag{4}$$

$$r' = \frac{\bar{\rho}_m}{2a'} + \sqrt{1 + \left(\frac{\bar{\rho}_m}{2a'}\right)^2} \tag{5}$$

with a_{i+} and a_{i+} activities of cations and anions inside the membrane, and $a' = \sum\limits_i a_{i+}' = \sum\limits_i a_{i-}'$ (the last egality arising from the electroneutrality condition) the activity of ion in the left compartment.

The steps in the iteration proceeding are the following : we choose a $\Delta\Phi_{diff}$ and from relation (1) we compute $(\Delta\Phi_D' - \Delta\Phi_D'')$ depending on V_0 and $\Delta\Phi_{Nernst}$. Solving the equations (4) and (5) and the analogous equations at the right interface, we can determine $\bar{\rho}_m$, as a function of $(\Delta\Phi_D' - \Delta\Phi_D'')$, a' and a''. With that $\bar{\rho}_m$ we can calculate $\bar{a}_i'$, $\bar{a}_i''$ from (3) and the analogous value at the right interface. These values will be introduced in equation (2) and will determine a new $\Delta\Phi_{diff}$. The iteration stops when the value of $\Delta\Phi_{diff}$ from the beginning and the calculated one are close enough. The values of ion activity and mobility are taken from tables [3].

Considering only one kind of ions in each compartment, A respectively B, one obtains with (2) :

$$\Delta\Phi_b = \frac{RT}{F}\ln\frac{a_A\gamma_B\bar{u}_A}{a_B\gamma_A\bar{u}_B} \tag{6}$$

where $\gamma = \frac{a}{c}$ is the "activity coefficient" ; the other symbols correspond to that introduced before. $\Delta\Phi_b$ is called biionic potential and this value is proportional with the ratio of the mobilities which is finally proportional with the ratio of the permeabilities.

Results and Discussion

The results of measuring the transmembrane potential at some distance from the membrane, for different gradients of concentration, are presented in table 1. One can observe (figure 3) that the measured potential V_0 and the membrane potential $\Delta\Phi_{memb}$ varies un, lineary, as a function of $\lg \frac{c'}{c''}$. This fact is in accordance with other observations made on fixed electric charge membranes [4]. For bigger concentration gradients, e.g. 100 mM versus 0.01 mM, it could be explained in terms of variable electric charge density of the collagen molecule with the ionic strength of solution $\left(I = \frac{1}{2} \sum_i c_i z_i^2\right)$. If the ionic strengths of solutions from the two compartments are very different, it can be expected that the charges fixed at the interfaces are very different, and as a consequence, the potential will change unlineary with the concentration ratios.

Table 1

The measured potential V_0 and the membrane potential as a function of $\lg \frac{c'}{c''}$

Crt. no.	c′ (mM)	c″ (mM)	$\lg \frac{c'}{c''}$	V_0 (mV)	$\Delta\Phi_{memb}$(mV)
1	100	0.01	4	100	−124.5
2	100	0.1	3	102	− 65
3	200	2	2	78.5	− 30
4	200	20	1	51	− 2
5	100	20	0.7	35	− 5
6	20	200	−1	− 49	+ 4
7	0.1	200	−3.3	−113	+ 69.5

It can be stated that, within experimental errors, (table 1), the membrane is simetrical, i.e. re-

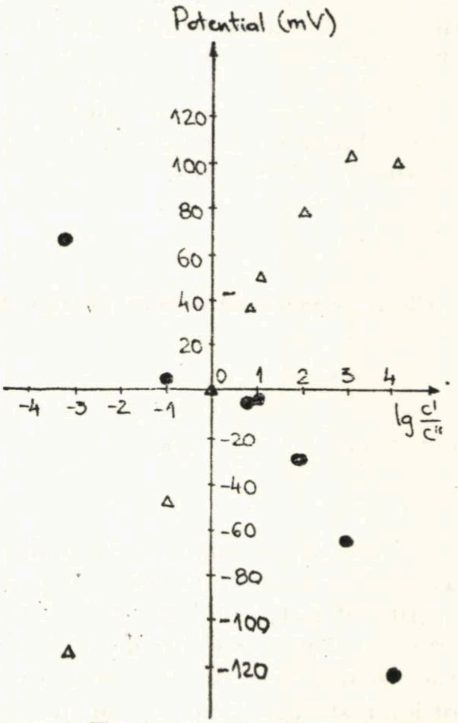

Figure 3. The change of the measured potential $V_0(\Delta)$and the membrane potential $\Delta\Phi_{memb}(\circ)$ as a function of lg c'/c''.

versing the concentration gradient we obtain the same potential (in modulus).

Table 2 presents the measured (V_0) and the membrane ($\Delta\Phi_{memb}$) potential variations depending on pH. It will be observed the decrease, in absolute value, of membrane potential, $\Delta\Phi_{memb}$, with pH (figure 4), in accordance with results on other types of collagen membranes [5]. This my be explained by a modification of the effective fixed electric charge on membrane [5].

Table 2

The change of $\Delta\Phi_{memb}$ and V_0 with the pH, for an initial gradient of concentration of NaCl 10 mM–5mM

Salt	Concentrations	$\Delta\Phi_{memb}$(mV)	V_0 (mV)	pH
NaCl	10 mM–5 mM	−26	16	4.3
		−24.5	17.5	6.0
		−22	20	7.1
		−13	29	7.65

The results regarding the biionic potential, as well as the mobility ratio (relation 6) for the two cations, are presented in tabel 3. The ratio of the cationic mobilities approaches the unity, i.e. both cations cross the membrane with similar speed. Analogous results have been obtained in some studies on cell wall of Nitella flexibilis [4]; the authors concluded that the "permeation channels" of the wall are highly hydrated and the permeability of the cations does not depend on the stength of the field of the fixed charges.

Table 3

Biionic potential and mobility ratio for NaCl and KCl at equal concentrations and pH

Salts	c	pH	$\Delta\Phi_{memb}$(mV)	u_k/u_{Na}
KCl–NaCl	10 mM	6.1	+2	1.08

We also estimated by calculus $\Delta\Phi_{memb}$ and $\bar{\rho}_m$ for two cases (table 4). The concentration in one compartment was maintained constant ($c' = 10$ mM NaCl) and in the other compartment we choosed two concentrations (5 mM and 1 mM). The pH was constant in the first respectively the second case. In this way we have evidenced the cumulative effect of ionic strength and pH on the fixed effective electric charge density $\bar{\rho}_m$. The values for $\Delta\Phi_{memb}$ calculated are in accordance with typical values for $\Delta\Phi_{memb}$ calculated for protein membranes [6].

Table 4

The diffusion potential $\Delta\Phi_{\text{diff}}$ and the effective fixed electric charge density for the collagen membrane, c = 10 mM

Salt	c″ (mM)	$\Delta\Phi_{memb}$(mV)	pH	$\Delta\Phi_{diff}$(mV)	$\bar{\rho}_m$, (mols/l)
NaCl	5	−13	7.65	1.979	−23.76
	1	−7	5.5	11.54	− 1.78

It is remarcable that the sign of the effective fixed electric charge, as obtained in our experimental conditions, is negative.

From calculus it results also the variation of ionic activities at the interfaces (figure 5), according to Henderson conditions. The behaviour of NaCl salt towards the collagen membrane with effective fixed electric charge is similar to other types of synthetical membranes with electric charge [1].

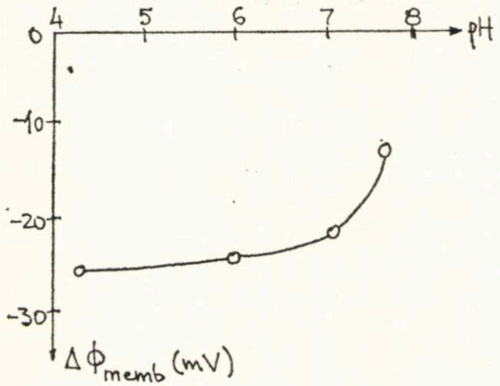

Figure 4. The change of membrane potential $\Delta\Phi_{memb}$ with the pH. The initial gradient of concentration was10 mM−5 mM.

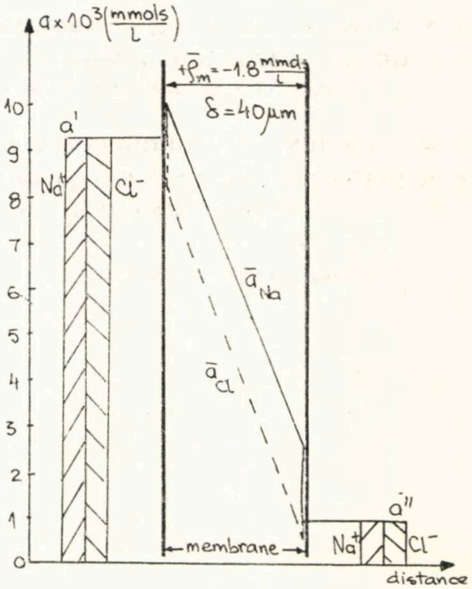

Figure 5. The change of ion activities (Na^+ and Cl^-) inside the collagen membrane (the gradient of concentration was 10 mM−1 mM). We supposed a linear change of the potential inside the membrane Henderson conditions).

Conclusion

We have studied the variations of membrane potential on synthetic collagen membrane depending on two important parameters : the gradient of concentration and the pH. The unlinear, change, of the membrane potential as a function of these parameters is in accordance with the studies on other types of protein membranes.

By means of a relatively simple theory we have calculated the diffusion potential and the effective fixed electric charge density in the membrane. The density $\bar{\rho}_m$ is negative in the studied cases. Even if some of the hypothesis of Teorell-Meyer-Sievers theory could be violated by some of the experimental conditions, it is still established that the calculated values can be used in comparing different types of membranes.

This work represents an attempt to characterize some synthetic membranes for current purposes, by a relatively simple and rapid technique.

REFERENCES

1. R. PLONSEY, *Bioelectric Phenomena*, Mc Graw-Hill Book Comp., 53–62, 78–112, 1969.
2. J. BURES, M. PÉTRAN, J. ZACHAR, *Electrophysiological Methods in Biological Research*, Publ. House of Czech. Acad. Sci., Praga, 178–190, 1960.
3. N. A. LANGE, *Handbook of Chemistry*, Handbook Publ. Inc., 1956.
4. C. GILLET, J. LEFEBRE, *Echanges ioniques transmembranaires chez les végétaux*, Colloque du CNRS nr. 258, 1976, Eds. du CNRS et de l'Université de Rouen, 75–81, 1977.
5. M. A. PICHENY, A. J. GRODZINSKY, Biopolymers, 15, 1845, (1976).
6. M. DELMOTTE, J. CHANU, *Echanges ioniques transmembranaires chez les végétaux*, Colloque du CNRS nr. 258 d 1976, Eds. du CNRS et de l'Université de Rouen, 55–59, 1977.

Received, December 20, 1979

ANALELE UNIVERSITĂŢII BUCUREŞTI, FIZICĂ XXIX, 1980, PAG. 107–111

NOTICES ON THE VARIATION OF SEISMIC WAVES VELOCITY BENEATH THE VRANCEA ZONE

ST. LASCU

Faculty of Physics, University of Bucharest *

ABSTRACT

The azimuthal distribution of the travel times for the earthquajes in Vrancea, caming to the conclusion that ont he azimuthal direction of 260°–330°, seismic waves velocity does not represent the specific fulling of the astenospheric stratum, the litospheric one going on with an increased velocity stratum.

Introduction

A lot of authors have noticed anomalies of velocity propagation of seismic waves P and especially S for the Vrancea seismic zone including. They came to some conclusions from studying the distribution of seismic waves velocity as well as of the earthquake focuses regarding the way the two sides of tectonic plates that contact each other are confrunting, and in some cases regarding the subduction process.

For the Vrancea seismic zone, although it has been established that the earthquakes of it take place due to a subduction process, estimating that one of the directions is oriented at about 300° azimuth, though the pointing out of some azimuthal anomalies of velocity propagation of the whole subduction, mechanism that has implications on the understanding of physical processes within the earthquake focuses.

The Matdrial Used and The Analysis of Data.

For a better pointing out of some anomalies of seismic waves velocity the travel times of the two direct waves P and S were used, times that were recorded at most seismic stations all over the world for 15 of the more powerful earthquakes taken place in the Vrancea zone within the

---

[*] National Center of Physics, Măgurele, Bucharest, P.O. Box 5211.

last century, earthquakes whose depths do not vary too much as they were comprised into the limits of 100 –160 km.

The study of these earthquakes pointed out [1, 3, 4, 5, 6] the existence in the superior mantle of this part of our earth of an astenospheric velocity fulling stratum and whose superior limit is lower than in other zones. We can't point out the accidental different limits of astenosphera for different directions.

Table 1

$\theta < 19°$				$\theta > 19°$			
Az deg	Az deg	$P_0 - P_c$ sec	n *	Az deg	Az deg	$P_0 - P_c$ sec	n*
0–30	25	0,4	8	0–30	15	1,5	2
30–60	40	−0,6	2	30–60	52	0,1	19
60–90	—	—	—	30–90	80	0,4	44
90–120	103	2,2	38	90–120	103	1,0	23
120–150	146	0,1	7	—	—	—	—
150–180	161	0,6	12	150–180	175	−0,1	6
180–210	198	2,1	9	180–210	—	—	—
210–240	221	1,5	6	210–240	229	−0,7	3
240–270	260	−1,1	30	240–270	262	−1,8	25
270–300	285	0,2	95	270–300	287	−1,3	3
300–330	316	−0,4	64	300–330	322	−1,7	51
330–360	356	−0,8	20	330–360	350	1,2	58

* n = No. of observ.

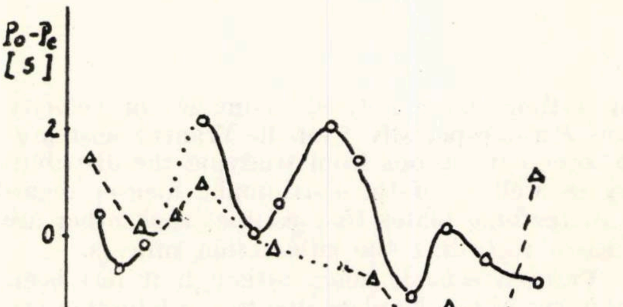

Fig. 1. P residuals (Observed — J—B) as a function of azimuth for : nearer stations($\theta < 19°$, circles) and distant stations ($\theta > 19°$.

In figure 1, we represented the residuals of travel times of longitudinal waves in comparison with the table J –B [2]. The values in graph represent the mediums of more times obtained the residuals of the travel times are due to some causes such as :

— lateral variations of waves velocity in superior mantle under the epicentre ;

— regional variations of waves velocity in superior mantle found under the stations that recorded the earthquakes;

— the imperfect distribution of stations in azimuth and distance;

— the tables of travel time used in determining the focus and of the reading of errors of phases.

The weight of the last causes is small reporting to the first one the lateral each of omogenity of superior mantle under the epicentre of the earthquake. That is why in figure 1 the azimuthal variation of residuals for nearer stations (points represented by circles) is compared with the azimuthal variation for distant stations (points represented by triangles).

The values in table 1 and points in figure 1 respectively are obtained for azimuthal intervals of 30°. It is clear that both the value and the way of warying of the two sets of stations are very different. The residuals variation for nearer stations points out the existence of the low velocity stratum between the azimuth 90° –200° as well as near the value of 360°, and on the direction 260° –330° we could notice an increased velocity of *P* waves. The residuals distribution for the distant stations do not seem to point out the presence of a low velocity stratum, the travel times oscilating about the values given in tables J –B ; that is understandable because the waves that reached these stations were oriented downside on their leaving the focus and did not penetrate the low velocity stratum but partially.

Within the azimuthal interval of 260° –330° a parallelism is noticed between the two curves ; the minimum being more stressed for the distant stations. This parallelism leads to the conclusion that the subduction in the Vrancea zone on the siegned direction is studdenly finished, the mather being in compression, passing into the low velocity stratum.

Table 2

h = 160 km				h = 112 km			
Az=0° – 360°		260° – 330°		Az = 0° – 360°		260° – 330°	
θ°	δk [× 10⁻³]	θ°	δk [× 10⁻³]	θ°	δk [× 10⁻³]	θ°	δk [× 10⁻³]
				5,8	4	6,1	–10
9,2	–1	8,7	100	10,4	35	10,3	25
10,9	50	11,2	77	12,6	8	12,7	3
12,9	29	12,7	61	14,2	47	14,2	33
16,1	28	16,2	51	16,4	27	16,4	22
20,0	12	20,0	19	19,5	17	19,4	2
				22,9	28	22,5	24
				26,9	38	26,9	30
				34,0	4		

For a more striking pointing out of this fact in table 2 we calculated the differences δk between the reports of longitudinal and transversal waves velocity that were noticed and of those calculated in tables J –B – for two earthquakes whose depths of 160 km and 122 km are placed at the extremes of the used earthquakes depths. These differences were calculated using all the stations situated at an epicentral distance comprised between 5° and 20° as well as separately tacking into account only the stations having their azimuth of 260° –330° and clearly out having in mind the same epicentral limits. The results are represented in figures 2 and 3.

It is noticed that for earthquakes with a smaller depth (figure 3) these variations are paralleled for two sets of stations, the reports being positive, caming to the conclusion that the aproximatelly uniform distribution of the low velocity stratum at a small depth. For earthquakes having a bigger depth (figure 2), at small distances, that is at small depths the variations of the two sets of stations are parallel, while for big epicentral distances, so, for big depths of seismic waves penetration these variations are paralleled giving an exponential falling more stressed for the sets of stations having the directions 260° –330°, pointing out the same sudden penetration to the increased velocity stratum.

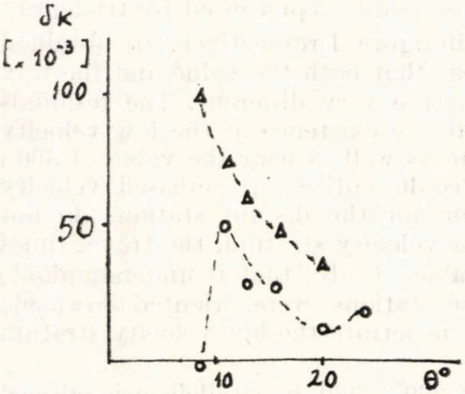

Fig. 2. **k residuals (Observed – J–B) as a function of epicentral distance θ, for earthquakes with h = 160 km. Triangles represent residuals for stations with azimuth of 260° to 330°, and circles are for all directions.**

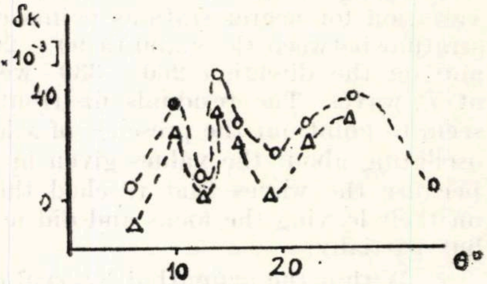

Fig. 3. **k residuals (Observed – J–B) as a function of epicentral distance θ, for earthquakes with h = 122 km. Triangles represent residuals for stations with azimuth of 260° to 330°, and circles are for all directions.**

Conclusion

The low velocity stratum beneath the Vrancea zone is not distributed homogeneously in azimuth, on the direction comprised between 260° –330°, it being almost absent, the litospheric zona being joined to the increased velocity zone.

REFERENCES

1. IOSIF T., Revue Roum. Géophys., Tome 10 No. 1,,1966, 33–41.
2. JEFFREYS H. and BULLEN K. E., *Seismological Tables – Britisch Association for the Advancement of Sciences*, London, 1948.
3. LASCU ST., Analele Univ. Buc., XXV, 1975, 41–48.
4. MITRONOVAS W. and ISACKS B. L., Journ. of Géophys. Res., vol. 66, No. 29, 1971, 7154–7180.
5. PETRESCU G. and RADU C., Revue Roum. Géophys., Tome 9, No. 1, 1965, 29–33.
6. PETRESCU G., RADU C. and LASCU ST., Revue Roum. Géophys., Tome 9, No. 1, 1965, 36–47.

Received, Januury 30, 1980

ANALELE UNIVERSITĂŢI BUCUREŞTI, FIZICĂ XXIX, 1980, PAG. 113–114

LE PROFESSEUR NICOLAE BĂRBULESCU À SON 80ème ANNIVERSAIRE

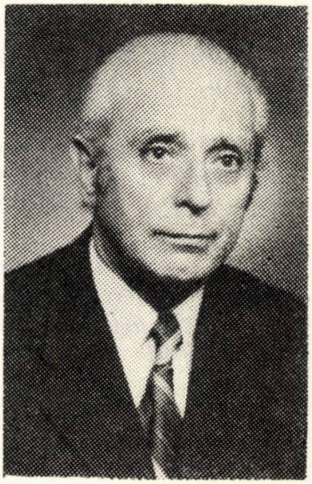

Le professeur Nicolae Bărbulescu est né le 10 Juillet 1900, à Bucarest.

Il suit les cours du lycée à Bucarest. En 1921, à la fin de ses études universitaires, il est intégré dans le laboratoire d'Acoustique et Optique de l'Université de Bucarest.

Entre 1926 et 1932 il fonctionne comme maître assistent au laboratoire de chimie physique de l'Université de Cluj, ensuite il y devient maître de conférences et professeur de physique générale.

Dans les années 1940–1948 il donne des cours de physique médicale à la faculté de Médecine de Bucarest.

Après qu'il a fonctionné comme recteur et professeur de physique générale à l'Ecole Supérieure de Textiles de Bucarest, il devient professeur et doyen à la faculté de chimie de l'Université de Bucarest (1948–1957).

Il donne des cours de Physique générale (1951–1953) à la faculté de Métallurgie de l'Institut Polytechnique de Bucarest.

Entre 1952–1962 il est professeur titulaire de chaire a l'Institut de Constructions de Bucarest.

De 1962 à 1970 il donne des cours de physique moléculaire et chaleur, étant en même temps professeur titulaire de chaire et le doyen de la faculté de physique de Bucarest (1966–1968).

Par son activité fructueuse et de longue durée, le professeur Nicolae Bărbulescu se situe parmi les plus représentatifs physiciens, maîtres d'école et chercheurs qui ont mis et consolidé les bases de la physique moderne en Roumanie.

Eminent professeur et effervescent chercheur scientifique, le professeur Nicolae Bărbulescu a également une prodigieuse et remarcable activité de publiciste dans la specialité, élaborant de nombreux cours, manuels, traités et monographies d'une réelle utilité pour l'enseignement de physique.

Ses préoccupations didactiques, scientifiques et philosophiques sont éloquemment illustrées par de nombreux et valeureux travaux concernant la *physique et la chaleur, la physique médicale, l'électricité biologique, la théorie cinétique des gaz, la pression osmotique, la théorie de la relativité, la chimie physique, la thermodynamique des phénomènes superficiels, l'énergétique, l'état liquide, les solutions, les mélanges binaires, les liquides raréfiés, la causalité et le déterminisme, la certitude mathématique, le problème du temps dans la théorie de la relativité restreinte, etc. Beaucoups de ses travaux, publiés chez nous ou à l'étranger, jouissent d'authentique considération et reconnaissance méritoire.*

Ses travaux d'histoire de la science, de pédagogie et de popularisation, ainsi que les articles publiés dans la presse, montrent éloquement son dévouement multiple mis avec une supérieure compétence et un rare humanitarisme au bénéfice de nombreuses générations de bénéficiaires, élèves, étudiants, professeur, ingénieurs, médecins, philosophes, etc. Commençant par l'article écrit en 1916 dans le journal des sciences populaires sur « Le Verrier et la découverte de la planète « Neptune », continuant par « L'histoire de l'électron » (Natura, 11, 1925), « La reforme de l'enseignement universitaire » (Scînteia, 1946) « Les exigences de l'enseignement supérieur » (Gazeta învățămîmtului XV, 723? 1963) « La science et la vie sociale », « Culture et democratie », etc., le professeur N. Bărbulescu ajoute, aujord'hui même, à ses manuscrits d'insolites epigrammes, des essais et des travaux littéraires.

À son 80-ème anniversaire, nous tous ceux qui connaissons et apprécions son oeuvre dans toute sa beauté et son utilité, apportons au vénérable magister, le professeur Nicolae Bărbulescu, un vibrant hommage et chaleureux souhaits de santé et prosperité.

I. C. PETREA **C. N. PLĂVIȚU** **I. DIMA**

BUDAPEST • MŰSZAKI EGYETEM

Abonamentele în ţară se pot contracta la oficiile P.T.T.R., agenţii poştali şi factorii poştali.

Cititorii din străinătate se pot abona, adresîndu-se la ILEXIM Departamentul Export-Import Presă, P.O. Box 136—137, telex: 11226, Bucureşti str. 13 Decembrie nr. 3.

Lei 22